

**The superconducting phase diagram
of the t-J model**

by

Menke Ubbo Heert Ubbens

M.Sc., Physics, University of Groningen (1989)

M.Sc., Mathematics, University of Groningen (1989)

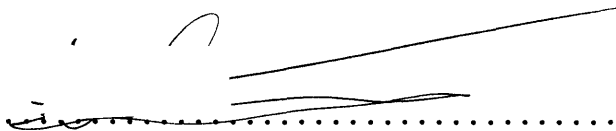
Submitted to the Department of Physics
in partial fulfillment of the requirements for the degree of
Doctor of Philosophy

at the

MASSACHUSETTS INSTITUTE OF TECHNOLOGY

February 1994


© Massachusetts Institute of Technology 1994. All rights reserved.

Author 

Department of Physics
December 6, 1993

Certified by 

Patrick A. Lee
William & Emma Rogers Professor of Physics
Thesis Supervisor

Accepted by 

George F. Koster
Chairman of Graduate Committee

science
LIBRARIES
FEB 08 1994

MASSACHUSETTS INSTITUTE OF TECHNOLOGY

The superconducting phase diagram of the t - J model

by

Menke Ubbo Heert Ubbens

Submitted to the Department of Physics
on December 6, 1993, in partial fulfillment of the
requirements for the degree of
Doctor of Philosophy

Abstract

In this thesis I present a microscopic model for the high- T_c cuprates, and analyze the phase diagram predicted by this model. The model is based on the t - J Hamiltonian, which describes the physics of a single copper-oxide plane. An important feature of the t - J model is that close to half filling the motion of the electrons is controlled by the empty sites in the system. This leads to spin-charge separation, which I take into account using the slave-boson formalism. In this approach the electrons are split into spinons and holons, which carry, respectively, the spin and the charge degrees of freedom of the electrons. Superconductivity will occur when the spinons form Cooper pairs and the bosons are Bose condensed.

I first analyze the model in the mean-field approximation. Novel flux phases are found at low doping, indicating that the system tries to simulate a Néel ordered state to minimize its magnetic energy. At intermediate doping the mean-field analysis predicts a superconducting gap with a d -wave symmetry.⁷ A drawback of the mean-field analysis is that it grossly overestimates the superconducting transition temperature, especially at low doping.

One can improve on the mean-field results by including a fluctuating gauge field in the analysis. This gauge field mediates the interactions between the spinons and the holons, which are strongly coupled. I show in Chapter 3 that the fluctuating gauge field suppresses the tendency of the holons to Bose condense.⁸ In order to obtain this result I developed a new technique based on a summation over Feynman paths,⁹ which is a very convenient approach in the strong-coupling limit $t \gg J$.

Chapter 4 focuses on the pair-breaking effects of the gauge field, which can be analyzed by studying the contribution of the gauge field to the total free energy. I show that there is a significant reduction of free energy due to gauge field fluctuations, which

⁷M.U. Ubbens and P.A. Lee, Phys. Rev. B **46**, 8434 (1992).

⁸M.U. Ubbens, P.A. Lee, and N. Nagaosa, Phys. Rev. B **48**, 13762 (1993).

⁹M.U. Ubbens and P.A. Lee, submitted to Phys. Rev. B (1993).

is partly lost when a gap opens up in the spinon excitation spectrum.¹⁰ At low doping this cost of free energy prevents the system from going into a superconducting state. At higher doping the pair-breaking effects of the gauge field become less important, and as a result superconductivity can survive in an intermediate range of doping $0.05 \lesssim x \lesssim 0.35$. An important consequence of this analysis is that for a single CuO_2 plane the spin-gap phase is completely destroyed by gauge-field fluctuations.

In Chapter 5 a model for two coupled CuO_2 planes is presented, to explain the spin-gap phase in multi-layered materials such as $\text{YBa}_2\text{Cu}_3\text{O}_{6.6}$.¹¹ This model uses the t - J Hamiltonian to describe each CuO_2 plane, with an additional antiferromagnetic inter-plane interaction coupling the two planes. I show that the presence of antiferromagnetic correlations strongly enhances the pairing between spinons on adjacent CuO_2 planes.¹² I propose that the spin-gap phase in multi-layered cuprates is due to enhanced inter-plane pairing, described by an inter-plane order parameter $\Delta_{\perp}(\mathbf{r}_{ij}) = \langle f_{i\uparrow}^{(1)} f_{j\downarrow}^{(2)} - f_{i\downarrow}^{(1)} f_{j\uparrow}^{(2)} \rangle$. I argue that the gauge field, which is very effective in destroying the in-plane order parameter Δ_{\parallel} , is less effective in destroying the inter-plane order parameter Δ_{\perp} . I use this model to calculate the NMR-relaxation rate, the echo-decay rate, and the Knight shift. The numerical results are in good agreement with the experimental data on $\text{YBa}_2\text{Cu}_3\text{O}_{6.6}$.

Thesis Supervisor: Patrick A. Lee

Title: William & Emma Rogers Professor of Physics

¹⁰M.U. Ubbens and P.A. Lee, to appear in Phys. Rev. B (1994).

¹¹M.U. Ubbens and P.A. Lee, submitted to Phys. Rev. Lett. (1993).

¹²M.U. Ubbens and P.A. Lee, M.I.T. preprint (1993).

Acknowledgements

It has been a great pleasure to work with my advisor, Patrick Lee, whose experience and insight in the field of condensed matter physics was invaluable for the progress of my research. Whenever I was temporarily stuck on a minor problem, or was anxious to show some new results, Patrick was always there to discuss my work and give suggestions on how to move on. The enthusiasm he showed for my work was greatly appreciated, especially at times when my progress was slow.

Special thanks go to Naoto Nagaosa, who was a postdoc at M.I.T. during my first two years as a graduate student. His ideas got me started on several projects, and I enjoyed his clear explanations during many fruitful conversations.

I am grateful to my past and present officemates Jari Kinaret, Michael Faas, Mitya Chklovskii, Bruce Normand and Hyunwoo Lee, for creating a pleasant atmosphere to work in, and for the daily conversations about life, physics, and everything in between.

I also wish to express my gratitude to Pieter Klaassen, Lars Schade, Timo Smit, Herre van der Zant, Jordina Vidal, Alexis Falicov, Susie Glass, Leslie Young, Paul Starkis, Katya Burns, Mike Peterson, Andreas Kussmaul and Reiko Oda. Thanks to these friends, and many others who I failed to mention here, my stay in Boston has been a very enjoyable and memorable period of my life, that I will undoubtedly look back upon with a smile.

Finally, I wish to thank my parents for encouraging a scientific career, and for their continuing love and support during my stay in the United States.

Contents

List of Figures	12
1 High-T_c superconductivity	13
1.1 History of the high- T_c cuprates	13
1.2 The phase diagram of the high- T_c superconductors	14
1.3 The material structure of cuprates	17
1.4 How to model a CuO_2 plane?	20
1.5 The t - J model	22
1.6 Spin-charge separation	25
1.7 The phase diagram of spinons and holons	27
1.8 Outline of this thesis	30
2 Flux phases in the t-J model	33
2.1 Introduction	33
2.2 Hartree-Fock-Bogoliubov decomposition	34
2.3 Flux phases	36
2.4 Phase diagram	38
2.5 Conclusions	42
3 Path-integral analysis of bosons interacting with a gauge field	44
3.1 Introduction	44
3.2 The gauge-field model	46
3.3 Annealed versus quenched averaging	49
3.4 The single-particle partition function	53

3.5	Response to an external field	63
3.6	Discussion	70
4	The superconducting phase diagram in the gauge-field description of the t-J model	73
4.1	Introduction	73
4.2	The role of gauge-field fluctuations in the t - J model	75
4.3	The gauge-field contribution to $F(\Delta_0)$ in the presence of a gap	85
4.3.1	The propagator at $T = 0$	89
4.3.2	The propagator for $\Delta_0 \ll T$	92
4.4	Numerical analysis of $F_{\text{gauge}}(\Delta_0)$	94
4.5	Conclusions	98
5	Spin-gap formation in bi-layer cuprates due to enhanced inter-layer pairing	100
5.1	Introduction	100
5.2	RPA analysis of two coupled CuO_2 planes	103
5.3	Inter-plane pairing	110
5.4	Numerical analysis of inter-plane pairing	114
5.5	Pair-breaking effects of the gauge field	119
5.6	NMR-relaxation rates	123
5.7	Discussion	130
A	Decoupling of $\mathbf{S}_i \cdot \mathbf{S}_j$	135
B	Diagonalization of H^{MF}	138
C	Calculation of ρ_{ret}^x	140

List of Figures

1-1	The phase diagram of $\text{La}_2\text{Sr}_{2-x}\text{CuO}_4$ measured by Keimer <i>et al.</i> [5].	15
1-2	The chemical structure of La_2CuO_4	18
1-3	The chemical structure of $\text{Tl}_2\text{Ba}_2\text{Ca}_{n-1}\text{Cu}_n\text{O}_{2n+3+x}$ for $n = 1, 2, 3$	19
1-4	The structure of a single CuO_2 plane.	20
1-5	The Fermi surface of the t - J model close to half filling.	24
1-6	The t - J model in the slave-boson approach. On each site there is either a spinon or a holon.	26
1-7	A qualitative phase diagram of the t - J model, based on the pairing transition of the spinons and the Bose condensation of the holons.	28
2-1	The symmetry of the order parameters χ_{ij} and Δ_{ij}	37
2-2	The global phase diagram for $t/J = 0.5$. For $\delta \lesssim 0.6$ the gap Δ has a d -wave symmetry. For $\delta \lesssim 0.12$ staggered-flux phases become favorable.	39
2-3	Phase diagram for $t/J = 0.5$. For $\delta \lesssim 0.12$ staggered-flux phases become energetically favorable. For $\delta \lesssim 0.06$ a π -flux phase becomes stable. The shaded area represents the hysteresis of a first-order transition between the d -wave-pairing state and the flux-phase region.	40
2-4	Phase diagram for $t/J = 2$. Comparison with the phase diagram for $t/J = 0.5$ shows that for larger values of t/J the whole phase diagram gets pushed towards lower values of δ . The staggered-flux phase region still extends to $\delta \sim 0.02$, but the π -flux region is only stable for $\delta \lesssim 0.002$. For $\delta > 0.02$ there is a continuous transition from the d -wave-pairing state to the flux-phase region.	41

2-5	The onset of the staggered-flux phase and the π -flux phase as a function of t/J . The onset of the staggered-flux phase is inversely proportional to t/J : $\delta_{c1} \sim 0.08J/t$	42
3-1	Fig. (a) shows the unaveraged diagram for a response function, where the wavy lines denote the gauge field. A quenched average over the gauge field means that the wavy lines have to be connected in all possible ways, as shown in Fig. (b). This does not include diagrams with internal boson loops, like the one shown in Fig. (c).	52
3-2	A certain class of diagrams with internal boson loops can be included in the quenched average, by including strings of boson bubbles in the gauge field propagator, as shown in Fig. (a). This is equivalent to replacing χ_F by $\chi = \chi_F + \chi_B$. Similarly one should also include these strings of boson bubbles in the response function to an external field, as is shown in Fig. (b). The gauge field now screens the external field, and one obtains the Ioffe-Larkin rule $\chi_{\text{phy}}^{-1} = \chi_F^{-1} + \chi_B^{-1}$	53
3-3	Fig. (a) shows the typical boson-path in a strongly fluctuating gauge field. At short time-scales $\tau < \tau_\phi$ the bosons follow random walks. At longer time-scales $\tau > \tau_\phi$ the typical path retraces itself, to minimize the total area of the path. Fig. (b) is obtained by “stretching” the coarse-grained reference path.	55
3-4	Three different approximations for the boson susceptibility $\chi_B(T)$ for a fixed boson density $n_B = 0.1$ and $t/J = 1$. The dashed line is the quenched susceptibility $\chi_B^Q(T) \propto (gT)^{-1}$. The solid line is the self-consistent $\chi_B^{\text{SC}}(T)$. Below a crossover temperature T_{BE} the susceptibility χ_B^{SC} diverges exponentially, analogous to the non-interacting value χ_B^0 (dash-dotted line). Notice that due to gauge field fluctuations the crossover temperature is strongly suppressed, $T_{\text{BE}} \ll T_{\text{BE}}^0$	68

- 3-5 The (inverse) boson susceptibility $\chi_B^{\text{SC}}(T)^{-1}$ for various values of t/J at a fixed density $n_B = 0.1$. At high temperatures $\chi_B^{\text{SC}}(T)^{-1}$ is linear in T , with a slope proportional to t/J , and an intercept independent of t/J . Below $T_{\text{BE}} \simeq 0.08 T_{\text{BE}}^0$ one enters the weak-coupling regime, and $\chi_B^{\text{SC}}(T)^{-1}$ decays exponentially. Note that T_{BE} is reduced by a factor of $\simeq 12$ compared to T_{BE}^0 69
- 4-1 A schematic mean-field phase diagram of the t - J model. The mean-field pairing line (dotted) and the Bose-condensation line (solid) divide the phase diagram into four regions. Region I is a Fermi-liquid phase, region II is the spin-gap phase, region III is the superconducting phase, and region IV is the strange metal phase. 76
- 4-2 The phase-diagram of the t - J model for $t/J = 3$ using a mean-field expression for the susceptibility χ_B^0 . The self-consistent dissipative model χ_B^{SC} produces a phase diagram that is essentially indistinguishable. The line denoted by black diamonds is our best guess of the correct phase boundary within this model. For $x \lesssim 0.05$ superconductivity vanishes completely, which is directly related to the fact that the gauge field becomes unstable against flux phases at low doping. 78
- 4-3 The phase-diagram of the t - J model for $t/J = 3$, using the dissipative model for the susceptibility χ_B^{diss} . The solid line for $T_c(x)$ uses $T = 0$ expressions for the propagator $\Pi_F(\nu)$, while the dashed line is obtained by expanding $\text{Im } \Pi_F(\nu)$ and $\text{Re } \Pi_F(\nu)$ in Δ_0^2 . Note that in this phase diagram the transition temperature $T_c(x)$ is much lower than in Fig. 4-2. 79

- 4-4 The boson susceptibility $\chi_B(T)$ for three different models for a doping $x = 0.07$. The fact that $\chi_B(T)$ increases rapidly at low temperatures indicates that the bosons effectively condense into a superfluid state below a certain crossover temperature. The dotted line is the mean-field value χ_B^0 , the dashed line represents the dissipative model for χ_B^{diss} and the solid line is the self-consistent dissipative χ_B^{SC} . In the absence of a full theory χ_B^{SC} is a reasonable guess for the behavior of the susceptibility $\chi_B(T)$ 82
- 4-5 This figure shows $\text{Im } \Pi_F(\nu)$ at $T = 0$ for $\Delta'/\Delta = 1, 0.3, -0.3$ and -1 . Notice that there is no absorption for $\nu < |\Delta| + |\Delta'|$. For $\nu > |\Delta| + |\Delta'|$ it depends on the relative sign of Δ and Δ' whether $\text{Im } \Pi_F(\nu)$ is enhanced or suppressed by the gap. 90
- 4-6 This figure shows $\text{Re } \Pi_F(\nu)$ at $T = 0$ for $\Delta'/\Delta = 1, 0.3, -0.3$ and -1 . Similar to the case of $\text{Im } \Pi_F(\nu)$ it depends on the relative sign of Δ and Δ' whether $\text{Re } \Pi_F(\nu)$ is positive or negative. 91
- 4-7 This figure shows $\Delta_{00}(x)$, the gap at $T = 0$. By comparing this to $T_c(x)$ in Figs. 4-2 and 4-3 we find that the ratio $2\Delta_{00}/T_c$ is approximately 3 if one uses the mean-field χ_B^0 (or the self-consistent χ_B^{SC}), and approximately 8 if one uses the dissipative χ_B^{diss} . This should be compared to the mean-field d -wave value of $2\Delta_{00}/T_c^0 \simeq 2.6$ 97
- 5-1 The renormalized susceptibility $\chi^{\text{RPA}}(q)$ in the RPA approximation. The wavy line denotes the in-plane exchange $\mathbf{S}_i^{(n)} \cdot \mathbf{S}_j^{(n)}$, and the jagged line denotes the inter-plane exchange $\mathbf{S}_i^{(n)} \cdot \mathbf{S}_i^{(n')}$ 106
- 5-2 The effective in-plane coupling $J_{\parallel}^{\text{eff}}(\mathbf{q})$ (left axis) and the effective inter-plane coupling $J_{\perp}^{\text{eff}}(\mathbf{q})$ (right axis) for various values of the doping x . Close to the AF instability at $x_c = 0.08$, $J_{\parallel}^{\text{eff}}(\mathbf{q})$ and $J_{\perp}^{\text{eff}}(\mathbf{q})$ have strong incommensurate peaks at $\mathbf{Q}_{\text{AF}} \simeq (\pi, \pi \pm 0.19)$ 109

- 5-3 The pairing order parameter $\Delta_{\perp}(\mathbf{r})$ for $x = 0.085$. Due to the antiferromagnetic correlations $\Delta_{\perp}(\mathbf{r})$ decays over a correlation length of approximately 3-4 lattice spacings. Also notice that $\Delta_{\perp}(\mathbf{r})$ is relatively strong along the diagonals $r_x = \pm r_y$. This implies that in momentum space $\Delta_{\perp}(\mathbf{k})$ is enhanced around the diamond-shaped Fermi surface. 115
- 5-4 A contour plot of the gap $\Delta_{\perp}(\mathbf{k})$ for $x = 0.085$ and $J_{\perp}^0 = 0.2 J_{\parallel}^0$. The diamond-like Fermi surface is indicated by the black dotted line. Notice that the gap $\Delta_{\perp}(\mathbf{k})$ has an extended s -wave symmetry, with peaks at the four corners $\mathbf{k} = (\pm\pi, 0)$ and $\mathbf{k} = (0, \pm\pi)$, and without nodes. 116
- 5-5 The inter-plane gap $\Delta_{\perp}(\mathbf{k})$ around the Fermi surface for $x = 0.085$, $x = 0.09$ and $x = 0.10$. The gap $\Delta_{\perp}(\mathbf{k})$ has an extended s -wave symmetry, and is anisotropic around the Fermi surface, with peaks at the corners. For higher doping the amplitude of the gap decreases rapidly, and the anisotropy almost disappears. 117
- 5-6 A logarithmic plot of the gap Δ_{\perp}^{\max} at the corner of the Fermi surface as a function of the inter-plane coupling constant $(J_{\perp}^0)^{-1}$, assuming that the effective coupling is given by $J_{\perp}^{\text{eff}}(\mathbf{r}) = \pm J_{\perp}^0 \exp(-r/r_0)$. The straight lines show that Δ_{\perp}^{\max} depends exponentially on $(J_{\perp}^0)^{-1}$. Notice that for $r_0 = 3$ the slope of the line is 2.7 times smaller than for $r_0 \rightarrow 0$. 118
- 5-7 The diagrams for the gauge field propagators $\Pi_{\parallel}(q)$ and $\Pi_{\perp}(q)$. The indices n and n' indicate plane 1 or plane 2 (and $n \neq n'$). In Sec. 5.5 we show that the in-phase propagator $\Pi_+ = \Pi_{\parallel} + \Pi_{\perp}$ becomes massive when an inter-plane gap Δ_{\perp} opens up, while the out-of-phase propagator $\Pi_- = \Pi_{\parallel} - \Pi_{\perp}$ remains massless. 120
- 5-8 The NMR-relaxation rate $(T_1 T)^{-1}$ on the copper and the oxygen sites for two values of the scattering rate Γ . This calculation uses a BCS-like temperature dependence for the spin-gap $\Delta_{\perp}(T)$. The Hebard-Schlichter peak gets less pronounced when Γ increases. 127

5-9	The NMR-relaxation rate $(T_1 T)^{-1}$ on the copper and the oxygen sites, using a pseudo-gap $\Delta_{\perp}(T)$ which has a finite tail for $T > T_P^0$, as is shown in the inset. The main difference with Fig. 5-8 is that the Hebard-Schlichter peak gets smeared out over a wider range of temperature.	128
5-10	The echo-decay rate T_2^{-1} as a function of temperature for two values of the scattering rate Γ . The dashed lines assume a BCS-like temperature dependence of the spin-gap $\Delta_{\perp}(T)$, and the solid lines assume a pseudo-gap behavior.	129
5-11	The Knight shift as a function of temperature. The dashed line assumes a BCS-like temperature dependence of the spin-gap $\Delta_{\perp}(T)$, and the solid line assumes a pseudo-gap behavior. The Knight shift decays exponentially when $T \lesssim \Delta_{\perp}(T)$	130
5-12	A schematic phase diagram for bi-layer cuprates. We predict that the spin-gap phase is due to inter-layer fermion pairing, enhanced by antiferromagnetic correlations. Below the superconducting transition (thick solid line) the s -wave inter-plane pairing and the d -wave in-plane pairing coexist.	133
C-1	The exponent γ' as a function of $\alpha = 2R/N/\sqrt{\tau_{\phi}/M}$. This exponent modifies the enhancement of the density of states near the band edge.	142

Chapter 1

High- T_c superconductivity

1.1 History of the high- T_c cuprates

Once in a while the physics community is stirred by a major discovery that creates an important new field of research. The discovery of high-temperature superconductivity will undoubtedly be remembered as one of those events. It all started in 1986, when Bednorz and Müller reported the discovery of a new material that remained superconducting at a much higher temperature than any other material known at that time [1]. Their material was a layered ceramic, La_2CuO_4 doped with Ba, which appeared to be superconducting below a critical temperature of about 30 Kelvin. It quickly became clear that this new material was an example of a much larger class of so-called *copper oxides* or *cuprates* with similar properties. The most striking feature of these cuprates was their unusually high superconducting transition temperature. This discovery started a frantic race to find similar materials with higher and higher transition temperatures. This race involved material scientists to grow these complicated compounds, experimental physicists to carry out measurements, and theoretical physicists trying to understand the very abnormal behavior of these cuprates.

The first few years the progress on the materials side was quite impressive [2]. Regularly new cuprates were discovered with higher and higher transition temperatures, mostly by replacing certain elements in the compounds by other elements. An important breakthrough was reached in 1987 with the discovery of $\text{YBa}_2\text{Cu}_3\text{O}_7$,

which has a T_c of 92 K. This discovery made it possible to obtain superconductivity above the boiling point of liquid nitrogen, which is at 77 K. Because of the low cost of liquid nitrogen, this opened a whole new field of applications.

In that period the hopes were high that much higher transition temperatures were going to be reached in the near future, and people even talked about superconductivity at room temperature. In 1988 a T_c of 125 K was attained with the thallium compound $\text{Tl}_2\text{Ba}_2\text{Ca}_2\text{Cu}_3\text{O}_{10}$ [3], but for many years it appeared to be impossible to push the transition temperature any higher than that. Recently, in June 1993, the highest T_c was pushed slightly higher to 135 K with the mercury compound $\text{HgBa}_2\text{Ca}_{n-1}\text{Cu}_n\text{O}_{2n+3+x}$ [4].

Although the highest reported T_c has hardly increased during the last few years, there has been significant improvement in better preparation of the compounds. Larger and purer single crystals have become available, as well as greatly improved epitaxial films. The availability of these large and pure single crystals is important for experimental physicists, in order to get clean results about the interesting physical properties of the cuprates. At this moment, seven years after the discovery of the high- T_c cuprates, there is a rather complete picture of the physical properties of these materials. However, there is no consensus yet among theorists what is the correct microscopic model that *explains* the physics of these materials, although there is a reasonably good understanding of what are the main ingredients of this puzzle.

1.2 The phase diagram of the high- T_c superconductors

The enormous interest in the cuprates since their discovery in 1986 was initiated by their unusually high superconducting transition temperature. However, the high superconducting transition temperature of the cuprates is just one of the unusual physical properties of these materials. These unusual properties are best illustrated by the phase diagram for $\text{La}_{2-x}\text{Sr}_x\text{CuO}_4$ in Fig. 1-1, calculated by Keimer *et al* [5]. This phase diagram for $\text{La}_{2-x}\text{Sr}_x\text{CuO}_4$ is characteristic for all the high- T_c cuprates.

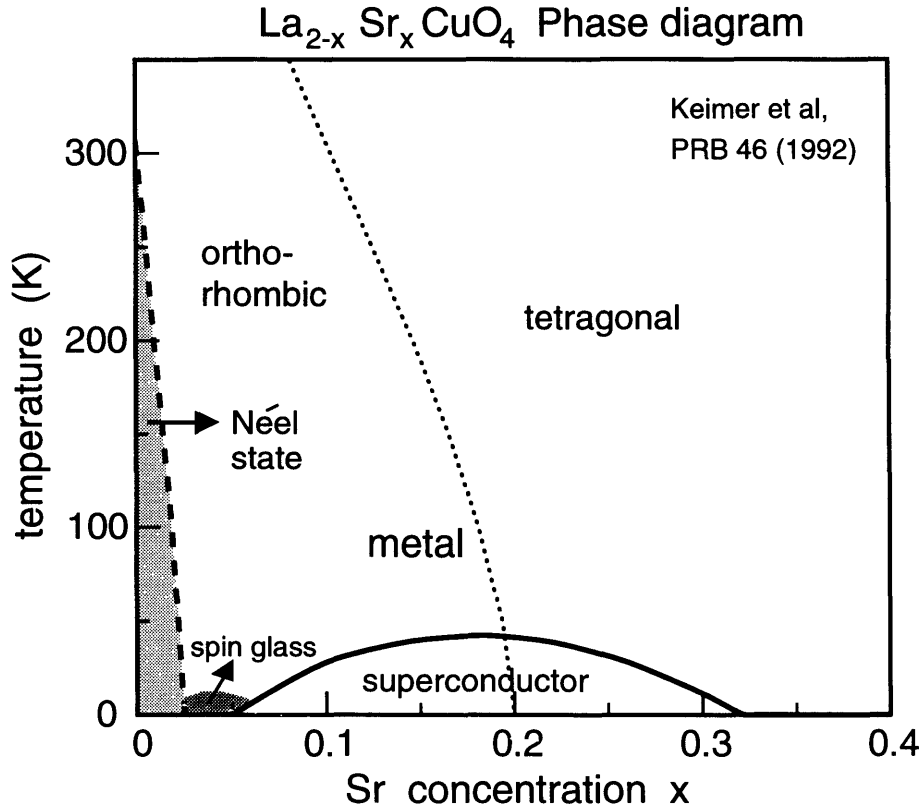


Figure 1-1: The phase diagram of $\text{La}_2\text{Sr}_{2-x}\text{CuO}_4$ measured by Keimer *et al.* [5]. At very low doping this material is an antiferromagnetic insulator, with a long-range Néel ordering. For slightly higher doping the material becomes metallic, with very unusual properties. Superconductivity survives in an intermediate range of doping $0.05 \lesssim x \lesssim 0.3$. The optimum T_c is at approximately 40 K.

In the undoped case the parent compound La_2CuO_4 is an insulator with antiferromagnetic (Néel) ordering. The physical properties change dramatically if one dopes the material with strontium, which amounts to replacing some La atoms by Sr atoms in the crystal structure. Fig. 1-1 shows that for a small amount of doping the long-range Néel ordering disappears, but the system remains an insulator. For higher doping the system becomes metallic. By lowering the temperature the system becomes eventually superconducting. Notice that superconductivity only survives in an intermediate range of doping $0.05 \lesssim x \lesssim 0.3$. The optimum T_c for $\text{La}_{2-x}\text{Sr}_x\text{CuO}_4$ is at approximately 40 K. Although much higher transition temperatures have been achieved for other high- T_c cuprates, a T_c of 40 K is already much higher than what one could possibly expect for a normal metal. In normal metals superconductivity

has never been observed above 23 K, and for most metals the transition temperature remains well below 10 K.

Except for the unusually high transition temperature, the properties of the superconducting state are quite similar to that of a conventional superconductor. Many physicists nowadays agree that the “normal-state” properties of the cuprates are much more unusual than the properties of the superconducting state. At very high doping ($x \gtrsim 0.25$) the cuprates are still reasonably well described by the Fermi-liquid theory for normal metals. But if one lowers the doping further and further, the cuprates start to behave stranger and stranger in the “normal” state. Below follow a few examples of irregularities of the cuprates in the normal state at low doping.

- The in-plane resistivity ρ_{ab} is almost exactly proportional to T , from the transition temperature up to 500 K.
- The Hall-effect has an unusual temperature dependence. The Hall resistance R_H increases with decreasing temperature, and the Hall angle varies like $\theta_H^{-1} \sim T^2$.
- There are indications for a gap in the spin-excitation spectrum, which remains visible well above T_c .

It is widely believed that the unusual properties of the normal state are directly related to the high superconducting transition temperature of the cuprates.

In addition to the Néel transition and the superconducting transition, Fig. 1-1 also shows a phase transition between an orthorhombic phase and a tetragonal phase. This structural phase transition is characteristic for La_2CuO_4 , but this transition will in general be different (or not exist at all) for other high- T_c compounds. This structural phase transition is not important for the understanding of the physical properties of the cuprates, and we will therefore not discuss this transition any further.

Perhaps one of the most surprising aspects of the high- T_c cuprates is that the phase diagram is qualitatively the same for all the different compounds. The exact value of the transition temperature might vary strongly from compound to compound, but for all the high- T_c cuprates one observes an insulating Néel phase at very low

doping ($x \lesssim 0.015$), and a superconducting phase at an intermediate range of doping $0.05 \lesssim x \lesssim 0.3$. This general behavior of the cuprates is somewhat surprising, because at first glance the different high- T_c compounds seem to have very different chemical compositions. Clearly there must be some kind of unifying feature that controls the physics of the whole class of high- T_c cuprates. It was known from the very beginning that all these compounds have one feature in common, namely the two-dimensional CuO_2 planes that are present in all the high- T_c materials. Considering that this is the only similarity between all the different high- T_c compounds, it was understood early on that these CuO_2 planes must be responsible for the unusual physics of the high- T_c cuprates.

In the next section we will show a few examples of how the structure of some of the high- T_c cuprates looks like, and how the CuO_2 planes are built into the structure.

1.3 The material structure of cuprates

The high- T_c cuprates can have widely varying chemical compositions, but they all have in common that they have a layered structure that contains two-dimensional CuO_2 planes. In Figs. [reflco.fig](#) and 1-3 we show a few examples of the structure of some selected high- T_c cuprates:

- (a). La_2CuO_4 , the compound that started high- T_c superconductivity. By replacing 20 % of the La atoms by Sr atoms one can reach an optimum T_c of 38 K.
- (b). $\text{Tl}_2\text{Ba}_2\text{Ca}_{n-1}\text{Cu}_n\text{O}_{2n+3+x}$ for $n = 1, 2, 3$. This family of compounds has an optimum T_c of, respectively, 80 K, 108 K and 125 K for $n = 1, 2, 3$. The last compound was until recently the record holder, with the highest T_c of all known materials.

The two-dimensional CuO_2 planes are the horizontal planes bisecting the octahedra in Figs. 1-2 and 1-3, and the horizontal planes at the basis of the pyramids. The oxygen atoms are on the vertices of these octahedra and pyramids. The other elements (La, Sr, Tl, Ca, Ba, etc.) are located on planes between the CuO_2 layers. The current

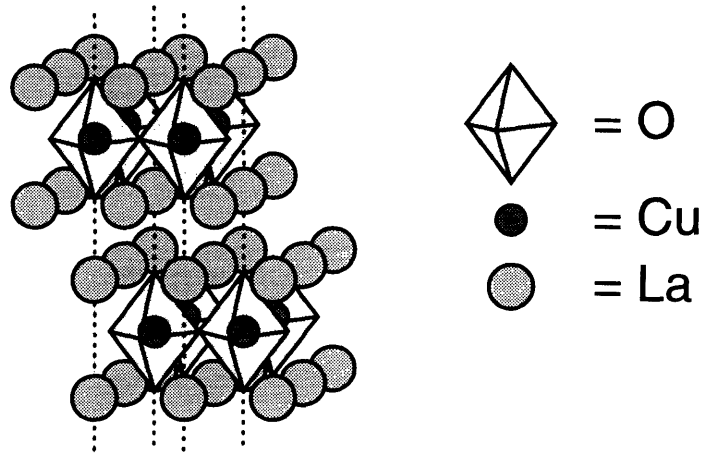


Figure 1-2: The chemical structure of La_2CuO_4 . The CuO_2 planes are the horizontal planes bisecting the octahedra. The oxygen atoms are on the vertices of these octahedra. If one dopes this material with strontium a small percentage of La^{3+} atoms gets replaced by Sr^{2+} atoms. This has the effect of creating holes in the CuO_2 planes.

understanding is that this structure between the CuO_2 layers merely acts as a charge reservoir, whose main role is to influence the charge density *within* the CuO_2 layers. If by means of doping one modifies the chemical composition of these charge reservoirs, one alters the charge density in the CuO_2 planes, which consequently changes the electronic properties of the material. In La_2CuO_4 this can be achieved by replacing a La^{3+} atom by a Sr^{2+} atom. The Sr^{2+} atom has a different valency than the La^{3+} atom, and therefore “sucks” an electron out of the nearby CuO_2 plane. This means that a hole is created in a CuO_2 plane if one dopes La_2CuO_4 with a Sr atom. As was shown in the phase diagram in the previous section, the physical properties of $\text{La}_{2-x}\text{Sr}_x\text{CuO}_4$ strongly depend on the amount x of Sr doping.

In order to derive a microscopic theory for the high- T_c cuprates we will from now on focus on the CuO_2 planes, because that is the only common feature of the whole class of high- T_c cuprates. We will derive a model for a *single* CuO_2 plane, assuming that the role of the chemical elements between the CuO_2 planes is only to fix a certain density of electrons in this CuO_2 plane. In the next few chapters we use this model for a single CuO_2 plane to calculate the superconducting phase diagram for the high- T_c cuprates. Only in the last chapter we will also consider the coupling between adjacent

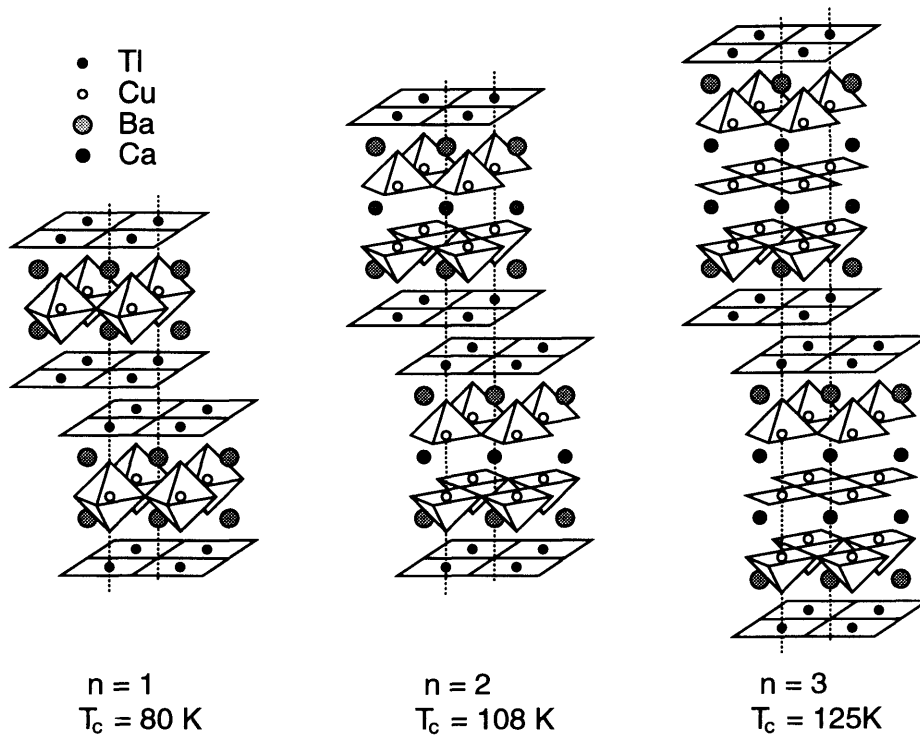


Figure 1-3: The chemical structure of $\text{Tl}_2\text{Ba}_2\text{Ca}_{n-1}\text{Cu}_n\text{O}_{2n+3+x}$ for $n = 1, 2, 3$. The CuO_2 planes are the horizontal planes bisecting the octahedra and the horizontal planes at the basis of the pyramids. The oxygen atoms are on the vertices of these octahedra and pyramids. Note that for $n = 2$ and $n = 3$ there are several CuO_2 planes close together in each unit cell.

CuO_2 planes. The motivation for this is that there is clear experimental evidence that the properties of single-layer materials are qualitatively different from the properties of multi-layer materials, that have two or more CuO_2 planes close together in each unit cell. One of the differences is that the superconducting transition temperature tends to increase if there are several CuO_2 planes in a unit cell. This is illustrated by the three thallium structures in Fig. 1-3. The transition temperatures of these three structures are respectively 80 K, 108 K and 125 K for $n = 1, 2$ and 3 CuO_2 planes per unit cell. This indicates that the interaction between nearby CuO_2 planes enhances superconductivity. Another difference is that in multi-layer cuprates such as $\text{YBa}_2\text{Cu}_3\text{O}_{6.6}$ one observes a (pseudo) *spin gap* in the excitation spectrum of the electrons. This spin gap, which is absent in single-layer materials, is observed at low doping, and survives well above the superconducting transition temperature. A

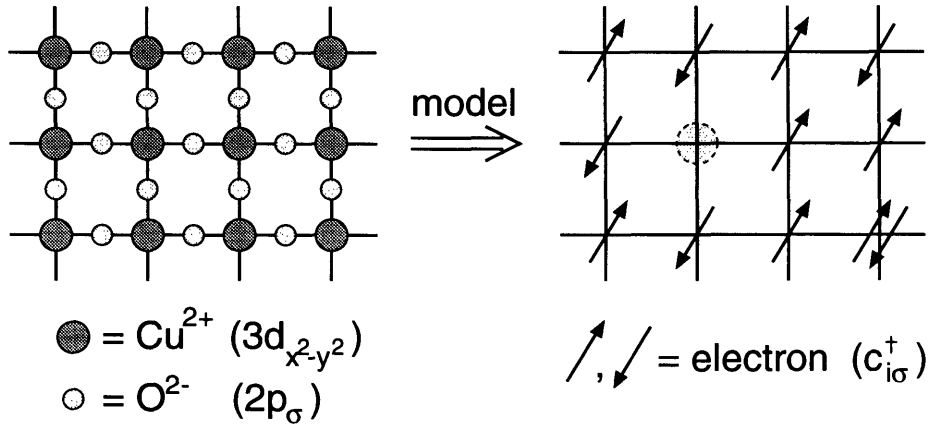


Figure 1-4: The structure of a single CuO_2 plane, which is a square lattice with Cu atoms on the vertices and O atoms on the bonds. By focusing on the electron in the hybridized d - p band, this reduces to the model on the right, which has one electron per unit cell, with a strong antiferromagnetic superexchange interaction between neighboring sites.

possible mechanism for this spin-gap phase will be discussed in Chapter 5, where we study a system of two coupled CuO_2 layers.

1.4 How to model a CuO_2 plane?

A copper-oxide plane consists of a square lattice with copper atoms on the vertices and oxygen atoms between adjacent Cu atoms. This is shown in Fig. 1-4. We can simplify this electronic system by focusing only on the electron states that lie close to the Fermi level. In this case these states correspond to the $3d$ orbital on the Cu atom and the $2p$ orbital on the O atom. Because of their closeness in energy the $d_{x^2-y^2}$ orbital and the p_{σ} orbital are strongly mixed, leading to a hybridized d - p band. The electrons in this d - p band are usually identified with the Cu sites. Due to the strong hybridization between the electron states on the Cu atoms and the O atoms the electrons in this band can easily hop from one site to the next.

One might wonder what is so special about Cu and O atoms, and whether the same story can also hold for two-dimensional planes that consists of other atoms. There are two features of the CuO_2 planes that are very characteristic for Cu and O atoms. First the $3d_{x^2-y^2}$ band of the Cu atom is very flat, and second the $3d_{x^2-y^2}$

band and the $2p_\sigma$ band are very close in energy, which leads to strong hybridization. This will in general not be true for two-dimensional planes that consist of other atoms.

After this simplification we have reduced the system to an effective model of electrons on a square lattice, on which the electrons can hop from one site to the next. Perhaps the most popular Hamiltonian to describe this system is the so-called Hubbard Hamiltonian, given by

$$H = -t \sum_{\langle i,j \rangle} (c_{i\sigma}^\dagger c_{j\sigma} + \text{c.c.}) + U \sum_i n_{i\uparrow} n_{i\downarrow}, \quad (1.1)$$

where $n_{i\sigma} = c_{i\sigma}^\dagger c_{i\sigma}$ is the number operator of electrons $c_{i\sigma}^\dagger$ with spin σ on site i . The first term in the Hubbard Hamiltonian is a kinetic term that indicates that the electrons like to hop from site to site. The second term is a potential term due to the Coulomb repulsion. This term tells us that the system pays a big energy U if a particular site is occupied by two electrons at the same time.

Another popular Hamiltonian to describe a CuO_2 plane is the so-called t - J Hamiltonian, given by

$$H = -t \sum_{\langle i,j \rangle} (c_{i\sigma}^\dagger c_{j\sigma} + \text{c.c.}) + J \sum_{\langle i,j \rangle} (\mathbf{S}_i \cdot \mathbf{S}_j - \frac{1}{4} n_i n_j), \quad (1.2)$$

where $\mathbf{S}_i = \frac{1}{2} c_{i\alpha}^\dagger \boldsymbol{\sigma}_{\alpha\beta} c_{i\beta}$ is the spin operator of the electron on site i . The first term in Eq. (1.2) is again the kinetic hopping term. The second term indicates that it is favorable for the spins to have an antiferromagnetic orientation. For the t - J model there is the additional constraint that it is not allowed that any site is double occupied. In the limit $t \gg J$ (or $U \gg t$), which is the appropriate limit for the high- T_c cuprates, the t - J model and the Hubbard model become equivalent, if one chooses $J = 4t^2/U$.

The Hubbard model, the t - J model, and variations of these two models are the most widely used starting points in efforts to develop a microscopic theory for the high- T_c cuprates. In order to describe the cuprates accurately, typical values for U , t

and J are

$$\begin{aligned}U &\sim 5 \text{ eV}; \\t &\sim 0.4 \text{ eV}; \\J &\sim 0.12 \text{ eV}.\end{aligned}\tag{1.3}$$

These values are obtained by comparing the low energy spectrum of the Hubbard model and the t - J model with the actual energy spectrum of a CuO_2 plane.

Both the Hubbard model and the t - J model are difficult to deal with for the values of the parameters given in Eq. (1.3). In the case of the Hubbard model it is impossible to use standard perturbation theory, because of the large value of U , while in case of the t - J model it is hard to deal with the constraint of no double occupancy. In this thesis we will focus exclusively on the t - J model, which is somewhat easier to analyze than the Hubbard model. In Chapter 5 we will generalize the t - J model somewhat to take the coupling between adjacent CuO_2 planes into account, which is important in multi-layer systems such as YBCO.

1.5 The t - J model

The t - J model, which was introduced in section 1.4 as a model for a single CuO_2 plane, is one of the most widely used microscopic models for high- T_c superconductivity. The purpose of this section is to give the reader a better understanding of the basic properties of the t - J model, before we dive into a more detailed analysis in the next few chapters.

The t - J model is a model for electrons on a two-dimensional square lattice, whose dynamics are described by the Hamiltonian in Eq. (1.2). This Hamiltonian is under the important constraint that no site is allowed to be double occupied. We will first consider the t - J model in the important case of half filling, i.e. when there is on average one electron per site. Because of the constraint of no double occupancy this implies that there is *exactly* one electron on each site. In the absence of empty sites

the electrons do not have any opportunity to move around, and thus we are dealing with an insulator that consists of quantum spins pinned on a lattice. Clearly the hopping term in Eq. (1.2) becomes irrelevant, and at half filling the Hamiltonian therefore reduces to the Heisenberg Hamiltonian

$$H = J \sum_{\langle i,j \rangle} \mathbf{S}_i \cdot \mathbf{S}_j. \quad (1.4)$$

It is well known that below the Néel temperature T_N this Hamiltonian describes an insulator with long-range antiferromagnetic order. Experiments indeed show that the undoped cuprates are Néel ordered below a certain temperature. For La_2CuO_4 this Néel temperature is at $T_N(0) \simeq 325\text{K}$.

The situation changes drastically away from half filling, i.e. when the system contains a small amount of holes. The phase diagram for $\text{La}_{2-x}\text{Sr}_x\text{CuO}_4$ in Fig. 1-1 shows that the Néel temperature $T_N(x)$ decreases rapidly if one dopes La_2CuO_4 with a small amount of strontium atoms. At a Sr concentration of $x \simeq 0.015$ the long-range antiferromagnetic order has disappeared completely. We will now use t - J model to explain this behavior qualitatively. In the language of the t - J model doping means that a certain amount of electrons have been removed, so that there are on average $1 - x$ electrons per site, while a fraction of x sites is unoccupied. It is clear that the empty sites control the dynamics of the electrons, because an electron can only hop to an adjacent site if that particular site is one of the few sites that is unoccupied. The kinetic term in the t - J Hamiltonian favors these empty sites to move around. However, the empty sites can not move around freely in a background of antiferromagnetically ordered spins, because every time an empty site changes places with an electron, it leaves behind an electron whose spin is pointing in the wrong direction. This creates a string of overturned spins, which costs a lot of energy [6]. When the system is sufficiently close to half filling, i.e. when there are very few empty sites, the antiferromagnetic order prevails, and the system remains in the Néel-ordered phase. This phase describes an insulator, because the Néel order prevents the empty sites from moving around freely.

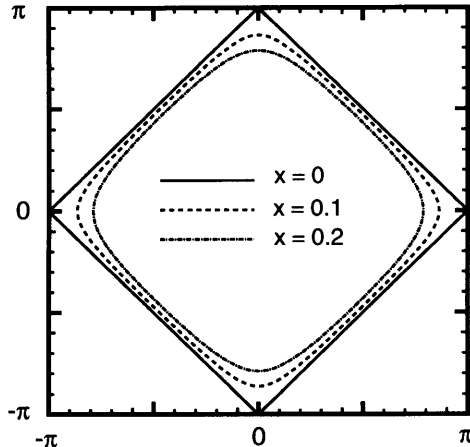


Figure 1-5: The Fermi surface of the t - J model for various values of the doping x . At half filling the Fermi surface is a diamond with sharp corners, and the density of states diverges at these corners. Note that at half filling there is perfect nesting of the Fermi surface over the wave vector $\mathbf{Q}_{\text{AF}} = (\pi, \pi)$. For larger doping the nesting properties of the Fermi surface become less and less pronounced.

Surprisingly enough this result is exactly the opposite of what one would expect from bandtheory. According to bandtheory the system should be a metal, because close to half filling there is a large Fermi surface, as is shown in Fig. 1-5. This is the usual argument to distinguish a metal from an insulator. The reason why this simple band-theory argument is not valid is due to the fact that it does not take the constraint of no double occupancy into account. This constraint played a crucial role in the arguments given above why the system is in reality an insulator close to half filling. This system, which has a Fermi surface but is still an insulator, is sometimes called a *doped Mott insulator*, emphasizing that the mechanism that is responsible for the insulating properties has nothing to do with band theory, but is more closely related to the mechanism originally proposed by Mott.

If one increases the doping above a certain value the long-range antiferromagnetic order disappears, but the system remains an insulator due to strong short-ranged antiferromagnetic correlations. If one increases the doping even further the system becomes eventually metallic, which is called the Mott-insulator transition. This is the regime we will focus on in this thesis, because this regime contains the supercon-

ducting phase at sufficiently low temperatures.

Until now our description of the physics of the t - J model has been very qualitative, emphasizing the importance of the empty sites for the transport properties. In the next section we will discuss a mathematical trick that puts these qualitative arguments on a solid basis.

1.6 Spin-charge separation

From the qualitative arguments in the previous section we learned that due to the constraint of no double occupancy the empty sites are very important for the transport properties of the t - J model. Clearly any successful analysis of the t - J model has to pay special attention to these empty sites. Fortunately there exists a mathematical trick, called the *slave-boson formalism*, which allows us to keep track of the empty sites by treating them as independent particles. These new objects are called “slave-bosons” in this formalism. Mathematically one simply replaces the original electron operator $c_{i\sigma}^\dagger$ by the product $f_{i\sigma}^\dagger b_i$, where $f_{i\sigma}^\dagger$ is a fermion operator that carries the *spin* of the electron, and b_i is a boson operator that corresponds with the empty sites, and that carries the *charge* of the electron. This leads to the Hamiltonian

$$\begin{aligned}
 H = & -t \sum_{\langle i,j \rangle \sigma} (f_{i\sigma}^\dagger b_i b_j^\dagger f_{j\sigma} + \text{c.c.}) + J \sum_{\langle i,j \rangle} (\mathbf{S}_i \cdot \mathbf{S}_j - \frac{1}{4} n_i n_j) \\
 & + \sum_i i \lambda_i (f_{i\sigma}^\dagger f_{i\sigma} + b_i^\dagger b_i - 1),
 \end{aligned} \tag{1.5}$$

where the field λ_i is a Lagrange multiplier field that one has to integrate over to enforce the local constraint that $f_{i\sigma}^\dagger f_{i\sigma} + b_i^\dagger b_i = 1$ at each site i . This constraint means that at every site there is either a fermion or a boson, but not both. The corresponding picture is shown in Fig. 1-6.

Notice that this approach leads to *spin-charge separation*, because the spin and the charge degrees of freedom of the electron are now carried by different particles, $f_{i\sigma}^\dagger$ and b_i^\dagger , which are often called “spinons” and “holons”. Spin-charge separation is a convenient concept to explain certain unusual properties of the high- T_c cuprates.

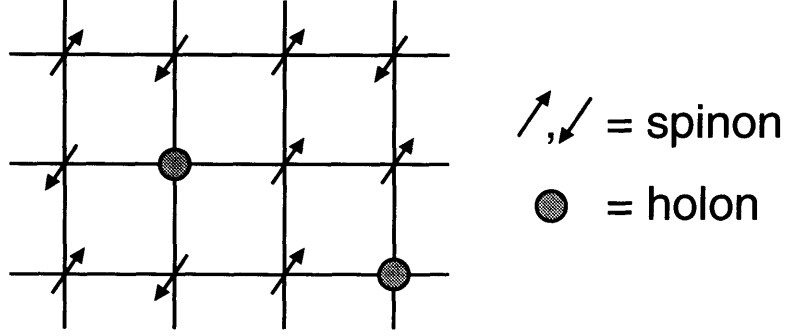


Figure 1-6: The t - J model in the slave-boson approach. The physical electrons are split into “spinons” and “holons”. On each site there is either a spinon or a holon. The spinons carry the spin degrees of freedom and the holons, which correspond to the empty sites in the original t - J model, carry the charge degrees of freedom. Close to half filling the dynamics is controlled by the holons.

For example, it can explain why experiments that probe the transport properties of the electrons, such as the conductivity or the Hall effect, indicate that there is only a small number of charge carriers, roughly proportional to the number of empty sites. This is naturally explained by noting that the holons are the charge carriers in the problem, and not the spinons. On the other hand, angular-resolved photo-emission experiments show a large Fermi surface, which is easily explained by identifying the experimental results with the Fermi surface of the spinons.

Although it is convenient to think in terms of spinons and holons, one has to keep in mind that they are mathematical objects, that can not exist outside a CuO_2 plane. To explain this we will make a few remarks about gauge invariance. The Hamiltonian in Eq. (1.5) is manifestly gauge invariant under the local gauge transformation

$$\begin{aligned} f_{j\sigma} &\longrightarrow e^{i\varphi_j} f_{j\sigma}; \\ b_j &\longrightarrow e^{i\varphi_j} b_j. \end{aligned} \tag{1.6}$$

The only observable quantities are quantities that are invariant under this local gauge transformation. Clearly the spinons and holons are objects that are not gauge invariant, and can therefore never be measured in physical experiments. On the other hand, the product $f_{i\sigma}^\dagger b_i$, which corresponds to the physical electron, remains gauge invariant. Considering that there exists a local gauge symmetry in the Hamiltonian in

Eq. (1.5), it is not surprising that a gauge field will appear in a more detailed analysis of this model. How this gauge field is introduced, and what are its properties, will be discussed in Chapters 3 and 4.

We would like to remark that one can also choose to work in the so-called *slave-fermion* formalism. In that approach the spinons are bosons with a spin index, and the holons are fermions that carry a charge but no spin. The slave-fermion approach is a good starting point at very low doping ($x \lesssim 0.04$), while the slave-boson approach is more appropriate at intermediate doping.

1.7 The phase diagram of spinons and holons

We will now explain some of the qualitative features of the phase diagram of the cuprates, using the concept of spin-charge separation. The underlying idea is to identify the various regimes that are observed in the high- T_c cuprates with the phase transitions of the spinons and the holons.

Let us discuss the different phase transitions that the spinons and the holons can undergo. The spinons obey Fermi statistics, so they will form Cooper pairs at sufficiently low temperatures, due to the antiferromagnetic spin interaction which creates an attractive interaction in the Cooper channel. This transition is indicated by the solid line in Fig. 1-7, which is a qualitative phase diagram in the doping-temperature plane. The transition temperature $T_P(x)$ decreases as a function of doping, because the antiferromagnetic interaction is strongest close to half filling. The holons on the other hand obey boson statistics, and will therefore Bose condense at low temperatures. This is indicated by the dashed line in Fig. 1-7. Note that the Bose-condensation temperature $T_{BE}(x)$ is proportional to the density of holons x .

The pairing transition line $T_P(x)$ and the Bose-condensation line $T_{BE}(x)$ divide the phase diagram in Fig. 1-7 in four regions, and each region will have a very different physical properties. We are most familiar with the regime $T < T_{BE}(x)$, because in that regime the physical electrons can be directly identified with the spinons. The reason for this is that for $T < T_{BE}(x)$ the holons are Bose condensed, and can therefore

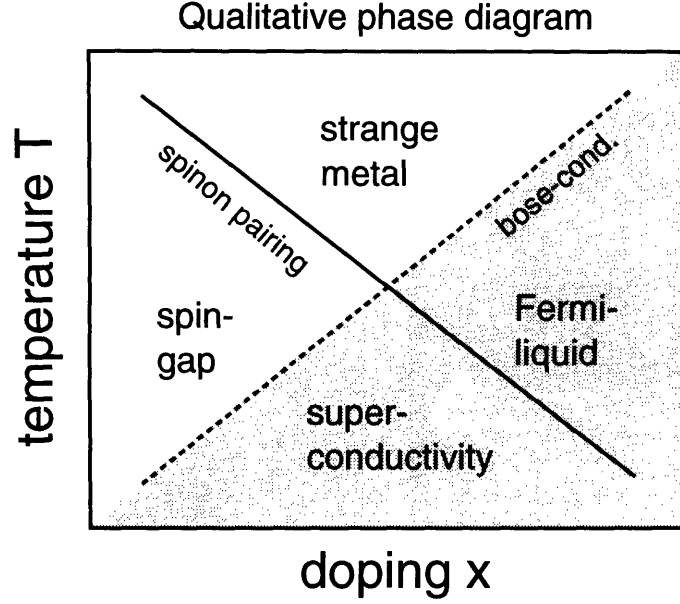


Figure 1-7: A qualitative phase diagram of the t - J model, based on spin-charge separation. The solid line is the pairing transition temperature, below which the spinons form Cooper pairs. The dashed line is the Bose-condensation temperature, below which the holons condense into a superfluid state. These two transition lines divide the phase diagram into four regimes: a Fermi-liquid phase, a superconducting phase, a strange-metal phase, and a spin-gap phase.

be treated as c -numbers instead of operators. In other words, the electron creation operator $c_{i\sigma}^\dagger = f_{i\sigma}^\dagger b_i$ can be replaced by

$$c_{i\sigma}^\dagger = f_{i\sigma}^\dagger b_i \longrightarrow \text{const.} \times f_{i\sigma}^\dagger. \quad (1.7)$$

This means that for $T < T_{\text{BE}}(x)$ the pairing transition temperature $T_P(x)$ coincides with the superconducting transition temperature $T_c(x)$ of the physical electrons. For $T > T_P(x)$ the system behaves like a normal metal, while for $T < T_P(x)$ the system behaves like a conventional superconductor.

The properties of the system are more unusual for $T > T_{\text{BE}}(x)$, i.e. when the bosons are not condensed yet. In that case we cannot simply identify the physical electrons with the spinons anymore. Instead the electrons are composite particles, made up of spinons and holons that strongly interact with each other. The spinons will not behave like a Fermi liquid anymore, because the holons provide a soft scattering

mechanism, altering the lifetime of the quasi particles. Due to the presence of low lying excitations one can expect a whole variety of unusual phenomena. This region is commonly referred to as the *strange metal* phase. An interesting consequence of the presence of non-condensed holons is that the pairing transition temperature $T_P(x)$ does not correspond with the superconducting transition anymore. This is easily understood by considering the superconducting order parameter

$$\begin{aligned}\Delta_{ij}^* &= \langle c_{i\uparrow}^\dagger c_{j\downarrow}^\dagger - c_{i\downarrow}^\dagger c_{j\uparrow}^\dagger \rangle \\ &= \langle f_{i\uparrow}^\dagger f_{j\downarrow}^\dagger - f_{i\downarrow}^\dagger f_{j\uparrow}^\dagger \rangle \langle b_i b_j \rangle.\end{aligned}\tag{1.8}$$

To obtain a finite superconducting gap Δ_{ij} it is not sufficient that $\langle f_i^\dagger f_j^\dagger \rangle$ is nonzero; the expectation value $\langle b_i \rangle$ has to be nonzero as well. This creates the interesting possibility of having a state in which the spinons form Cooper pairs, i.e. $\langle f_i^\dagger f_j^\dagger \rangle \neq 0$, while the system is not superconducting. This state has the feature that physical quantities which probe the spin degrees of freedom of the system, such as NMR relaxation rates and the Knight shift, will show a (pseudo) spin gap below a certain energy scale. This pseudo gap will not show up in the conductivity, or in other transport properties which are controlled by the holons. This very unusual phase is commonly referred to as the *spin-gap* phase.

Summarizing, the picture of spin-charge separation leads to the following four phases:

1. Normal metal: $T < T_{BE}(x)$ and $T > T_P(x)$;
2. Superconductor: $T < T_{BE}(x)$ and $T < T_P(x)$;
3. Strange metal: $T > T_{BE}(x)$ and $T > T_P(x)$;
4. Spin-gap phase: $T > T_{BE}(x)$ and $T < T_P(x)$.

These four phases are indeed observed in experimental studies of the high- T_c cuprates. The spin-gap phase is somewhat controversial, because it is only observed in multi-layer cuprates such as YBCO, but not in single-layer materials such as LaSrCuO.

We will explain in Chapter 4 why the spin-gap phase is not observed in single-layer materials. In Chapter 5 we present a model that shows that the spin-gap phase in multi-layer materials can be explained by the formation of Cooper pairs of spinons on nearby CuO_2 planes.

1.8 Outline of this thesis

The goal of this thesis is to explain the superconducting phase diagram of the high- T_c cuprates, using a microscopic model based on the t - J Hamiltonian. As explained in Sec. 1.7, this essentially boils down to determining the pairing transition temperature $T_c(x)$ of the spinons, and the Bose-condensation temperature T_{BE} of the holons. Determining these two transition lines is the central theme of this thesis. Each of the next four chapters deals with a different piece of this puzzle. In the final two chapters we are able to put all these pieces together, to obtain a theoretical phase diagram that agrees very well with the experimental phase diagram.

In Chapter 2 we start by analyzing the t - J model in the mean-field approximation [7], which is a logical starting point to obtain a qualitative understanding of the model. Within this approximation it is relatively straightforward to obtain the transition temperatures $T_P^0(x)$ and T_{BE}^0 . A drawback of the mean-field approximation is that $T_P^0(x)$ and T_{BE}^0 are much higher than the actual transition temperatures measured in experiments. This shows that the mean-field approximation is an over-simplification, which does not fully capture the physics of the high- T_c cuprates. The reason for this is that there is a very strong interaction between the spinons and the holons, because every time a spinon hops from one site to the next, a holon has to hop in the opposite direction. This feature, which is due to the local constraint of no double occupancy, is completely missed in the mean-field approximation.

In Chapter 3 and 4 we go beyond the mean-field approximation, by including a gauge field in the analysis, which takes Gaussian fluctuations around the mean-field result into account. The role of the gauge field is to mediate the strong interactions between the spinons and the holons. The picture that we have in mind is that one

can view the t - J model as a system of spinons and holons, that continuously scatter off a fluctuating gauge field. This gauge field is massless, and therefore creates a soft scattering mechanism for the spinons and the holons, which will significantly alter the properties of these particles.

Chapter 3 deals with the question of how the gauge field influences the behavior of the holons [8, 9]. We show that for the relevant parameters of the t - J model this is a strongly correlated problem, which cannot be treated with the standard perturbative methods. Instead we express the partition function in terms of closed Feynman paths, which turns out to be a very convenient method in the strong-coupling limit. In the strong-coupling limit the gauge field destroys the phase coherence of the holons, thereby suppressing the tendency of the holons to condense. The signature of this is that the diamagnetic susceptibility is strongly suppressed, and diverges at a much lower temperature than before. This temperature can be identified with the Bose-condensation temperature of the holons.

Chapter 4 focuses on the effect that the gauge field has on the pairing of the spinons [10]. The gauge field is strongly pair-breaking, because it acts as a large fluctuating magnetic field. Using the analogy with a magnetic field, it is not surprising that the gauge field suppresses the formation of Cooper pairs. The phase diagram that we obtain after taking the pair-breaking effects of the gauge field into account agrees very well with the experimental phase diagram of single-layer materials such as $\text{La}_{2-x}\text{Sr}_x\text{CuO}_4$. One of the most important conclusions of this analysis is that the fluctuating gauge field completely destroys the spin-gap phase. This agrees with the experimental evidence that there is no spin-gap phase in $\text{La}_{2-x}\text{Sr}_x\text{CuO}_4$.

In Chapter 5 we study a model for two coupled CuO_2 planes, in order to explain the different behavior of single-layer cuprates and multi-layer cuprates [12]. Measurements of the NMR relaxation rate and the Knight shift, which are quantities that probe the spin degrees of freedom of the material, indicate that multi-layer cuprates such as YBCO have a spin-gap in their excitation spectrum. The main objective of Chapter 5 is to present a microscopic model that is able to explain why this spin gap exists in underdoped $\text{YBa}_2\text{Cu}_3\text{O}_{6.6}$, but not in $\text{La}_{2-x}\text{Sr}_x\text{CuO}_4$. We propose that the

spin gap is due to pairing between spinons on adjacent CuO_2 planes, which is significantly enhanced by the antiferromagnetic correlations between spins on adjacent CuO_2 planes. Using this model we are able to calculate the NMR relaxation rates on the ^{63}Cu and the ^{17}O sites, the Knight shift and the spin-echo decay rate as a function of temperature. Our numerical results are in good agreement with the experimental data on $\text{YBa}_2\text{Cu}_3\text{O}_{6.6}$.

Chapters 2-5 were originally written as four separate articles, which over the last few years have been submitted to *Physical Review B* [7, 9, 10, 12]. Each chapter is self-contained, and can be read separately from the rest of the thesis.

Chapter 2

Flux phases in the t - J model

2.1 Introduction

Since the discovery of the copper oxide superconductors there is a renewed interest in strongly correlated electronic systems. The t - J model is one of the proposed models that might describe the essential physics of those materials [13].

Several schemes have been used to develop a mean-field theory for the t - J model, and many phases have been suggested to be energetically favorable away from half filling.

Generally a mean-field theory arises from decoupling the Hamiltonian either in the particle-hole channel ($f_i^\dagger f_j^\dagger \rightarrow \langle f_i^\dagger f_j^\dagger \rangle$) or in the particle-particle channel ($f_i^\dagger f_j \rightarrow \langle f_i^\dagger f_j \rangle$).

The early mean-field theories assumed a uniform (or s -wave) pairing state [13, 14, 15]. Kotliar and Liu however showed that a d -wave-pairing state has a higher pairing-gap transition temperature, and is energetically favored over an s -wave-pairing state [16, 17]. Affleck and Marston took a different approach by enlarging the unit cell for the particle-hole order parameter $\langle f_{i\sigma}^\dagger f_{i\sigma} \rangle$, while ignoring particle-particle correlations. They found that for low doping a lower ground-state energy is achieved by taking a π -flux phase for the particle-hole order parameter. [18, 19]. At half filling this phase is equivalent to the $s + id$ phase of Kotliar [16], due to a local gauge invariance at half filling [20]. A similar $s + id$ phase was also considered by Ye and Sachdev, in

their recent study of a 3-band model [21]. Other states that occur at low doping are dimerized states [18, 19, 22, 23] and commensurate-flux phases [24, 25, 26]. However, away from half-filling both the dimerized states and the commensurate flux phases are only stable for small values of t/J ($t/J \lesssim 1$).

A generalization of π -flux phase was proposed by Zhang [27], who combined the d -wave-pairing state with a staggered-flux phase for the particle-hole order parameter.

The aim of this paper is to see how these different phases fit together at finite temperatures. Most of the numerical work so far has dealt with the zero temperature ground state [28, 29]. In particular, we would like to know how the π -flux phase is connected to the uniform phase and the d -wave-pairing state. We will focus on a temperature range in the vicinity of the pairing-gap transition temperature. We compare the free energies of a class of phases that includes Zhang's staggered-flux phases and Kotliar's mixed phase. However, we exclude dimerized phases and commensurate flux phases, which is motivated by the numerical work cited above, that away from half-filling these phases are only feasible for $t/J \lesssim 1$. The experimental values of t and J for copper oxides give $t/J \sim 3$.

We find numerically that for $\delta \lesssim 0.08J/t$, a staggered-flux phase is favored over the d -wave-pairing state close to the pairing-gap transition temperature. We present a phase diagram that shows how at finite temperatures the staggered-flux phase interpolates in between a π -flux phase and the uniform phase. The occurrence of flux phases strongly suppresses the pairing-gap transition temperature.

In Appendix A we discuss a recipe that describes how to decouple the t - J model into its different channels, using Hubbard-Stratonovich fields.

2.2 Hartree-Fock-Bogoliubov decomposition

We use the slave-boson formalism and write the t - J model as [17]

$$H = -t \sum_{\langle i,j \rangle} (f_{i\sigma}^\dagger f_{j\sigma} b_j^\dagger b_i + c.c.) + J \sum_{\langle i,j \rangle} (\mathbf{S}_i \cdot \mathbf{S}_j - \frac{1}{4} n_i n_j)$$

$$-\mu_0 \sum_i f_{i\sigma}^\dagger f_{i\sigma} + i \sum_i \lambda_i (f_{i\sigma}^\dagger f_{i\sigma} + b_i^\dagger b_i - 1), \quad (2.1)$$

where $\mathbf{S}_i = \frac{1}{2} f_{i\alpha}^\dagger \boldsymbol{\sigma}_{\alpha\beta} f_{j\beta}$. The corresponding quantum partition function, $Z = \int \mathcal{D}[f, b, \lambda] \exp(-S)$, is a functional integral over a fermion field $f_{i\sigma}$, a bosonic field b_i to keep track of the empty sites, and a real field λ_i to enforce the local constraint $f_{i\sigma}^\dagger f_{i\sigma} + b_i^\dagger b_i = 1$ at each site i .

The usual way to derive a mean-field theory for the Hamiltonian (2.1) is by decoupling the Hamiltonian either in the particle-hole channel or the particle-particle channel. This leads to mean-field order parameters $\chi_{ij} = \langle f_{i\sigma}^\dagger f_{j\sigma} \rangle$ or $\Delta_{ij} = \langle f_{i\uparrow} f_{j\downarrow} - f_{i\downarrow} f_{j\uparrow} \rangle$. There is however a significant amount of freedom in choosing combinations of both order parameters. The SU(2) symmetry of the Hamiltonian at half filling suggests to treat both order parameters on the same footing [17, 20].

In Appendix A we discuss a recipe how to decouple the four-fermion term $\mathbf{S}_i \cdot \mathbf{S}_j$ into a combination of different channels, using 3 sets of Hubbard-Stratonovich fields. This leads to the following identity:

$$e^{-J \sum_{\langle i,j \rangle} \mathbf{S}_i \cdot \mathbf{S}_j} \propto \int \prod_{\langle i,j \rangle} d\chi_{ji}^* d\chi_{ji} d\Delta_{ji}^* d\Delta_{ji} \prod_i \prod_{k=1}^3 d\rho_i^k e^{-\sum_{\langle i,j \rangle} \mathcal{A}_{ji}(\chi, \Delta, \rho)}, \quad (2.2)$$

$$\begin{aligned} \mathcal{A}_{ji} = & \frac{3J}{8} \left[|\chi_{ji}|^2 + |\Delta_{ji}|^2 - \chi_{ji}^* (f_{j\sigma}^\dagger f_{i\sigma}) - c.c. + n_i \right. \\ & \left. - \Delta_{ji}^* (f_{j\uparrow} f_{i\downarrow} - f_{j\downarrow} f_{i\uparrow}) - c.c. \right] \\ & + \frac{J}{2} \left[|\rho_i|^2 - \sum_{k=1}^3 \rho_i^k (f_j^\dagger \sigma^k f_j) \right]. \end{aligned} \quad (2.3)$$

The hopping term $t \sum f_{i\sigma}^\dagger f_{j\sigma} b_j^\dagger b_i$ can be taken into account by replacing $\chi_{ji}^* (f_{j\sigma}^\dagger f_{i\sigma})$ by $\chi_{ji}^* (f_{j\sigma}^\dagger f_{i\sigma} + \frac{8t}{3J} b_j^\dagger b_i)$. In addition to the hopping term this modification also leads to four-boson terms of the form $b_i^\dagger b_j b_j^\dagger b_i$. In principle one needs an additional auxiliary field to decouple these terms. However, these four-boson terms give only a small contribution close to half filling, and at the mean-field level we can replace these terms by $\langle b_i^\dagger b_i \rangle b_j b_j^\dagger$, and incorporate them into the bosonic chemical potential term.

Putting everything together the decoupled Hamiltonian now becomes

$$\begin{aligned}
H = & \frac{3J}{8} \sum_{\langle i,j \rangle} \left[|\chi_{ji}|^2 + |\Delta_{ji}|^2 - \chi_{ji}^* (f_{j\sigma}^\dagger f_{i\sigma} + \frac{8t}{3J} b_j^\dagger b_i) - c.c. + n_i \right. \\
& \left. - \Delta_{ji}^* (f_{j\uparrow} f_{i\downarrow} - f_{j\downarrow} f_{i\uparrow}) - c.c. \right] + \frac{J}{2} \sum_{\langle i,j \rangle} \left[|\boldsymbol{\rho}_i|^2 - \sum_{k=1}^3 \rho_i^k (f_j^\dagger \sigma^k f_j) \right] \quad (2.4) \\
& - \mu_0 \sum_i f_{i\sigma}^\dagger f_{i\sigma} - i \sum_i \lambda_i (f_{i\sigma}^\dagger f_{i\sigma} + b_i^\dagger b_i - 1).
\end{aligned}$$

A mean-field theory is achieved by replacing the fields χ_{ij} , Δ_{ij} , $\boldsymbol{\rho}_i$ and λ_i by their saddlepoint values. We put $\boldsymbol{\rho}_i^{\text{MF}} = \langle \mathbf{S}_i \rangle = 0$. The field $i\lambda_i^{\text{MF}}$ will be interpreted as the chemical potential μ_b of the bosons. The effective chemical potential of the fermions is $\mu_f \equiv \mu_0 + \mu_b - 3J/4$. Our final result for H^{MF} is identical to the mean-field Hamiltonian used by Kotliar and Liu [17], except for the way we incorporated the hopping term into the order parameter χ_{ij} .

2.3 Flux phases

Several forms of χ_{ij} and Δ_{ij} have been suggested to give a minimum of the free energy. The simplest phases are the uniform phase ($\chi_{ij} = \chi$, $\Delta_{ij} = \Delta$ for all bonds $\langle i, j \rangle$) and the d -wave phase ($\chi_{ij} = \chi$, $\Delta_{ij} = \pm\Delta$, + if $\mathbf{ij} \parallel \hat{x}$, - if $\mathbf{ij} \parallel \hat{y}$) [16, 17]. Other suggested phases are mixed phases [16, 22], dimerized phases [18, 19, 22, 23] and several flux phases [18, 19, 24, 25, 26, 27].

Excluding dimerized phases, we parametrize χ_{ij} and Δ_{ij} by

$$\chi_{ij} = \chi e^{i\theta_{ij}}, \quad \Delta_{ij} = \Delta e^{i\tau_{ij}} \quad (2.5)$$

$$(\theta_{ij} = -\theta_{ji}, \tau_{ij} = \tau_{ji}).$$

We are interested in studying a class of phases, that satisfies the following criteria:

- (a) the class should include Zhang's staggered flux phases and Kotliar's mixed phases;
- (b) χ_{ij} and Δ_{ij} should be treated on the same footing.

Before discussing a simple class of phases that satisfies these criteria, it is important to note that many choices of χ_{ij} and Δ_{ij} are equivalent, due to the local gauge

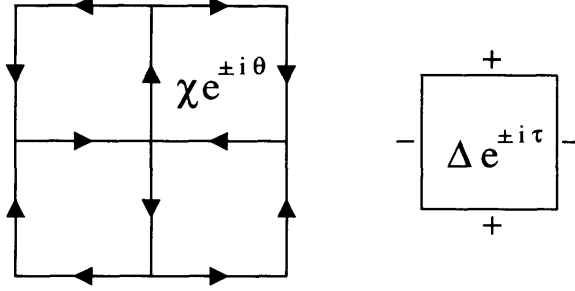


Figure 2-1: We doubled the unit cell for χ_{ij} , to allow the possibility of a flux around a plaquette. χ_{ij} is given a phase $\pm\theta$, depending on whether \mathbf{ij} goes along or against the arrow on the bond. Modulo gauge transformations, this is the most general parametrization of $\chi e^{\theta_{ij}}$ with a double unit cell. Δ_{ij} is given a phase $\pm\tau$, depending on whether the bond $\langle i, j \rangle$ is in the \hat{x} or the \hat{y} direction. As a result χ_{ij} has a staggered-flux of 4θ , and Δ_{ij} has a “flux” of 4τ .

transformation $f_{i\sigma}^\dagger \rightarrow f_{i\sigma}^\dagger e^{i\varphi_i}$, $\chi_{ij} \rightarrow \chi_{ij} e^{i\varphi_i - i\varphi_j}$ and $\Delta_{ij} \rightarrow \Delta_{ij} e^{i\varphi_i + i\varphi_j}$. The only gauge invariant property of χ_{ij} is its flux through a plaquette (i.e., $\theta_{ij} + \theta_{jk} + \theta_{kl} + \theta_{li}$) [18, 19]. The simplest way to allow the possibility of a nonzero flux is to double the unit cell for χ_{ij} . The most general parametrization of χ_{ij} with a double unit cell, modulo gauge transformations, is

$$\chi_{ij} = \chi e^{\pm i\theta} \quad (\pm \text{ if } \mathbf{ij} \text{ along or against arrow}) \quad (2.6)$$

(see Fig. 2-1). This is the same parametrization of χ_{ij} as used by Zhang [27].

Similarly, the only gauge invariant quantity for Δ_{ij} is the “flux” per plaquette $\tau_{ij} - \tau_{jk} + \tau_{kl} - \tau_{li}$. A single unit cell is sufficient to give Δ_{ij} a nonzero “flux”. This leads to the parametrization:

$$\Delta_{ij} = \Delta e^{\pm i\tau} \quad (+ \text{ if } \mathbf{ij} \parallel \hat{x}, - \text{ if } \mathbf{ij} \parallel \hat{y}). \quad (2.7)$$

This choice of Δ_{ij} ensures that our class of phases includes Kotliar’s mixed phases, and that χ_{ij} and Δ_{ij} are treated on the same footing. Note that χ_{ij} has a staggered-flux of 4θ around each plaquette, while Δ_{ij} has a “flux” of 4τ .

By going to Fourier space, and using a Bogoliubov transformation, H^{MF} can be

brought to the diagonal form (see Appendix B, cf. [27])

$$\frac{1}{J'} H^{\text{MF}} = N(\chi^2 + \Delta^2) + \sum_{k,s=\pm 1}' E_{ks}(\alpha_{ks}^\dagger \alpha_{ks} - \beta_{ks} \beta_{ks}^\dagger) + \sum_{k,s=\pm 1}' \Omega_{ks} \tau_{ks}^\dagger \tau_{ks} \quad (2.8)$$

where α_{ks} and β_{ks} are fermion fields, and τ_{ks} is a bosonic field. \sum_k' denotes a sum over half of the Brioullin zone and $J' \equiv 3/4J$ sets the energy scale. In units of J' the eigenvalues E_{ks} and Ω_{ks} are

$$\begin{aligned} E_{ks} &= \sqrt{(-\mu_f + s\chi\xi_k)^2 + \Delta^2\psi_k^2}, \\ \Omega_{ks} &= -\mu_b - 2st\chi\xi_k, \end{aligned} \quad (2.9)$$

where we defined

$$\begin{aligned} \xi_k &= \sqrt{\gamma_k^2 \cos^2 \theta + \varphi_k^2 \sin^2 \theta}, \\ \psi_k &= \sqrt{\gamma_k^2 \cos^2 \tau + \varphi_k^2 \sin^2 \tau} \end{aligned} \quad (2.10)$$

($\gamma_k = \cos k_x + \cos k_y$ and $\varphi_k = \cos k_x - \cos k_y$).

It is nice to check from the energyspectrum (2.9) that at half filling (i.e., $\mu_f = 0$) the order parameters χ and Δ are indeed treated equivalently.

For a given temperature T and doping $\delta = 1 - \sum f_{i\sigma}^\dagger f_{i\sigma} = \sum b_i^\dagger b_i$, the phase will be favored that gives the lowest free energy

$$\begin{aligned} F &= -2T \sum_{ks}' \ln \cosh(\beta E_{ks}/2) + T \sum_{ks}' \ln(1 - e^{-\beta \Omega_{ks}}) \\ &\quad - N\delta(\mu_f - \mu_b) + N(\chi^2 + \Delta^2). \end{aligned} \quad (2.11)$$

2.4 Phase diagram

Numerical analysis shows that the lowest free energy is generally given by $\tau = \pi/2$, except for very high doping ($\delta \gtrsim 0.5$). In the vicinity of $\delta \sim 0.5$ and at sufficiently low temperatures τ continuously rotates from $\tau = \pi/2$ (i.e., d -wave-pairing) to $\tau = 0$ (i.e., s -wave-pairing) (see Fig. 2-2).

Physically a doping $\delta \gtrsim 0.5$ is not of very much interest, so from now on we will only consider $\tau = \pi/2$ which corresponds to a d -wave symmetry for Δ_{ij} .

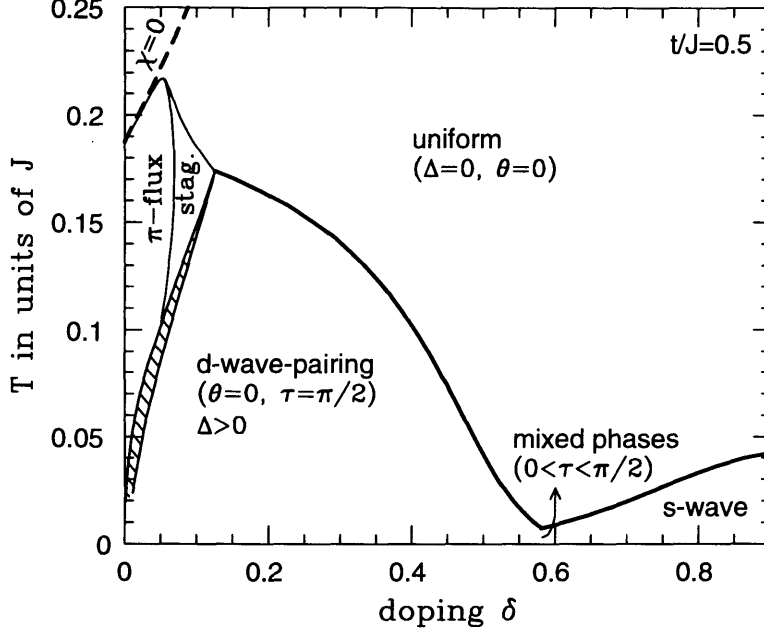


Figure 2-2: Global phase diagram for $t/J = 0.5$. Below the thick solid line a pairing gap Δ opens. For $\delta \lesssim 0.6$ this gap has a d -wave symmetry ($\tau = \pi/2$), but for $\delta \gtrsim 0.6$ it has an s -wave symmetry ($\tau = 0$). In between, at $\delta \sim 0.6$, we have mixed phases, where τ rotates continuously from $\tau = \pi/2$ to $\tau = 0$. Closer to half filling, for $\delta \lesssim 0.12$, staggered-flux phases become favorable. See Fig. 2-3 for a more detailed phase diagram.

Minimizing F with respect to χ , Δ and θ one obtains the self-consistency equations

$$\begin{aligned}
 \chi &= \frac{1}{2N} \sum'_{ks} s \xi_k \left[\frac{\epsilon_{ks}}{E_{ks}} \tanh(\beta E_{ks}/2) + \frac{2t}{e^{\beta \Omega_{ks}} - 1} \right], \\
 \Delta &= \frac{\Delta}{2N} \sum'_{ks} \frac{\varphi_k^2}{E_{ks}} \tanh(\beta E_{ks}/2), \\
 0 &= \frac{\chi \sin 2\theta}{N} \sum'_{ks} \frac{\gamma_k^2 - \varphi_k^2}{s \xi_k} \left[\frac{\epsilon_{ks}}{E_{ks}} \tanh(\beta E_{ks}/2) + \frac{2t}{e^{\beta \Omega_{ks}} - 1} \right]
 \end{aligned} \tag{2.12}$$

($\epsilon_{ks} = -\mu_f + s\chi\xi_k$). The chemical potentials μ_f and μ_b are determined by $\delta = \frac{1}{N} \sum' \epsilon/E \tanh(\beta E/2) = \frac{1}{N} \sum' (e^{\beta \Omega} - 1)^{-1}$. Without the bosonic terms it is straightforward to show that the above equations cannot hold simultaneously if both $\Delta \neq 0$ and $\sin 2\theta \neq 0$ (see Zhang [27]). However, due to the presence of the bosonic terms this is not necessarily true anymore.

Fig. 2-3 shows the phase diagram in the (δ, T) plane for $t/J = 0.5$. The different phases were found numerically by first minimizing the free energy directly with re-

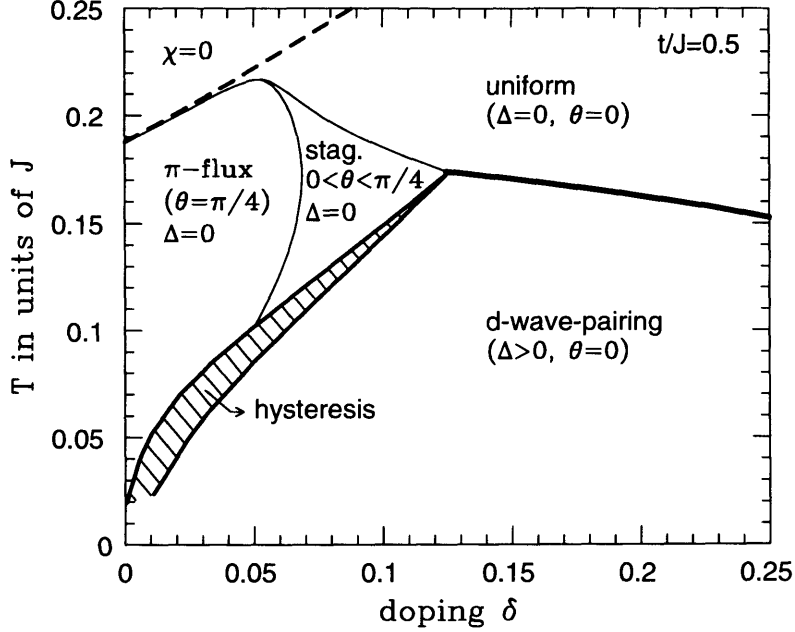


Figure 2-3: Phase diagram for $t/J = 0.5$. Below the thick solid line the d -wave-pairing state is stable. However, for $\delta \lesssim 0.12$ (left of the shaded area) staggered-flux phases become energetically favorable. For $\delta \lesssim 0.06$ a π -flux phase becomes stable. The shaded area represents the hysteresis of a first-order transition between the d -wave-pairing state and the flux-phase region.

spect to χ , Δ and θ , and then using the self-consistency equations to find the phase boundaries more accurately.

For $\delta \gtrsim 0.12$ the standard d -wave-pairing state (i.e., $\theta = 0$ and $\Delta > 0$) is favored at sufficiently low temperatures. But for lower doping (staggered) flux phases with $\theta \neq 0$ and $\Delta = 0$ are favored over the d -wave-pairing state, which leads to a suppression of the temperature below which a pairing gap opens.

The staggered-flux phase region has the shape of a triangle, which at intermediate temperatures extends from $\delta \sim 0.06$ to $\delta \sim 0.12$. If one decreases δ in this region, θ rotates continuously from 0 to $\pi/4$. Below $\delta \sim 0.06$ a π -flux phase with $\theta = \pi/4$ becomes stable. This π -flux phase has a flux of exactly π around each plaquette, and was previously considered by Affleck and Marston [18, 19].

If one decreases the temperature there is a first-order transition from the (staggered) flux-phase region (with $\theta > 0$ and $\Delta = 0$) to the d -wave region (with $\theta = 0$ and $\Delta > 0$). Characteristic for a first-order transition one observes hysteresis in a

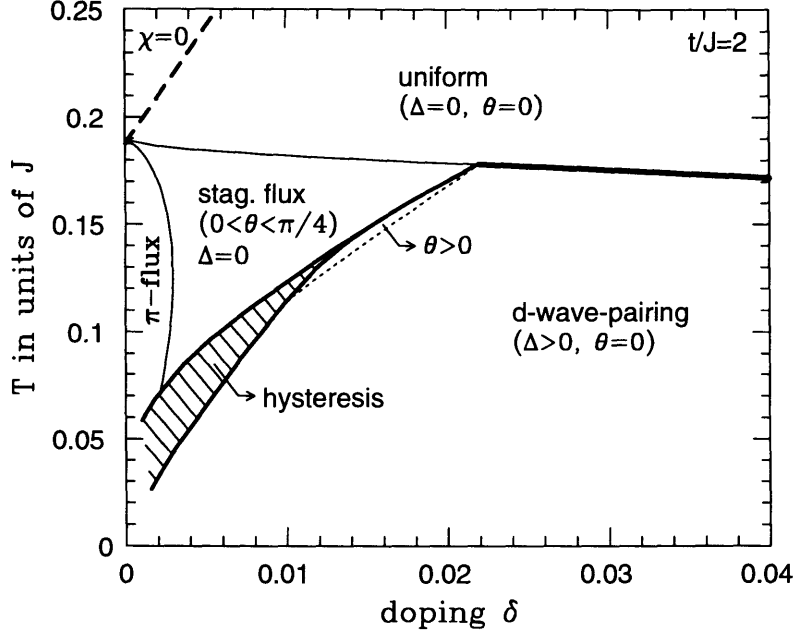


Figure 2-4: Phase diagram for $t/J = 2$. Comparison with the phase diagram for $t/J = 0.5$ shows that for larger values of t/J the whole phase diagram gets pushed towards lower values of δ . The staggered-flux phase region still extends to $\delta \sim 0.02$, but the π -flux region is only stable for $\delta \lesssim 0.002$. Note that the shaded area, which represents a first-order transition, ends at $(\delta, T) = (0.02, 0.18)$. For $\delta > 0.02$ there is a continuous transition from the d -wave-pairing state to the flux-phase region. The dotted line represents the threshold, at which θ is rotated all the way to 0.

small wedge around the transition line. Within this wedge one can in principle find a solution of the self-consistency equations with both $\theta > 0$ and $\Delta > 0$, but this solution does not correspond to a local minimum of the free energy.

For higher values of the hopping parameter t the entire phase diagram is pushed to lower values of δ (see Fig. 2-4 for $t/J = 2$). While the staggered-flux phase region still extends to an appreciable value of $\delta \lesssim 0.02$, the π -flux phase is only stable for very small doping ($\delta \lesssim 0.002$). This is consistent with the observations of Affleck and Marston that for $t/J \gtrsim 1$ the flux phase does not exist away from half filling [18, 19].

Furthermore note that, in contrast to Fig. 2-3, the first-order transition line between the staggered-flux phase and the d -wave-pairing phase does not extend all the way to the d -wave transition line anymore. Instead, Fig. 2-4 shows a small strip where a continuous rotation takes place from $\theta = \text{finite}$ to $\theta = 0$, while Δ increases continuously from 0 to its d -wave-pairing value.

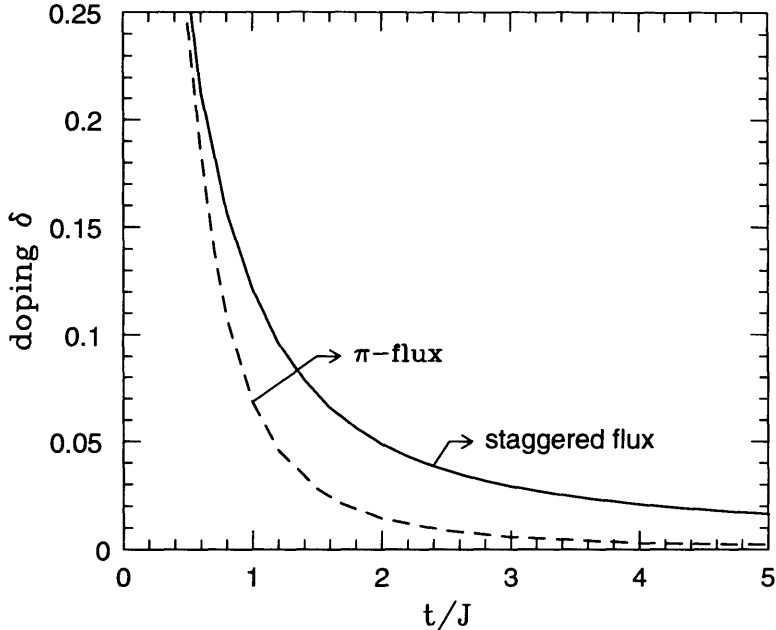


Figure 2-5: Onset of the flux phases. The solid line represents the maximum doping δ_{c1} to which the staggered-flux phase region extends. Note that δ_{c1} decreases inversely proportional with t/J : $\delta_{c1} \sim 0.08J/t$. The dashed line represents the maximum doping δ_{c2} at which the π -flux phase becomes unstable. Remark that δ_{c2} decreases much more rapidly than δ_{c1} .

Fig. 2-5 shows how far the staggered-flux phase region and the π -flux-phase region extend as a function of t/J . More specifically, the solid line shows the value of δ_{c1} at which the d -wave-pairing state becomes unstable against a staggered-flux phase in the limit of $\Delta \rightarrow 0$. One sees that δ_{c1} decreases quite slowly with t/J : $\delta_{c1} \sim 0.08J/t$. In contrast, the π -flux phase loses its stability much more rapidly (dashed line).

2.5 Conclusions

We showed that at finite temperatures the π -flux phase, which is stable at low doping, is connected to the uniform phase via a staggered-flux phase region. In this region the flux per plaquette decreases continuously from π to 0 if one increases the doping δ . A first-order transition line separates the staggered-flux phase from the d -wave-pairing state, which is more stable at lower temperatures. This pairing-gap transition line drops to $T = 0$ for $\delta \rightarrow 0$, hence even at the mean-field level the pairing-gap transition

temperature vanishes at half filling.

Acknowledgements

This work was done in collaboration with Patrick A. Lee [7]. The work was supported by the NSF through the Material Research Laboratory under Grant No. DMR-90-22933.

Chapter 3

Path-integral analysis of bosons interacting with a gauge field

3.1 Introduction

The discovery of the high- T_c cuprates has brought a renewed interest in strongly-correlated systems in two dimensions. It has been suggested that the cuprates are examples of so-called doped Mott insulators. The physics of a Mott insulator is that while according to band theory it appears to be metal with a Fermi surface, it still remains an insulator due to the fact that electrons cannot move without creating a double occupied site. Upon doping the transport properties are controlled by the few empty sites in the system. The simplest models that are believed to capture this physics are the Hubbard model and the t - J model [13, 15], and both models have been studied extensively. Because of the importance of the empty sites for the transport properties, it is convenient to consider these empty sites as fictitious particles called “holons”, that can hop around on the lattice by changing places with fermions. For the t - J model one can show that this picture naturally leads to an effective theory of fermions and bosons interacting with a fluctuating gauge field [23, 31, 32, 33, 34, 35, 36, 37].

The fermionic part of this effective action is reasonably well understood. The gauge field acts as a fluctuating electromagnetic field, and provides a soft scattering

mechanism for the fermions. The remaining degrees of freedom, the bosons interacting with a gauge field, are not as well understood. In the absence of the gauge field the bosons would condense into a superfluid state at a transition temperature $T_{\text{BE}}^0 \simeq 4\pi n_B t$, which is a very high temperature at any finite doping n of interest. One expects that a fluctuating gauge field tends to destroy the phase coherence of the bosons, and thereby suppress the Bose-condensation temperature to a much lower temperature $T_{\text{BE}} \ll T_{\text{BE}}^0$. It has been proposed that this Bose-condensation temperature appears in the phase diagram of the high- T_c cuprates as the transition line that separates the superconducting phase from the spin-gap phase [34, 35]. Another importance of the Bose-condensation temperature is that for $T \gtrsim T_{\text{BE}}$ the fluctuating gauge field destroys superconducting order parameter, so that at low doping the superconducting transition is controlled by T_{BE} [10].

Several attempts have been made to analyze this suppression of the Bose-condensation temperature T_{BE} . Diagrammatic techniques are complicated by the well-known fact that all diagrams with an internal gauge field line diverge [38], although these divergences should disappear if the object that one calculates is a gauge-invariant physical quantity [35]. Ioffe and Kalmeyer for example showed in a high-temperature calculation of the diamagnetic susceptibility that all divergences cancel each other to fourth order in perturbation theory [39]. They showed that the gauge-field corrections lower the susceptibility, which is an indication for the suppression of Bose condensation by the gauge field. Unfortunately their perturbative results become unreliable when T approaches T_{BE} [39]. A somewhat similar approach was taken by Kuboki [40], who calculated the suppression of Bose condensation by including the lowest-order gauge-field correction self-consistently in the total free energy. Higher order gauge-field corrections can be included by means of a perturbative renormalization-group analysis of the gauge field model [8]. The problem of these perturbative approaches is that it is inherently a perturbation around the weak-coupling limit $t \ll J$, while in reality we are more interested in the strong-coupling limit $t \gtrsim J$.

A completely different approach was taken by Wheatley *et al.* They used a path-integral formulation of the gauge field model, and showed that after averaging over

the gauge field one effectively generates a long-range retarded self interaction in the boson action [41, 42, 43]. To analyze this model they made the drastic approximation of replacing this complicated retarded interaction by a much simpler dissipative term. This simplified model could be solved exactly.

We will follow this path-integral approach in this paper, without making the drastic approximation mentioned above. We will argue that thanks to the interaction with the gauge field the path integral will be dominated by almost self-retracing paths [35, 36]. By focusing on these special paths we are able to evaluate the partition function, find an expression for the density of states, and calculate the diamagnetic susceptibility. We would like to emphasize that in contrast to the perturbative methods mentioned above that are only appropriate in the weak-coupling limit, this path-integral approach takes the strong-coupling limit as its starting point.

3.2 The gauge-field model

In this section we would like to show how an effective action of bosons interacting with a gauge field can be derived from the t - J model. This is a standard derivation, and we refer to other articles for a more lengthy discussion of this derivation [23, 31, 32, 33, 34, 35].

The original t - J model is a system of electrons on a square lattice. Close to half filling the transport properties are controlled by the empty sites, due to the constraint that no site can be double occupied. Our goal is therefore to derive an effective theory, that has the *empty* sites as its degrees of freedom. This can be achieved using the slave-boson approach in which one keeps track of the empty sites by putting a fictitious boson on every empty site. The local constraint is then satisfied by requiring that on every site there is exactly one particle, either a fermion or a boson. This leads to the Hamiltonian

$$\mathcal{H} = -t \sum_{\langle i,j \rangle \sigma} (f_{i\sigma}^\dagger b_i b_j^\dagger f_{j\sigma} + \text{c.c.}) + J \sum_{\langle i,j \rangle} (\mathbf{S}_i \cdot \mathbf{S}_j - \frac{1}{4} n_i n_j)$$

$$+ \sum_i i\lambda_i (f_{i\sigma}^\dagger f_{i\sigma} + b_i^\dagger b_i - 1), \quad (3.1)$$

where $\mathbf{S}_i = \frac{1}{2} f_{i\alpha}^\dagger \sigma_{\alpha\beta} f_{j\beta}$ and $n_i = \sum_\sigma f_{i\sigma}^\dagger f_{i\sigma}$. The field λ_i is a Lagrange-multiplier field, that enforces the local constraint $b_i^\dagger b_i + f_{i\sigma}^\dagger f_{i\sigma} = 1$. The fermion operator $f_{i\sigma}^\dagger$ carries the spin of the original electron, while the boson b_i carries the charge [7, 15, 17].

The hopping term and the spin-spin interaction term can be decoupled using a Hubbard-Stratonovich transformation. At the mean-field level the Hubbard-Stratonovich field, that we denote by ξ_{ij} , is equal to $\xi_{ij} = \langle f_{i\sigma}^\dagger f_{j\sigma} + 8t/3J b_i^\dagger b_j \rangle$ [7]. One obtains the gauge-field model from Eq. (3.1) if one takes phase fluctuations of the field ξ_{ij} into account, by writing $\xi_{ij} = \xi e^{ia_{ij}}$. The field a_{ij} is a gauge field, because the Hamiltonian (3.1) is invariant under the local gauge transformation [23]

$$\begin{aligned} f_{i\sigma} &\longrightarrow f_{i\sigma} e^{i\theta_i} \\ b_i &\longrightarrow b_i e^{i\theta_i} \\ a_{ij} &\longrightarrow a_{ij} + \theta_i - \theta_j \end{aligned} \quad (3.2)$$

The field λ_i can be considered as the time component of the gauge field, but we will ignore this field from now on.

We finally obtain an effective action for the bosons interacting with the gauge field, by integrating over the fermionic degrees of freedom. This leads to the effective action

$$\begin{aligned} S = & \int_0^\beta d\tau \int d^2r \left[-t\xi b^\dagger (\nabla_r + i\mathbf{a})^2 b + b^\dagger \left(\frac{\partial}{\partial \tau} - \mu_B \right) b + \frac{16t^2}{3J} (b^\dagger b)^2 \right] \\ & + \frac{T}{2} \sum_{i\nu_n} \int \frac{d^2q}{(2\pi)^2} \Pi_{\alpha\beta}(q, i\nu_n) a_q^\alpha a_{-q}^\beta. \end{aligned} \quad (3.3)$$

We will chose to work in the Coulomb gauge $\nabla \cdot \mathbf{a} = 0$, in which case the gauge-field propagator is purely transverse, $\Pi_F^{\alpha\beta}(\mathbf{q}, i\nu_n) = (\delta_{\alpha\beta} - q_\alpha q_\beta / q^2) \Pi_F(\mathbf{q}, i\nu_n)$. The transverse propagator $\Pi_F(q)$ has the form

$$\Pi_F(\mathbf{q}, i\nu_n) = \chi_F q^2 + \gamma_F(\mathbf{q}) |\nu_n| / q. \quad (3.4)$$

For the t - J model χ_F is actually negative for doping $x \lesssim 0.5$ [10]. However, one can argue that for the *total* gauge-field propagator (which is obtained by integrating over the bosons as well), χ_F should be replaced by $\chi = \chi_F + \chi_B$. The gauge field is stable as long as the sum $\chi_F + \chi_B$ remains positive.

In this paper we will use the static approximation for the gauge field propagator (i.e. $i\nu_n = 0$), which is an excellent approximation above the Bose-condensation temperature T_{BE} . In the static approximation we can use the simple correlator $\langle a_q a_{-q} \rangle = T/(\chi q^2)$. In terms of the gauge invariant flux $h\hat{\mathbf{z}} = \nabla \times \mathbf{a}$ this can be written as $\langle h(\mathbf{x})h(\mathbf{0}) \rangle = T/\chi\delta(\mathbf{x})$.

In the following sections we will take the boson action in Eq. (3.3) as our starting point, without the short-range repulsion term in the first bracket. We would like to remark that one has to restore this repulsion term if one wants to obtain a true superfluid state [8]. We will furthermore assume that the coupling to the gauge field has a given value, i.e. we will write

$$\langle h(\mathbf{x})h(\mathbf{0}) \rangle = gTM\delta(\mathbf{x}), \quad (3.5)$$

where $g \equiv (M\chi)^{-1}$ is the dimensionless coupling constant of the gauge field, and M is the boson mass, which sets the energy scale. For the t - J model one has $M^{-1} = 2\xi t$ and $\chi_F \sim (12\pi m_F)^{-1} \sim \xi J/12\pi$, so that the coupling constant g is approximately $g \sim 24\pi t/J$. For the high- T_c cuprates one has typically $t/J \sim 3$, and thus one clearly has to deal with the strong-coupling limit $g \gg 1$.

A problem of the effective action in Eq. (3.3) is that ordinary perturbation works very poorly. All diagrams with an internal gauge-field line diverge [38], which makes it hard to use standard diagrammatic techniques. Moreover, even if one is able to cancel all the divergences, one still faces the problem that higher orders diagrams in the perturbation expansion become equally important if $t \gtrsim J$. This is illustrated by the work of Ioffe and Kalmeyer, who showed in an explicit calculation of the diamagnetic susceptibility that the divergences cancel each other to fourth order in the coupling constant [39]. They found a significant correction to the susceptibility due to the

gauge-field interaction, but they emphasized that the results become unreliable when T approaches T_{BE}^0 , in which case higher order corrections cannot be ignored anymore. A similar result was obtained from a renormalization group analysis of the gauge-field model [8]. This approach has the advantage that one avoids all divergences, but again the perturbation expansion breaks down for $t \gtrsim J$.

A more promising way to deal with the problem of bosons interacting with a gauge field is to use Feynman's path-integral formulation [31, 35, 36, 41, 43]. This has the advantage that one can deal with the strong-coupling limit directly, by focusing on the boson paths that are most important in the path integral, instead of perturbing around the non-interacting limit. We will argue that in the strong-coupling limit the path integral is dominated by the almost self-retracing paths.

3.3 Annealed versus quenched averaging

Our goal is to calculate the free energy corresponding to the action in Eq. (3.3). This action can be written as $S = S_B[b, \mathbf{a}] + S_G[\mathbf{a}]$, where

$$S_B[b, \mathbf{a}] = \int_0^\beta d\tau d^2r \left[\frac{1}{2M} b^\dagger (\nabla_r + i\mathbf{a})^2 b + b^\dagger \left(\frac{\partial}{\partial \tau} - \mu_B \right) b \right] \quad (3.6)$$

is the action of non-interacting bosons moving in a *fixed* gauge-field configuration $\{\mathbf{a}\}$, and $S_G[\mathbf{a}]$ is the action of the gauge field itself. In order to find the free energy $F = -T \log Z$ we have to calculate the partition function Z , which is defined by

$$\begin{aligned} Z &= \int \mathcal{D}\mathbf{a} e^{-S_G[\mathbf{a}]} \int \mathcal{D}[b, b^\dagger] e^{-S_B[b, \mathbf{a}]} \\ &= \int \mathcal{D}\mathbf{a} e^{-S_G[\mathbf{a}]} e^{-\beta F_B[\mathbf{a}]} \\ &= Z_0 \langle e^{-\beta F_B[\mathbf{a}]} \rangle_{\mathbf{a}}, \end{aligned} \quad (3.7)$$

where $Z_0 = \int \mathcal{D}\mathbf{a} \exp(-S_G[\mathbf{a}])$ is a constant. The last line in Eq. (3.7) indicates that Z is an *annealed* average of the boson partition function over all possible gauge-field configurations.

Let us first consider $\exp(-\beta F_B[\mathbf{a}])$. This is the partition function of non-interacting bosons subject to a fixed gauge-field configuration, which can be written in terms of a summation over Feynman paths [44]. This is a sum over all trajectories $\mathbf{x}_n(\tau)$, with $n = 1, \dots, N$ and $0 \leq \tau \leq \beta$, that satisfy the condition that the set of end points $\{\mathbf{x}_n(\beta)\}$ is a permutation of the set of begin points $\{\mathbf{x}_n(0)\}$. Following Wheatley [42], a set of m permutating particles in imaginary time β can also be classified as a single particle in imaginary time $m\beta$, satisfying $\mathbf{x}(0) = \mathbf{x}(m\beta)$. If we denote the number of m -cycles by n_m and sum over all sets $\{n_m\}$, we obtain the expression

$$e^{-\beta F_B[\mathbf{a}]} = \sum_{\{n_m\}} \prod_{m=1}^{\infty} \frac{e^{n_m m \beta \mu}}{n_m! m^{n_m}} [z_{\{\mathbf{a}\}}(m\beta)]^{n_m}, \quad (3.8)$$

where

$$z_{\{\mathbf{a}\}}(u) = L^2 \int_{\mathbf{x}(0)=\mathbf{x}(u)} \mathcal{D}\mathbf{x}(\tau) e^{-\int_0^u d\tau \frac{M}{2} \dot{\mathbf{x}}(\tau)^2 - i \oint \mathbf{a}(l) \cdot d\mathbf{l}} \quad (3.9)$$

is the partition function of a single particle in imaginary time u moving in a gauge-field configuration $\{\mathbf{a}\}$, and L^2 denotes the total system size. At high temperatures the sum is dominated by short loops ($m = 1$) which do not overlap each other. As the temperature is lowered long loops proliferate, and Bose condensation occurs.

Next we consider the average over $\{\mathbf{a}\}$. This is difficult to do, because the phase factor $\exp(-i \oint \mathbf{a}(l) \cdot d\mathbf{l})$ in Eq. (3.9) depends on the projected area of the paths onto real space, and when the projected areas in the various terms in Eq. (3.8) overlap the gauge-field average becomes hopelessly entangled. However, if the overlap of the projected areas is ignored, each factor $z_{\{\mathbf{a}\}}$ in Eq. (3.8) can be averaged separately, and we obtain

$$\langle e^{-\beta F_B[\mathbf{a}]} \rangle_{\mathbf{a}} \simeq \sum_{\{n_m\}} \prod_{m=1}^{\infty} \frac{1}{n_m!} \left(\frac{e^{m\beta\mu} z(m\beta)}{m} \right)^{n_m}, \quad (3.10)$$

where $z(u) = \langle z_{\{\mathbf{a}\}}(u) \rangle_{\mathbf{a}}$ is the ensemble average of a single particle with a periodicity u in imaginary time. The sum in Eq. (3.10) is easily done, and we obtain $Z \simeq Z_0 \exp(-\beta \tilde{F})$, where

$$\tilde{F} = - \sum_{m=1}^{\infty} \frac{e^{m\beta\mu}}{m\beta} z(m\beta). \quad (3.11)$$

Next we show that the approximation of ignoring overlapping loops corresponds to

the approximation of replacing the annealed average over the gauge field in Eq. (3.7) by a quenched average. Let us again consider the free energy $F_B[\mathbf{a}]$ of the bosons, corresponding to the action $S_B[b, \mathbf{a}]$ in Eq. (3.6). Because $S_B[b, \mathbf{a}]$ is quadratic in the boson field we can in principle diagonalize this action for any given gauge-field configuration $\{\mathbf{a}\}$, so that the free energy $F_B[\mathbf{a}]$ can be written as

$$F_B[\mathbf{a}] = L^2 T \int d\epsilon N_{\mathbf{a}}(\epsilon) \log(1 - e^{-\beta(\epsilon-\mu)}), \quad (3.12)$$

where $N_{\mathbf{a}}(\epsilon)$ is the density of states of the exact eigenstates of a particle moving in a fixed gauge-field configuration $\{\mathbf{a}\}$. A quenched average is defined as an average over the free energy instead of an average over the partition function. This means that the quenched free energy can be written as

$$\begin{aligned} F_Q &= \langle F_B[\mathbf{a}] \rangle_{\mathbf{a}} \\ &= L^2 T \int d\epsilon N(\epsilon) \log(1 - e^{-\beta(\epsilon-\mu)}), \end{aligned} \quad (3.13)$$

where $N(\epsilon) = \langle N_{\mathbf{a}}(\epsilon) \rangle_{\mathbf{a}}$ is the average density of states. Upon expanding the logarithm in Eq. (3.13) we find

$$F_Q = - \sum_{m=1}^{\infty} \frac{e^{m\beta\mu}}{m\beta} z(m\beta), \quad (3.14)$$

where

$$z(u) = L^2 \int d\epsilon N(\epsilon) e^{-u\epsilon} \quad (3.15)$$

is the average partition function of a single particle at a temperature u^{-1} . Comparing Eq. (3.11) with Eq. (3.14) we see that Eq. (3.11) is just the path integral representation of the same quantity. We conclude that \tilde{F} and F_Q are identical. We would like to emphasize that unlike the annealed problem, the quenched average problem only requires the knowledge of the average *single* particle partition function $\langle z(m\beta) \rangle_{\mathbf{a}}$, which we will discuss in the next section.

How good is the approximation of replacing the annealed problem by the quenched problem? We expect this approximation to be good when the boson loops are isolated, which will be the case at temperatures above the physical Bose-condensation

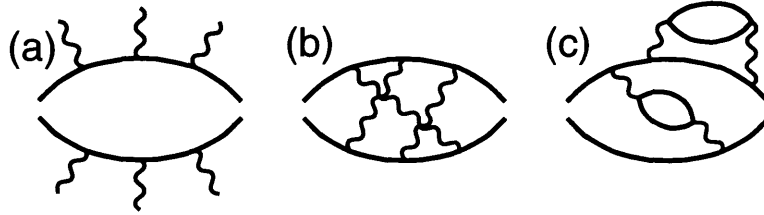


Figure 3-1: Fig. (a) shows the unaveraged diagram for a response function, where the wavy lines denote the gauge field. A quenched average over the gauge field means that the wavy lines have to be connected in all possible ways, as shown in Fig. (b). This does not include diagrams with internal boson loops, like the one shown in Fig. (c).

temperature T_{BE} , which we expect will be reduced relative to the non-interacting crossover temperature $T_{BE}^0 = 2\pi n_B/M$. As we will see in the next section, the most important boson loops are almost retracing, so that the loop area is relatively small. This will help to reduce the overlap between loops. Thus if our goal is to approach T_{BE} from above and estimate the suppression of T_{BE} , the quenched averaging is a reasonable approximation.

It is also useful to discuss which diagrams are included and excluded in the approximation scheme. Consider the diagrammatic calculation of a response function. The unaveraged diagram is shown in Fig. 3-1(a), where the wavy lines represent the gauge field. Quenched averaging corresponds to connecting the wavy lines in all possible ways, as shown in Fig. 3-1(b), and assigning the static gauge-field propagator $(\chi q^2)^{-1}$ to each wavy line. The diagrams that are excluded are those which involve closed boson loops, for example the diagram in Fig. 3-1(c) is not included. We can partially correct for this by including boson bubbles in the gauge-field propagator in a self-consistent way, as is shown in Fig. 3-2(a). This is equivalent to replacing the susceptibility χ_F by $\chi = \chi_F + \chi_B$. We will briefly discuss this scheme at the end of Sec. 3.5. In the same way we can also include boson bubbles in the response function, which is shown in Fig. 3-2(b). The crosses at the end denote an external field, and the double wavy line denotes the renormalized gauge-field propagator, which is given by a string of bubbles in Fig. 3-2(a). These RPA diagrams describe the screening of the external field by the gauge-field fluctuations, which is allowed in the annealed

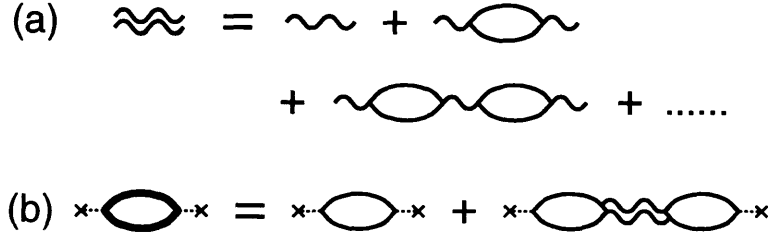


Figure 3-2: A certain class of diagrams with internal boson loops can be included in the quenched average, by including strings of boson bubbles in the gauge field propagator, as shown in Fig. (a). This is equivalent to replacing χ_F by $\chi = \chi_F + \chi_B$. Similarly one should also include these strings of boson bubbles in the response function to an external field, as is shown in Fig. (b). The gauge field now screens the external field, and one obtains the Ioffe-Larkin rule $\chi_{\text{phy}}^{-1} = \chi_F^{-1} + \chi_B^{-1}$.

problem but not in the quenched problem. The RPA approximation produces the Ioffe-Larkin rule for the physical susceptibility [23]

$$\chi_{\text{phy}}^{-1} = \chi_F^{-1} + \chi_B^{-1}. \quad (3.16)$$

In the quenched problem the RPA bubbles are not included (cf. Figs. 3-1(b) and (c)), so in that case one finds that the susceptibility of an external field is simply equal to χ_B . Thus the quenched approximation may provide a good estimate for χ_B , which we can then substitute in Eq. (3.16) to obtain the annealed χ_{phy} .

3.4 The single-particle partition function

The single-particle partition function $z(u)$ can be written as a path integral over all closed paths $\mathbf{x}(\tau)$ in imaginary time $0 \leq \tau \leq u$, where $u = m\beta$, and m is the length of a boson cycle. If the total system size is denoted by L^2 we obtain

$$z(u) = L^2 \int_{\mathbf{x}(0)=\mathbf{x}(u)} \mathcal{D}\mathbf{x}(\tau) e^{-\int_0^u d\tau \left[\frac{M}{2} \dot{\mathbf{x}}(\tau)^2 \right]} e^{-i\Phi}, \quad (3.17)$$

$$\Phi = \oint \mathbf{a}(l) \cdot d\mathbf{l}, \quad (3.18)$$

where Φ is the flux of the gauge field through the loop $\mathbf{x}(\tau)$. To find $\langle z(u) \rangle_{\mathbf{a}}$ we have to average $\langle e^{-i\Phi} \rangle_{\mathbf{a}}$ over the gauge field \mathbf{a} . Using that according to Eq. (3.5) the gauge

field is correlated as $\langle h(\mathbf{x})h(\mathbf{0}) \rangle = gTM\delta(\mathbf{x})$, where $h\hat{\mathbf{z}} = \nabla \times \mathbf{a}$, one obtains

$$\langle e^{-i\Phi} \rangle_{\mathbf{a}} = e^{-\frac{1}{2}\langle \Phi^2 \rangle} = e^{-\frac{1}{2}gTM \cdot [\text{area}]}. \quad (3.19)$$

Wheatley and Schofield pointed out that the area in the exponent is the *Ampérian* area of the loop $\mathbf{x}(\tau)$ [43]. For a simple area that does not fold over itself the Ampérian area is equal to the Euclidean area of the loop, but if the loop folds over itself the area that is traversed *twice* should be counted *four* times. A closed expression for this Ampérian area is given by [41, 43]

$$[\text{area}] = \oint \oint d\mathbf{r} \cdot d\mathbf{r}' \log |\mathbf{r} - \mathbf{r}'|. \quad (3.20)$$

The problem is now reduced to bosons that interact with themselves, according to the area cost given by Eqs. (3.19) and (3.20). Note that this is a long-range retarded self-interaction, because the area depends on the whole history of the loop $\mathbf{x}(\tau)$.

To evaluate the path integral in Eq. (3.17) we would like to know how the typical path in this path integral behaves. For $g = 0$ we would be dealing with a gas of non-interacting bosons, in which case the typical path of a boson is a random walk. Random walks have the property that there is no typical time scale or length scale (except for the overall time scale u), in the sense that if one takes a random walk and rescales time by a factor b and lengths by a factor \sqrt{b} , one ends up with a random walk that looks very much like the original random walk.

For $g \gg 1$ the typical path will look very different. Paths with a large area are very costly according to Eq. (3.19), so the dominant paths will be self-retracing paths that have a relatively small area. However, at very short time scales the bosons will still behave like free bosons that follow random walks, because the area cost only starts to be relevant at longer time and length scales. This introduces a new time scale τ_ϕ in the problem: for time scales $\tau \ll \tau_\phi$ we can treat the bosons as free particles, while for $\tau \gg \tau_\phi$ we have to use a retracing path approximation.

This picture suggests to coarse grain the path integral by dividing the time $[0, u]$ into short intervals of length τ_ϕ , denoted by $I_j = [\tau_j, \tau_{j+1}]$, where $\tau_j = j\tau_\phi$. After

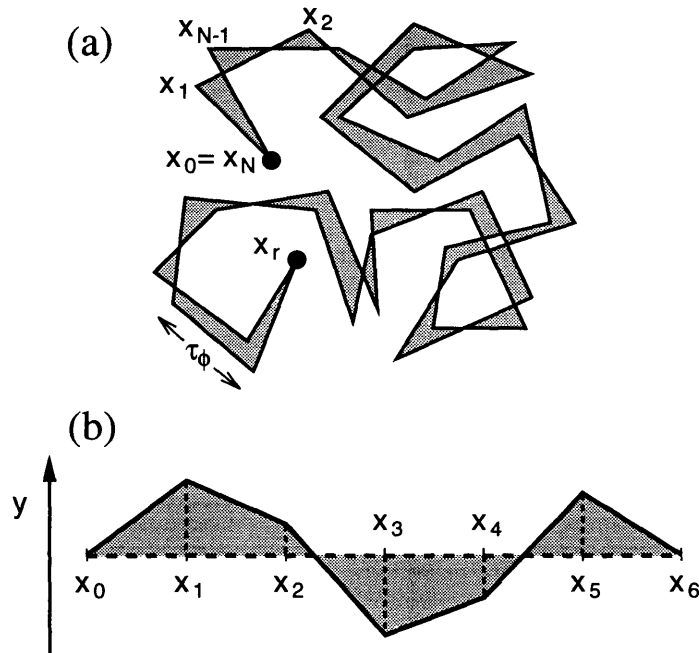


Figure 3-3: Fig. (a) shows the typical boson-path in a strongly fluctuating gauge field. At short time-scales $\tau < \tau_\phi$ the bosons follow random walks, denoted by the straight segments. At longer time-scales $\tau > \tau_\phi$ the typical path retraces itself, to minimize the total area of the path. Fig. (b) is obtained by “stretching” the coarse-grained reference path in Fig. (a), which does not change the area of the path. This allows us to decouple the x_j and y_j coordinates and to rewrite the problem as a one-dimensional quantum-mechanics problem.

coarse graining the typical path looks like the path in Fig. 3-3(a). In this figure the straight segments represent the random walks in the short time-intervals I_j . At longer time scales $\tau \gg \tau_\phi$ the path in Fig. 3-3(a) behaves like a retracing path. The partition function $z(u)$ can now approximately be written as an integral over all possible positions $\mathbf{x}_j = \mathbf{x}(\tau_j)$ at the discrete times τ_j ($j = 1, 2, \dots, N - 1$), which are the endpoints of the segments in Fig. 3-3(a). This gives

$$z(u) = L^2 \int \prod_{j=1}^{N-1} d^2 x_j \prod_{j=0}^{N-1} \rho(\mathbf{x}_j, \mathbf{x}_{j+1}) e^{-gTM\mathcal{A}[\mathbf{x}(\tau)]} \quad (3.21)$$

where $\mathcal{A}[\mathbf{x}(\tau)]$ is the Ampérian area of the polyhedron $[\mathbf{x}_0, \mathbf{x}_1, \dots, \mathbf{x}_N]$ with $\mathbf{x}_0 = \mathbf{x}_N = 0$. The density matrix $\rho(\mathbf{x}_j, \mathbf{x}_{j+1})$ is the contribution from the interval $\tau \in I_j$, represented by the straight segments in Fig. 3-3(a). Recall that τ_ϕ was chosen such that for time scales $\tau < \tau_\phi$ the paths behave like random walks. We can therefore

make the approximation of replacing $\rho(\mathbf{x}_j, \mathbf{x}_{j+1})$ by the free particle expression [44]

$$\rho_{2D}^0(\mathbf{r}, \tau_\phi) = \int_{\mathbf{x}(0)=0}^{\mathbf{x}(\tau_\phi)=\mathbf{r}} \mathcal{D}\mathbf{x}(\tau) e^{-S_0[\mathbf{x}]} = \frac{M}{2\pi\tau_\phi} e^{-\frac{1}{2}M\mathbf{r}^2/\tau_\phi}, \quad (3.22)$$

where $\mathbf{r} = \mathbf{x}_{j+1} - \mathbf{x}_j$. To evaluate $z(u)$ in Eq. (3.21) we notice that for $g \gg 1$ the dominant contribution comes from polyhedrons that have a small area, i.e. polyhedrons that are almost self-retracing, like the polyhedron in Fig. 3-3(a). We define the broken line $[\mathbf{x}_0, \mathbf{x}_1, \dots, \mathbf{x}_r]$ (with $r < N$) as the outgoing path, and the line $[\mathbf{x}_r, \mathbf{x}_{r+1}, \dots, \mathbf{x}_N]$ as the retracing path. The outgoing and retracing path have typically the same length, so we will always assume that the return time is exactly at $\tau_{N/2} = u/2$. We will use the outgoing path as a reference path, and measure the coordinates of the retracing points \mathbf{x}_j ($j > N/2$) relative to this reference path. If the retracing path follows the reference path very closely, we can “stretch” the reference path to a straight line, and the return path will look like the path shown in Fig. 3-3(b). We can now label the coarse-grained return path by the coordinates x_j along the reference path and y_j perpendicular to the reference path. Note that the result will depend on the total length $R = \sum_j |\mathbf{r}_j|$ of the coarse-grained reference path, but not on the shape of the path. Thus R is an essential parameter in our theory, which depends on τ_ϕ , and we will later in this section discuss how R is determined.

Accepting this picture of a retracing coarse-grained path, the partition function in Eq. (3.21) can now be written as

$$z(u) = L^2 \int \prod_{j=1}^{N/2} d^2 r_j \rho_{2D}^0(\tau_\phi, \mathbf{r}_j) \rho_{\text{ret}}(u/2, R). \quad (3.23)$$

In this expression ρ_{2D}^0 is the density matrix for free bosons in two dimensions, coming from the outgoing path, and $\rho_{\text{ret}}(u/2, R)$ is the density matrix for the retracing path from $R = \sum_j |\mathbf{r}_j|$ to $R = 0$. We now discuss the calculation of $\rho_{\text{ret}}(u/2, R)$. This calculation is quite similar to a calculation in a recent paper by Altshuler and Ioffe [45], who considered the propagation of a fermion in the presence of a fluctuating static gauge field. They evaluated the average of the gauge-invariant Green function

$\langle \Psi(\mathbf{r}, \tau) \Psi^\dagger(0, 0) \rangle \exp(i \int \mathbf{a} \cdot d\mathbf{l})$, where the phase factor is evaluated along a classical straight path connecting \mathbf{r} to the origin. Our approach is to adopt some of their ideas, with the reference path in Fig. 3-3(b) playing the role of the classical straight path. However, the fermion problem has the additional simplifying feature that the particle moves with the Fermi velocity along the classical path, so that the contribution along the classical path can easily be factored out and evaluated. In the present problem our approach is based on the notion that the evolution of the coarse-grained coordinates x_j can be described approximately by a constant velocity v_x , which can be determined self-consistently. The evaluation of the motion along the reference path must then be done with some care to be consistent with this notion.

The area of the path, on the other hand, depends mainly on the y_j coordinates, and can be approximated by

$$\mathcal{A} \simeq \frac{R}{N/2} \sum_{j=N/2+1}^{N-1} |y_j|. \quad (3.24)$$

With this approximation we can still decouple the x_j and y_j integrations, and hence we can write ρ_{ret} in Eq. (3.23) as

$$\rho_{\text{ret}}(u/2, R) = \rho_{\text{ret}}^x(u/2, R) \rho_{\text{ret}}^y(u/2, R). \quad (3.25)$$

The calculation of ρ_{ret}^y is the most interesting, because ρ_{ret}^y contains the area cost of the gauge field. According to Eqs. (3.21)–(3.23) ρ_{ret}^y is given by

$$\rho_{\text{ret}}^y(u/2, R) = \int \prod_{j=N/2+1}^{N-1} dy_j \prod_{j=N/2}^{N-1} dy_j \rho_{2D}^0(\tau_\phi, y_{j+1} - y_j) e^{-gTM\mathcal{A}/2} \quad (3.26)$$

We will do the y_j integrations by taking the continuum limit, and transforming the problem into a one-dimensional quantum-mechanics problem, similar to the problem analyzed by Altshuler and Ioffe [45]. Taking the continuum limit means that we replace the broken line in Fig. 3-3(b) by a smooth, continuous path. In the continuum

limit ρ_{ret}^y can be written as

$$\rho_{\text{ret}}^y(u/2, R) = \int_{y(0)=y(u/2)} \mathcal{D}y(\tau) \exp \left\{ - \int_0^{u/2} d\tau \left[\frac{M}{2} \dot{y}^2 + \alpha |y| \right] \right\}. \quad (3.27)$$

It is easy to see that the second term in the exponent in Eq. (3.27) corresponds to the area cost of the path if we define

$$\alpha = \frac{1}{2} g T M v_x, \quad (3.28)$$

where $v_x = R/(u/2)$ plays the role of the Fermi velocity in the Altshuler-Ioffe problem. Finding ρ_{ret}^y is equivalent to solving a 1D quantum mechanics problem, because ρ_{ret}^y can be written as [44]

$$\rho_{\text{ret}}^y(\tau) = \langle y = 0 | e^{-\tau \mathcal{H}} | y = 0 \rangle = \sum_n |\varphi_n(0)|^2 e^{-\tau E_n}, \quad (3.29)$$

where E_n and $\varphi_n(y)$ are the eigenvalues and eigenfunctions of the 1D Hamiltonian

$$\mathcal{H} = -\frac{1}{2M} \frac{\partial^2}{\partial y^2} + \alpha |y|. \quad (3.30)$$

The eigenfunctions are proportional to the Airy functions

$$\varphi_n(y) \propto \text{Ai} \left((2M\alpha)^{1/3} |y| - \tau_* E_n \right), \quad (3.31)$$

where $\tau_* = (2M/\alpha^2)^{1/3}$ and the eigenvalues E_n are the zeros of the functions $\text{Ai}(-\tau_* E_n)$ and $\text{Ai}'(-\tau_* E_n)$. Note that for $g \gg 1$ one has $\tau_* \ll u$, so that we can approximate $\rho_{\text{ret}}^y(\tau)$ in Eq. (3.29) by only using the lowest eigenvalue $E_0 = c/\tau_*$, where $c \simeq 1.019$ is the first zero of $\text{Ai}'(-x)$. This gives the simple expression

$$\rho_{\text{ret}}^y(u/2) \propto \sqrt{\frac{2M}{\tau_*}} e^{-cu/2\tau_*}. \quad (3.32)$$

To obtain ρ_{ret}^x in Eq. (3.25) we have to capture the physics that the motion is a random walk for $\tau < \tau_\phi$. Furthermore, the set $\{x_j\}$ should be ordered as shown in

Fig. 3-3(b), to be consistent with the concept of having a nearly retracing path. A reasonable approximation to ρ_{ret}^x is to sum over all paths with the restriction that $0 < x_{N-1} < \dots < x_{N/2} = R$. Relabeling each integration variable x_{N-n} by x_n one can then write

$$\begin{aligned} \rho_{\text{ret}}^x(u/2, R) &\simeq \int_0^R dx_{N/2+1} \cdots \int_0^{x_3} dx_2 \int_0^{x_2} dx_1 \\ &\rho_{1D}^0(\tau_\phi, x_1) \rho_{1D}^0(\tau_\phi, x_2 - x_1) \cdots \rho_{1D}^0(\tau_\phi, R - x_{N/2+1}). \end{aligned} \quad (3.33)$$

This integral is evaluated approximately in the limit of N large. The details are shown in the Appendix, and the result is (cf. Eq. (C.6))

$$\rho_{\text{ret}}^x(u/2, R) \propto \rho_{1D}^0(u/2, R) \left(\frac{u}{\tau_\phi} \right)^{\gamma'} e^{-c'u/\tau_\phi}, \quad (3.34)$$

where according to Eq. (C.7) $\gamma' \simeq 0.144$ and $c' \simeq 0.086$. Note that if the restriction of $x_j < x_{j+1}$ was not made, $\rho_{\text{ret}}^x(u/2, R)$ would simply be equal to the non-interacting diffusion propagator $\rho_{1D}^0(u/2, R)$, and the exponent γ' would be equal to 0. Not making this restriction would clearly overestimate the entropy of the return path.

Now we can substitute Eqs. (3.32) and (3.34) into Eq. (3.23), and perform the \mathbf{r}_j integrations. These integrations are still not simple, because $\rho_{\text{ret}}(\sum |\mathbf{r}_j|)$ contains the variables \mathbf{r}_j as well, and hence the integrations are not simple Gaussians. The simplest way to find an approximation for the integrals is by replacing $\rho_{\text{ret}}(R)$ by $\rho_{\text{ret}}(\langle R \rangle)$ self-consistently, where $R = \sum |\mathbf{r}_j|$ is the coarse-grained pathlength of the reference path. Each of the $d^2 r_j$ integrals is then exactly equal to 1, and for $\langle R \rangle$ we will take the root mean square

$$\langle R \rangle = \frac{N}{2} \langle |\mathbf{r}_j| \rangle_{\text{RMS}} = \frac{u}{2\tau_\phi} \sqrt{\frac{\tau_\phi}{M}}. \quad (3.35)$$

Substituting Eqs. (3.32) and (3.34) into the expression for $z(u)$ in Eq. (3.23) we obtain

$$z(u) \simeq L^2 \rho_{\text{ret}}^x(u/2, \langle R \rangle) \rho_{\text{ret}}^y(u/2, \langle R \rangle) \quad (3.36)$$

$$\propto \frac{ML^2}{u} \left(\frac{u}{\tau_*} \right)^{\frac{1}{2} + \gamma'} e^{-M(R)^2/u - c'u/\tau_\phi - cu/2\tau_*}. \quad (3.37)$$

What remains is to determine the cross-over time scale τ_ϕ , that separates the random walk limit from the retracing path limit. Our criterion to determine τ_ϕ is to require that the typical “vertical” deviation y_{typ} from the reference path is equal to the typical “horizontal” length $|x_j - x_{j+1}|$ of each segment. This criterion for τ_ϕ is consistent with the assumptions made about how the typical path behaves at different time scales. Indeed, for short time scales $|\tau - \tau'| \ll \tau_\phi$ the vertical deviation becomes much larger than the length $|x(\tau) - x(\tau')|$ of the segment, which indicates that the path behaves like a random walk. For long time scales $|\tau - \tau'| \gg \tau_\phi$ the vertical deviation is much smaller than $|x(\tau) - x(\tau')|$, so that at long time scales the retracing path approximation is appropriate.

The functional form of the eigenfunction $\varphi_n(y)$ in Eq. (3.31) immediately tells us the typical deviation y_{typ} from the reference path:

$$y_{\text{typ}} \simeq (2M\alpha)^{-1/3}. \quad (3.38)$$

Recall that $\alpha = gTMR/u$ (cf. Eq. (3.28)), and R is given by Eq. (3.35). Setting y_{typ} equal to $|x_{j+1} - x_j| = \sqrt{\tau_\phi/M}$ gives

$$\tau_\phi = \frac{1}{gT}. \quad (3.39)$$

This shows that our picture is only valid for $g \gg 1$, because for $g \lesssim 1$ the number of segments u/τ_ϕ becomes smaller than 1 for $u = \beta$. It is also worth pointing out that $R \sim \sqrt{gu/\beta} \sqrt{u/M} \gg \sqrt{u/M}$, i.e. for $g \gg 1$ the coarse-grained path length R is much greater than the RMS diameter of the random walk shown in Fig. 3-3(a). Using expression (3.39) for τ_ϕ we can express α and τ_* in terms of τ_ϕ : $\alpha = \frac{1}{2} \sqrt{M/\tau_\phi^3}$ and $\tau_* = 2\tau_\phi$. Substituting this into Eq. (3.37) we obtain the following simple expression

for the single-particle partition function:

$$z(u) \propto \frac{L^2 M}{u} \left(\frac{u}{\tau_\phi} \right)^\gamma e^{-\tilde{c}u/\tau_\phi}. \quad (3.40)$$

The exponent γ is equal to $1/2 + \gamma' \simeq 0.644$. According to Eq. (3.37) the numerical constant \tilde{c} is approximately by $\tilde{c} = c' + (1 + c)/4 \simeq 0.591$, using $c \simeq 1.019$ and $c' \simeq 0.086$. This is clearly only a crude estimate for \tilde{c} , because we made several approximations to derive this result. For instance, we replaced R by its root mean square average $\langle R \rangle$, which affects the value of \tilde{c} .

The expression in Eq. (3.40) displays two striking differences compared to the partition function $z_0(u) = M/(2\pi u)$ for free bosons. First $z(u)$ is suppressed by an exponential factor $\exp(-\tilde{c}u/\tau_\phi)$, and second $z(u)$ has a pre-factor that varies like $u^{-1+\gamma}$ instead of u^{-1} . We will show that these two differences will modify the density of states by shifting the band edge to $\epsilon_0 = \tilde{c}/\tau_\phi$ and by enhancing the density of states near the new band edge.

We will now determine the density of states $N(\epsilon)$ using Eq. (3.15), which states that $N(\epsilon)$ is the inverse Laplace transform of the single-particle partition function $z(u)/L^2$. Using the expression for $z(u)$ in Eq. (3.40) we can invert Eq. (3.15), which gives

$$N(\epsilon) \propto \frac{M^2}{[\tau_\phi(\epsilon - \epsilon_0)]^\gamma}. \quad (3.41)$$

The shift $\epsilon_0 = \tilde{c}/\tau_\phi$ in the band edge is due to the exponential factor $\exp(-\tilde{c}u/\tau_\phi)$ in $z(u)$, and can easily be incorporated as a shift in the chemical potential $\mu = \mu_0 - \epsilon_0$. Note that thanks to the shift in the band edge the bare chemical potential μ_0 can be *positive*, what is not allowed for free bosons. The enhancement of $N(\epsilon)$ at the band edge is due to the fact that $z(u)$ in Eq. (3.40) has a pre-factor that varies like $u^{-1+\gamma}$ instead of u^{-1} . We remark that in Wheatley's treatment, who replaced the gauge field fluctuations with a coupling to a heat bath, the exponent γ was equal to 1, leading to a δ -function singularity in the density of states at the band edge [42]. Clearly that approximation overestimates the effect of the gauge field fluctuations.

The enhancement of the density of states $N(\epsilon)$ has important consequences for

the density equation

$$n_B = \int_{\epsilon_0}^{\infty} \frac{d\epsilon N(\epsilon)}{e^{\beta(\epsilon-\mu_0)} - 1} \propto \int_0^{\infty} \frac{d\epsilon' M}{(\tau_\phi \epsilon')^\gamma} \left(\frac{1}{e^{\beta(\epsilon'-\mu)} - 1} \right). \quad (3.42)$$

It is instructive to compare this expression with the density equation for free bosons. For free bosons one has $N_0(\epsilon) = M/2\pi$, which leads to a chemical potential of the form $\mu = T \log(1 - e^{-T_{\text{BE}}^0/T})$, where $T_{\text{BE}}^0 = 2\pi n_B/M$. This implies that for $T \ll T_{\text{BE}}^0$ the only way to accommodate a high density of bosons is to make the chemical potential exponentially small: $\mu \simeq -T \exp(-T/T_{\text{BE}}^0)$. Having a chemical potential that is orders of magnitude smaller than any other energy scale in the problem is a somewhat awkward situation, and it is well-known that in the case of free bosons a small short-range repulsion is sufficient to create a superfluid state below a Bose-condensation temperature $T_{\text{BE}}^0 \simeq 2\pi n_B/M$ [8, 46, 47].

The situation is clearly very different in Eq. (3.42), where the gauge field interaction has introduced a singularity in the density of states at the band edge. This means that one can easily accommodate a high density of bosons, without having to make the chemical potential exponentially small. Bose condensation might still survive if there is a short-range repulsion between the bosons, but the strong enhancement of the density of states indicates that the transition will occur at a much lower temperature $T_{\text{BE}} \ll T_{\text{BE}}^0$. Our approximation of the density of states is not accurate enough to produce band tail states, which are states that correspond to an exponentially small density of states at low energies. According to a Lifshitz argument band tail states should be present due to unlikely voids in the gauge field configuration. These band tail states are localized and cause problems if bosons are allowed to condense into them. However, they are not expected to be important if hard-core repulsion is taken into account.

An important physical quantity that can be used to characterize the condensation of the bosons into a superfluid state is the diamagnetic susceptibility. In the weak-

coupling limit the boson susceptibility is given by

$$\chi_B^0 = \frac{1}{24\pi M} \left(e^{T_{\text{BE}}^0/T} - 1 \right), \quad (3.43)$$

where $T_{\text{BE}}^0 = 2\pi n/M$. For $T < T_{\text{BE}}^0$ the susceptibility χ_B^0 diverges exponentially, and T_{BE}^0 can therefore be identified as the crossover temperature below which the bosons start to behave like a superfluid. We will show in the next section that in the strong-coupling limit one obtains a very different expression for χ_B , that increases much slower below T_{BE}^0 , indicating that Bose condensation is suppressed.

3.5 Response to an external field

In this section we will couple the system to an external magnetic field $H\hat{z} = \nabla \times \mathbf{A}$, and calculate the diamagnetic susceptibility $\chi_B = L^{-2} \partial^2 F / \partial H^2$. In a quenched random gauge field we can again express the free energy $F_Q(\beta, H)$ in terms of the single-particle partition function $z(u, H)$ (with $u = m\beta$), averaged over the gauge field, similar to Eq. (3.14):

$$F_Q(\beta, H) = -T \sum_{m=1}^{\infty} \frac{e^{m\beta\mu}}{m\beta} \langle z(m\beta, H) \rangle_{\mathbf{a}}. \quad (3.44)$$

The susceptibility $\chi_B = L^{-2} \partial^2 F_Q / \partial H^2$ is determined by solving the two equations

$$\chi_B = -\frac{1}{L^2} \sum_{m=1}^{\infty} \frac{e^{m\beta\mu}}{m\beta} \frac{\partial^2 z}{\partial H^2}; \quad (3.45)$$

$$n_B = \frac{1}{L^2} \sum_{m=1}^{\infty} z(m\beta) e^{m\beta\mu}. \quad (3.46)$$

Eq. (3.46) is the density equation $n_B = -L^{-2} \partial F_Q / \partial \mu$, which determines the chemical potential μ .

The path-integral expression for $z(u, H)$ is identical to the expression for $z(u)$ in Eq. (3.9), except that due to the external field there is an additional factor $\exp(-i \oint \mathbf{A} \cdot d\mathbf{l})$ in the integrand. This means that the total flux Φ through a loop is now given

by:

$$\Phi = \oint \mathbf{a} \cdot d\mathbf{l} + \oint \mathbf{A} \cdot d\mathbf{l}. \quad (3.47)$$

The external gauge field \mathbf{A} is chosen such that $H\hat{\mathbf{z}} = \nabla \times \mathbf{A}$. Remark that for a constant external field H the contribution of this field to the flux Φ is simply equal to H times the *oriented* area of the loop. After averaging over the gauge field the total area cost of a closed loop is therefore equal to

$$\frac{1}{2}gTM \times [\text{Ampérian area}] + iH \times [\text{oriented area}]. \quad (3.48)$$

We will first give a qualitative estimate of $\chi_B = \partial^2 F / \partial H^2$. Due to the second term in Eq. (3.48), the single-particle partition function can be expanded in H^2 as $z(u, H) \simeq z(u)[1 - \frac{1}{2}H^2 \langle \mathcal{A}'^2 \rangle]$ for $H^2 \rightarrow 0$, where \mathcal{A}' is the oriented area of a path. The average $\langle \mathcal{A}'^2 \rangle$ can be estimated by dividing the retracing path into $N = u/\tau_\phi$ segments, which gives $\langle \mathcal{A}'^2 \rangle \simeq N \langle \mathcal{A}_0^2 \rangle$, where \mathcal{A}_0 is the area of a single segment. A single segment behaves like a random path, so $\langle \mathcal{A}_0^2 \rangle \simeq (\tau_\phi/M)^2$. This implies that $\langle \mathcal{A}'^2 \rangle \simeq N(\tau_\phi/M)^2$. Substituting $N = u\tau_\phi$ and $\tau_\phi = (gT)^{-1}$ gives $\langle \mathcal{A}'^2 \rangle \simeq u/(gTM^2)$, so that

$$\frac{\partial^2 z}{\partial H^2} = \langle \mathcal{A}'^2 \rangle z(u) \simeq \frac{u}{gTM^2} z(u). \quad (3.49)$$

Substituting this expression into Eq. (3.45), one notices that the factor $u = m\beta$ in Eq. (3.49) cancels $m\beta$ in the denominator of Eq. (3.45), so that Eqs. (3.45) and (3.46) become proportional to each other. This immediately gives us the result $\chi_B \simeq n_B/(gTM^2)$.

We will now calculate $z(u, H)$ more accurately, using the same approach as in Sec. 3.4. We again introduce a time scale τ_ϕ such that the paths are retracing for time scales $\tau > \tau_\phi$, and behave like random walks for time scales $\tau < \tau_\phi$. Just like in Sec. 3.4 we can define a reference path and a retracing path, and analogous to Eq. (3.36) we can derive that $z(u, H)$ can be written as

$$z(u, H) \simeq L^2 \rho_{\text{ret}}^x(u/2, \langle R \rangle) \rho_{\text{ret}}^y(u/2, \langle R \rangle, H). \quad (3.50)$$

The dependence on H is contained entirely in $\rho_{\text{ret}}^y(u/2, H)$. To calculate this quantity we will again use the trick of rewriting the problem as a 1D quantum mechanics problem (see Eq. (3.27)), but now the 1D Hamiltonian is replaced by

$$\mathcal{H} = -\frac{1}{2M} \frac{\partial^2}{\partial y^2} + \alpha|y| + iHv_x y. \quad (3.51)$$

Notice that in the last term y does not have absolute value bars, because the last term measures the *oriented* area of the loop. The eigenfunctions of \mathcal{H} can still be expressed in terms of Airy functions (cf. Eq. (3.31)):

$$\varphi_n(y) \propto \text{Ai}\left((2M\alpha_{\pm})^{1/3}|y| - \tau_{\pm} E_n\right), \quad (3.52)$$

where $\tau_{\pm} = (2M/\alpha_{\pm}^2)^{1/3}$, $\alpha_{\pm} = \alpha \mp iv_x H$, and \pm denotes the sign of y . The eigenfunctions E_n are found by requiring that $\varphi_n(y)$ and $\varphi_n'(y)$ are continuous at $y = 0$, which gives the transcendental equation

$$\frac{\text{Ai}'(-\tau_+ E_n)}{\text{Ai}(-\tau_+ E_n)} = -\frac{\text{Ai}'(-\tau_- E_n)}{\text{Ai}(-\tau_- E_n)}. \quad (3.53)$$

For $u/\tau_{\phi} \gg 1$ it is sufficient to focus on the lowest eigenvalue $E_0(H)$ of this equation. In the limit $H \rightarrow 0$ the solution of Eq. (3.53) can be written as

$$\frac{E_0(H) - E_0(0)}{E_0(0)} = c_H \left(\frac{v_x H}{\alpha}\right)^2, \quad (3.54)$$

where $c_H \simeq 0.218$ is a numerical constant. Substituting this into Eq. (3.29) we obtain

$$\rho_{\text{ret}}^y(u/2, H) \propto \sqrt{\frac{2M}{\tau_*}} \exp\left[-\frac{cu}{2\tau_*} \left(1 + c_H \left(\frac{v_x H}{\alpha}\right)^2\right)\right]. \quad (3.55)$$

This implies that

$$\left.\frac{\partial^2 \rho_{\text{ret}}^y}{\partial H^2}\right|_{H=0} = -\frac{cc_H u}{\tau_*} \left(\frac{v_x}{\alpha}\right)^2 \rho_{\text{ret}}^y. \quad (3.56)$$

A similar equation has to hold for $z(u, H)$, because ρ_{ret}^y is the only part of $z(u, H)$ that depends on H . Expressing τ_* and v_x/α in terms of τ_{ϕ} , as explained after Eq.

(3.39), we obtain

$$\left. \frac{\partial^2 z}{\partial H^2} \right|_{H=0} \simeq -2cc_H \frac{u\tau_\phi}{M^2} z(u). \quad (3.57)$$

Using this equation, which relates $\partial^2 z/\partial H^2$ to $z(u)$, we can now express the diamagnetic susceptibility in terms of the density:

$$\begin{aligned} \chi_B &= -\frac{1}{L^2} \sum_{m=1}^{\infty} \frac{e^{m\beta\mu}}{m\beta} \frac{\partial^2 z}{\partial H^2} \\ &= 2cc_H \frac{\tau_\phi}{M^2 L^2} \sum_{m=1}^{\infty} z(m\beta) e^{m\beta\mu} \\ &= 2cc_H \frac{n_B/T}{gM^2} = \frac{cc_H}{\pi} \frac{T_{BE}^0}{gMT}. \end{aligned} \quad (3.58)$$

If we substitute $g \equiv 1/(\chi M)$ with $\chi \simeq \chi_F$, this result is identical to the expression for χ_B derived by Wheatley *et al.* [43], except that the numerical factor here (i.e., $cc_H/\pi \simeq 0.071$) is somewhat smaller. Also note that Eq. (3.58) is similar to the qualitative expression for χ_B that we derived after Eq. (3.49). We will refer to the result in Eq. (3.58) as χ_B^Q , where the superscript Q denotes that this is the susceptibility of the *quenched* problem. Now compare the result $\chi_B^Q \sim 0.07 T_{BE}^0/(gMT)$ in Eq. (3.58) to the non-interacting expression $\chi_B^0 \sim T_{BE}^0/(24\pi MT)$ in Eq. (3.43) for $T > T_{BE}^0$. The conclusion is that at high temperatures χ_B^Q is reduced by a factor of $0.2g$ compared to χ_B^0 .

We will now discuss the self-consistency of the expression for χ_B^Q in Eq. (3.58). In the self-consistent scheme discussed at the end of Sec. 3.3 we argued that χ_F has to be replaced by $\chi = \chi_F + \chi_B$, in order to include a class of diagrams that are not included in the quenched problem, but should be included in the annealed problem. At high temperatures this does not change the results much, because $\chi_B \ll \chi_F$ for $T \gg T_{BE}$. Let us now consider what happens at lower temperatures, when χ_B becomes of the same order as χ_F . In that case $g \simeq (M\chi_F)^{-1}$ has to be replaced by $g = M^{-1}(\chi_F + \chi_B)^{-1}$, so that the right-hand side of Eq. (3.58) becomes a function

of χ_B as well. Solving this equation gives

$$\chi_B = \left(\frac{\pi}{cc_H} \frac{T}{T_{BE}^0} - 1 \right)^{-1} \chi_F. \quad (3.59)$$

According to this equation χ_B blows up at a finite temperature

$$T_{BE} = \frac{cc_H}{\pi} T_{BE}^0 \simeq 0.071 T_{BE}^0, \quad (3.60)$$

which we interpret as the Bose-condensation temperature. The fact that χ_B in Eq. (3.59) diverges at T_{BE} indicates that the validity of Eqs. (3.58) and (3.59) breaks down for $T \lesssim T_{BE}$. The reason for this is that Eq. (3.58) was derived under the assumption that $\tau_\phi \ll u$, or equivalently that $g = (\chi M)^{-1} \gg 1$. This is a valid assumption as long as χ is much smaller than M^{-1} , i.e. when $T > T_{BE}$. However, when T approaches T_{BE} , the susceptibility $\chi_B(T)$ increases so rapidly, that the assumption $g \gg 1$ breaks down, and thus Eqs. (3.58) and (3.59) are not valid anymore. To obtain an expression for χ_B we then have to consider the opposite limit $u \lesssim \tau_\phi$, which is equivalent to $g \lesssim 1$ for $u = \beta$. For $u \lesssim \tau_\phi$ the retracing behavior of the boson paths disappears, and instead the paths are random walks at all time scales, so that we should recover the non-interacting limit. In order to calculate χ_B self-consistently we have to find explicit expressions for $z(u)$ and $\partial^2 z / \partial H^2$ that are valid in both limits $u \gg \tau_\phi$ (strong coupling) and $u \ll \tau_\phi$ (weak coupling). We therefore define a time scale u_c , which is proportional to τ_ϕ , that separates the two limits:

$$z(u) \simeq \begin{cases} K \frac{L^2 M}{2\pi u} \left(\frac{u}{\tau_\phi} \right)^\gamma e^{-\tilde{c}u/\tau_\phi} & \text{for } u > u_c; \\ \frac{L^2 M}{2\pi u} & \text{for } u < u_c; \end{cases} \quad (3.61)$$

$$\frac{\partial^2 z}{\partial H^2} \simeq \begin{cases} -2cc_H \frac{u\tau_\phi}{M^2} z(u) & \text{for } u > u_c; \\ -\frac{u^2}{12M^2} z(u) & \text{for } u < u_c. \end{cases} \quad (3.62)$$

For $u > u_c$ these expressions are identical to Eqs. (3.40) and (3.58), while for $u < u_c$ they are equal to the well-known non-interacting expressions for $z(u)$ and $\partial^2 z / \partial H^2$. The parameters u_c and K have to be determined self-consistently, so that $z(u)$ and

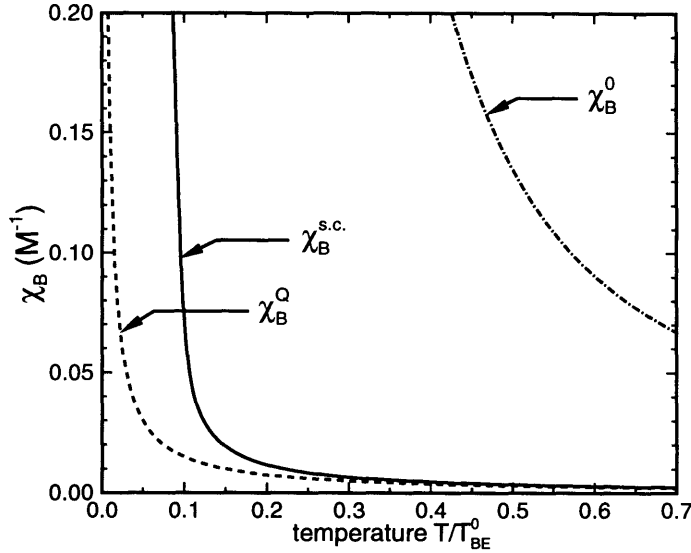


Figure 3-4: Three different approximations for the boson susceptibility $\chi_B(T)$ for a fixed boson density $n_B = 0.1$, using $\chi_F M = (24\pi t/J)^{-1}$ and $t/J = 1$. The dashed line is the quenched susceptibility $\chi_B^Q(T) \propto (gT)^{-1}$, which we derived in Eq. (3.58). The solid line is the self-consistent $\chi_B^{\text{SC}}(T)$, which we obtained by solving Eqs. (3.45) and (3.46) numerically. For high temperatures χ_B^{SC} approaches the dashed line, because in that case χ_B is small and can be ignored compared to χ_F . Below a crossover temperature T_{BE} the susceptibility χ_B^{SC} diverges exponentially, analogous to the non-interacting value χ_B^0 (dash-dotted line). Notice that due to gauge field fluctuations the crossover temperature is strongly suppressed, $T_{\text{BE}} \ll T_{\text{BE}}^0$.

$\partial^2 z / \partial H^2$ are continuous at $u = u_c$. This gives

$$\begin{aligned} u_c &= (24cc_H) \tau_\phi \simeq 5.331 \tau_\phi; \\ K &= \left(\frac{\tau_\phi}{u_c}\right)^\gamma e^{\tilde{c}u_c/\tau_\phi} \simeq 7.925. \end{aligned} \quad (3.63)$$

We can now substitute Eqs. (3.61)–(3.63) into the two Eqs. (3.45) and (3.46) that determine χ_B and μ . Notice that in contrast to Eq. (3.58), χ_B and n_B are not directly proportional to each other anymore. We remark that χ_B also enters the right-hand side of the Eqs. (3.45) and (3.46) via $\chi = \chi_F + \chi_B$.

We solved Eqs. (3.45) and (3.46) numerically at the density $n_B = 0.1$, using $\chi_F M = (24\pi t/J)^{-1}$. In Fig. 3-4 we show our results for $t/J = 1$. The solid line denotes the self-consistent χ_B^{SC} . Notice that at high temperatures $\chi_B^{\text{SC}}(T)$ approaches the dashed line, which corresponds to the quenched $\chi_B^Q(T)$ in Eq. (3.58). For low

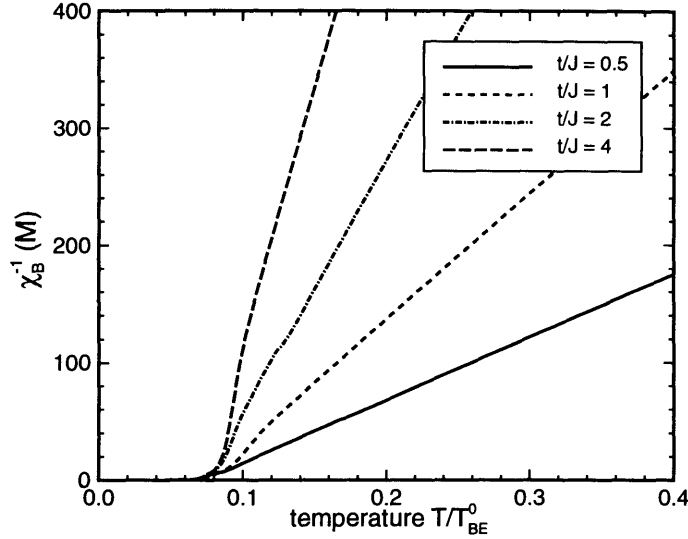


Figure 3-5: The (inverse) boson susceptibility $\chi_B^{\text{SC}}(T)^{-1}$ for various values of t/J at a fixed density $n_B = 0.1$, using $\chi_F M = (24\pi t/J)^{-1}$. The results were obtained by solving Eqs. (3.45) and (3.46) numerically, using an expression for the partition function $z(u)$ that is valid in both the strong-coupling and the weak-coupling limit. At high temperatures $\chi_B^{\text{SC}}(T)^{-1}$ is linear in T , with a slope proportional to t/J , and an intercept independent of t/J . Below $T_{\text{BE}} \simeq 0.08 T_{\text{BE}}^0$ one enters the weak-coupling regime, and $\chi_B^{\text{SC}}(T)^{-1}$ decays exponentially. Note that T_{BE} is reduced by a factor of $\simeq 12$ compared to T_{BE}^0 .

temperatures $\chi_B^{\text{SC}}(T)$ diverges exponentially, and behaves similar to the mean-field susceptibility $\chi_B^0(T)$ in Eq. (3.43), except that the crossover temperature T_{BE} , at which $\chi_B \sim \chi_F$, is significantly reduced. In Fig. 3-5 we show how the behavior of χ_B^{SC} changes for different values of t/J . At high temperatures χ_B^{-1} is linear in T , with a slope proportional to t/J , and an intercept at a finite temperature $T \simeq 0.07 T_{\text{BE}}^0$. This corresponds very well with the expression for χ_B in Eq. (3.59). At lower temperatures χ_B^{-1} decays exponentially. According to Fig. 3-5 the crossover temperature between the two regimes is at approximately $T_{\text{BE}} \simeq 0.08 T_{\text{BE}}^0$. These results remain almost the same if one repeats the analysis at a different density, keeping in mind that $T_{\text{BE}}^0 = 2\pi n_B/M$ scales linearly with the boson density n_B . The main difference is that at a higher density $\chi_B(T)$ diverges more quickly below T_{BE} .

3.6 Discussion

In this paper we analyzed an effective action of bosons moving in a fluctuating gauge field, using a path-integral approach. The effective action was obtained from the t - J model by averaging over the fermionic degrees of freedom. The advantage of using path integrals is that the interaction with the gauge field can be taken into account by associating an area cost to every closed path in the path integral. The fluctuating gauge field favors loops with a small area, which allows us to focus on self-retracing paths. This is a very appealing approach, because by focusing on self-retracing paths we essentially take the strong-coupling limit as our starting point, which is not possible if one uses standard diagrammatic techniques.

To find the partition function one in principle has to calculate an *annealed* average over the gauge field. We approximated this annealed average by a *quenched* average, in which case the total free energy can be written in terms of the single-particle partition function, averaged over the gauge field. The difference between a quenched and an annealed average is that a quenched average treats all boson loops as being independent, while in reality two or more boson loops can overlap. We believe that the quenched problem is a good approximation of the annealed problem for $T > T_{\text{BE}}$, because in that case the probability that boson loops overlap is small. For $T \lesssim T_{\text{BE}}$ the typical size of a loop increases, and one has to deal with a system of tangled loops. In that case the quenched problem and the annealed problem become very different.

An important aspect of our derivation of the partition function was the observation that there is a crossover time scale $\tau_\phi = (gT)^{-1}$, that distinguishes random-walk behavior from retracing-path behavior. At short time scales $\tau < \tau_\phi$ the bosons do not really feel the presence of the gauge field, and the bosons essentially follow random walks. At longer time scales $\tau > \tau_\phi$ the bosons realize that it is costly to form loops with a large area, so they try to retrace themselves to minimize the area cost. Note that $g \gg 1$ is equivalent to $\beta \gg \tau_\phi$, which means that in the strong-coupling limit the paths are indeed self retracing.

One of the main consequences of the retracing-path approximation is the effect

on the density of states. We found that the band edge is shifted, which allows the chemical potential to become positive. More importantly there is an enhancement of the density of states near the band edge. This suppresses Bose condensation, because due to this enhancement of the density of states one can accommodate a higher density of bosons in the system.

An important signature for Bose condensation is provided by the boson susceptibility χ_B . For non-interacting bosons it is well-known that χ_B diverges exponentially below a crossover temperature $T_{BE}^0 \simeq 2\pi n_B/M$. In other words, even though there is no *true* superfluid state, for all practical purposes the bosons still behave as if they were condensed, which is indicated by $\chi_B \gg 1/(24\pi M)$. One can therefore argue that the equation $\chi_B = \mathcal{O}(1/(24\pi M))$ determines a crossover temperature between a normal state and a (pseudo) superfluid state.

We calculated the susceptibility using our path-integral approach, by analyzing the effect that an external magnetic field has on the single-particle partition function. Because of the fact that the typical area of a closed loop is suppressed by the gauge field, one expects that the diamagnetic susceptibility, which is related to the area of loops, will be quite small in the strong-coupling limit. We indeed found that above the Bose-condensation temperature the susceptibility χ_B is a factor $0.2g$ smaller than the non-interacting expression χ_B^0 , and has the functional form $\chi_B^Q \simeq 0.44 n_B/(gTM^2)$. It is interesting to note that in the strong-coupling limit our expression for χ_B is similar to the expression derived by Wheatley *et al*, even though they analyzed a different model, in which the gauge field interaction was replaced by a simple dissipative term. They obtained a somewhat different expression for the density of states, but the expression for χ_B was the same as ours. This is due to the fact that the susceptibility χ_B can be directly related to the density of bosons, independent of the details of the density of states.

The expression $\chi_B^Q(T) \sim (gT)^{-1}$ is only valid above the Bose-condensation temperature T_{BE} . At lower temperatures one has to include χ_B in the total gauge-field susceptibility $\chi = \chi_F + \chi_B$ to obtain self-consistent results. This implies that the dimensionless coupling constant $g = (\chi M)^{-1}$ decreases rapidly, and at sufficiently

low temperatures one approaches the weak-coupling limit $g \ll 1$. Thus one expects that at low temperatures the strong-coupling result $\chi_B \sim (gT)^{-1}$ breaks down. Instead one has to solve a more complicated set of coupled equations to determine a self-consistent susceptibility χ_B^{SC} . We solved this numerically using an expression for $z(u, H)$ that is valid in both the strong-coupling limit $u \gg \tau_\phi$ and in the weak-coupling limit $u \ll \tau_\phi$. We showed that below T_{BE} the self-consistent χ_B^{SC} does not vary like $1/T$ anymore, but instead diverges exponentially below a crossover temperature $T_{\text{BE}} \simeq 0.08 T_{\text{BE}}^0$. This crossover temperature corresponds to the situation when $\chi_B \simeq \chi_F$. We conclude that the bosons still condense into a superfluid state, but due to the fluctuating gauge field this happens at a reduced temperature $T_{\text{BE}} \simeq 0.08 T_{\text{BE}}^0$.

Acknowledgements

This work was done in collaboration with Patrick A. Lee [9]. We would like to thank Naoto Nagaosa for several helpful discussions. The work was supported by the NSF through the Material Research Laboratory under Grant No. DMR-90-22933.

Chapter 4

The superconducting phase diagram in the gauge-field description of the t - J model

4.1 Introduction

Due to an intense effort by many researchers the unusual properties of the high- T_c copper-oxides are now quite well documented. In the normal state the copper-oxides seem to be an example of a strongly correlated electronic system, which cannot be described by conventional Fermi-liquid theory. One of the unusual normal-state properties is the resistivity, which is proportional to temperature over a large range of temperature. The superconducting state is in some sense less unusual than the normal state, because in many respects it behaves like a BCS superconductor, but with an unusual pairing mechanism. The onset of superconductivity occurs at temperatures that are so high, that the pairing between electrons cannot be solely due to phonons. Moreover, microwave measurements of the quasi-particle contribution to the conductivity have shown that the scattering rate decreases strongly below T_c , which is inconsistent with a scattering mechanism due to phonons [48]. It is therefore more likely that the pairing mechanism has an unconventional origin, which could be magnetism. This is further supported by experimental reports of gapless excitations

[48, 49, 50, 51, 52], and even evidence for a d -wave symmetry of the order parameter [53]. Another peculiar aspect of the superconducting state is that it only occurs in an intermediate range of doping of $0.05 \lesssim x \lesssim 0.3$, but disappears when the doping is too small or too big.

Many of the microscopic models that have been proposed to describe the properties of the high- T_c copper-oxides are based on the two dimensional Hubbard model or the t - J model [13, 14]. In the case of the t - J model one can obtain a crude approximation of the onset of superconductivity, by means of a BCS-like mean-field decoupling of the Hamiltonian. Several mean-field phases have been suggested, and depending on the doping and temperature different phases can be energetically favored [7, 15, 16, 17, 18, 19, 22, 23, 24, 27]. In general these mean-field phases predict a pairing-transition temperature of the order of $T_c^0 \simeq 0.15J$ close to half-filling, which corresponds to a temperature of several hundred degrees Kelvin. The reason for this overestimate of T_c is that a simple mean-field theory ignores fluctuations, which are very important in a strongly correlated system.

We will take the gauge-field formulation of the t - J model as our starting point, which goes beyond mean-field theory by including Gaussian fluctuations of a gauge field [23, 33, 35, 37, 54]. The gauge-field model has been successful in explaining some of the normal-state properties, such as the linear resistivity, in the regime above the Bose-condensation temperature [33, 35, 37]. So far little work has been done on what the effect is of the gauge field on the superconducting state. This article will focus on how the interaction with the gauge field can suppress the pairing-transition temperature to a temperature scale that agrees more with the experimental values of $T_c \lesssim 100K$. The main argument for this suppression is that the gauge field introduces an additional term in the free energy [55], which opposes the opening of a superconducting gap. Our numerical calculations show that this suppression is very significant, and that in fact superconductivity only survives at an intermediate range of doping, with a maximum T_c at a doping of $x \simeq 0.15$.

4.2 The role of gauge-field fluctuations in the t - J model

In this section we will first give a quick review of how the gauge-field model is derived from the t - J model. We refer to other papers for a more lengthy discussion of this derivation [23, 35, 32, 54]. Our starting point is the t - J model on a square lattice

$$H = -t \sum_{\langle i,j \rangle \sigma} c_{i\sigma}^\dagger c_{j\sigma} + J \sum_{\langle i,j \rangle} (\mathbf{S}_i \cdot \mathbf{S}_j - \frac{1}{4} n_i n_j), \quad (4.1)$$

where $\mathbf{S}_i = \frac{1}{2} c_{i\alpha}^\dagger \boldsymbol{\sigma}_{\alpha\beta} c_{j\beta}$ and $n_i = \sum_{\sigma} c_{i\sigma}^\dagger c_{i\sigma}$. This Hamiltonian is under the important constraint that no site is double occupied. In order to satisfy this constraint we employ the slave-boson formalism [56, 57], in which the electron operator $c_{i\sigma}^\dagger$ is replaced by $c_{i\sigma}^\dagger = f_{i\sigma}^\dagger b_i$. The boson operator b_i^\dagger keeps track of the empty sites, and the fermion operator $f_{i\sigma}^\dagger$ carries the spin [15, 17]. The constraint of no double occupancy is satisfied by requiring that $b_i^\dagger b_i + \sum_{\sigma} f_{i\sigma}^\dagger f_{i\sigma} = 1$ at each site i . In order to get a superconducting state in the slave-boson picture it is not sufficient that the fermions form Cooper-pairs, but the bosons have to be Bose condensed as well.

The gauge-field model is obtained from Eq. (4.1) by decoupling the hopping term and the Heisenberg term using Hubbard-Stratonovich fields, and then making the approximation of only considering fluctuations of the phase of one of these new fields. Denoting the Hubbard-Stratonovich fields by $\xi_{ij} = \xi e^{ia_{ij}}$ and $\Delta_{ij} = \pm \Delta_0$, this leads to the Hamiltonian [7, 17]

$$H = \frac{1}{2} \sum_{\langle i,j \rangle} \left[\frac{3J}{4} |\xi|^2 + \frac{4}{3J} |\Delta_0|^2 - \xi e^{-ia_{ij}} \left(\frac{3J}{4} f_{i\sigma}^\dagger f_{j\sigma} + 2t b_i^\dagger b_j \right) - \text{c.c.} - \Delta_{ij}^* (f_{i\uparrow} f_{j\downarrow} - f_{i\downarrow} f_{j\uparrow}) - \text{c.c.} \right] \\ + \frac{8t^2}{3J} \sum_{\langle i,j \rangle} b_i^\dagger b_j b_j^\dagger b_i - \mu_0 \sum_i f_{i\sigma}^\dagger f_{i\sigma} - i \sum_i \lambda_i (f_{i\sigma}^\dagger f_{i\sigma} + b_i^\dagger b_i - 1), \quad (4.2)$$

where λ_i is a Lagrange-multiplier field that enforces the local constraint $b_i^\dagger b_i + f_{i\sigma}^\dagger f_{i\sigma} = 1$. The role of the field a_{ij} will be discussed later on.

We will first consider the mean-field solution of this Hamiltonian, which corre-

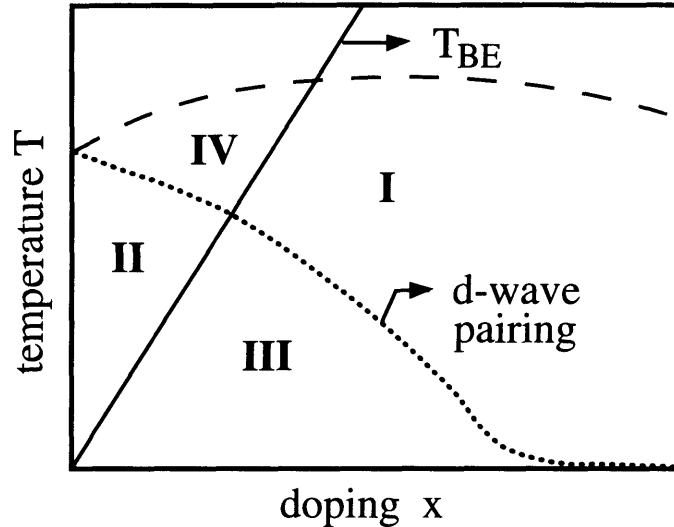


Figure 4-1: A schematic mean-field phase diagram of the t - J model. Below the dashed line the uniform RVB-order parameter ξ is nonzero. The mean-field pairing line (dotted) and the Bose-condensation line (solid) divide the phase diagram into four regions. Region I is a Fermi-liquid phase, region II is the spin-gap phase, region III is the superconducting phase, and region IV is the strange metal phase. In this paper we argue that the spin-gap phase is destroyed by gauge field fluctuations.

sponds to $a_{ij} = 0$. At the mean-field level $i\lambda_i = \mu_B$ plays the role of a chemical potential for the bosons, and μ_B is chosen such that the average boson density is equal to the doping concentration x . The mean-field phase diagram is schematically shown in Fig. 4-1 [34, 35, 58]. Below the dashed line the uniform RVB-order parameter ξ is nonzero. At a lower temperature, denoted by the dotted line, d -wave pairing between fermions occurs, i.e. $\Delta_{i,i+\hat{x}} = -\Delta_{i,i+\hat{y}} = \Delta_0$. Below the solid line the bosons condense into a superfluid state. According to mean-field theory Bose condensation occurs at a temperature scale given by $T_{BE}^0 \simeq 2\pi x/m_B$, where $1/m_B = 2t\xi$. The mean-field phase diagram divides naturally into four regions. Region I with $\langle b \rangle \neq 0$ is a Fermi-liquid phase. Region II with $\Delta_0 \neq 0$ but $\langle b \rangle = 0$ is called the *spin-gap* phase, because an anisotropic gap appears in the fermion spectrum which represents the spin degrees of freedom. In region III both Δ_0 and $\langle b \rangle$ are nonzero, so that d -wave pairing between physical electrons occurs, resulting in a superconducting phase. Region IV has been called the *strange metal* phase, because it exhibits some of the unusual properties of the normal state of the high- T_c copper-oxides [34, 35].

Since $f_{i\sigma}$ and b_i are fictitious entities, the only true phase boundary in Fig. 4-1 is the transition to the superconducting state in region III. Nevertheless it is possible that the other transition lines single broaden to cross-over lines, such that one can still identify the regions I, II and IV in the phase diagram, characterized by the physical properties described above. In particular much attention has been paid to the spin-gap phase, because NMR and susceptibility experiments indicate the appearance of a gap in the spin excitation spectrum in a temperature range above the superconducting T_c in underdoped materials. On the other hand, a recent analysis of the data by Millis and Monien indicated that the spin-gap phase may be absent in simple layer materials such as $\text{La}_{2-x}\text{Sr}_x\text{CuO}_4$, and present in double layer materials such as the YBCO compounds [59]. Thus the identification of the spin-gap phase with region II is quite uncertain at this point.

A serious difficulty with the schematic mean-field diagram shown in Fig. 4-1 is that the temperature scale for Bose condensation is much too high, if one uses the mean-field expression $T_{\text{BE}}^0 \simeq 4\pi t \xi x$. Furthermore, close to half-filling ($x \lesssim 0.04$) the d -wave pairing state is unstable to more complicated phases, such as dimerized phases [18, 19, 23], incommensurate flux phases [24] and staggered flux phases [7, 27]. We restrict our attention to $x \gtrsim 0.04$, which is indicated by the shaded region in Figs. 4-2 and 4-3. The dotted line in this phase diagram is the mean-field transition to a d -wave pairing state. On the same plot the T_{BE}^0 -line would lie entirely *inside* the shaded area.

For non-interacting bosons Bose condensation does not really exist in two dimensions, but one can still consider T_{BE}^0 as a cross-over temperature below which the boson susceptibility diverges exponentially:

$$\chi_B^0 = \frac{1}{24\pi m_B} \left(e^{T_{\text{BE}}^0/T} - 1 \right). \quad (4.3)$$

It has been argued that the characteristic temperature scale for the increase in χ_B will be strongly suppressed by fluctuations around the mean-field solution [8, 33, 39, 41, 42, 43].

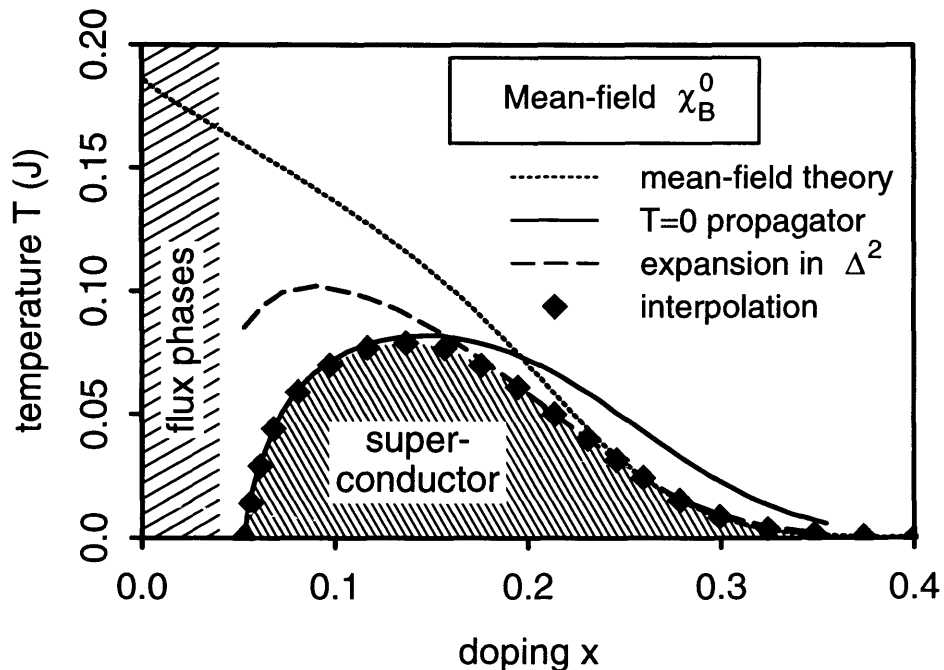


Figure 4-2: The phase-diagram of the t - J model for $t/J = 3$ using a mean-field expression for the susceptibility χ_B^0 , given by Eq. (4.3). The self-consistent dissipative model χ_B^{SC} produces a phase diagram that is essentially indistinguishable. The solid line for $T_c(x)$ uses $T = 0$ expressions for the propagator $\Pi_F(\nu)$ (see Sec. 4.3.1), while the dashed line is obtained by expanding $\text{Im } \Pi_F(\nu)$ and $\text{Re } \Pi_F(\nu)$ in Δ_0^2 (see Sec. 4.3.2). The first-order jump in Δ_0 at the transition is quite small for $x \gtrsim 0.1$, and hence the expansion in small Δ_0^2 (dashed line) is a good approximation in this case. For $x \lesssim 0.1$ the first-order jump in Δ_0 becomes so large, that the solid line is more appropriate. The line denoted by black diamonds is our best guess of the correct phase boundary within this model. For $x \lesssim 0.05$ superconductivity vanishes completely, which is directly related to the fact that the gauge field becomes unstable against flux phases for $x \lesssim 0.04$. For $x \gtrsim 0.2$ the gauge field becomes so stiff, that the transition line $T_c(x)$ approaches the d -wave BCS value $T_c^0(x)$ (dotted line).

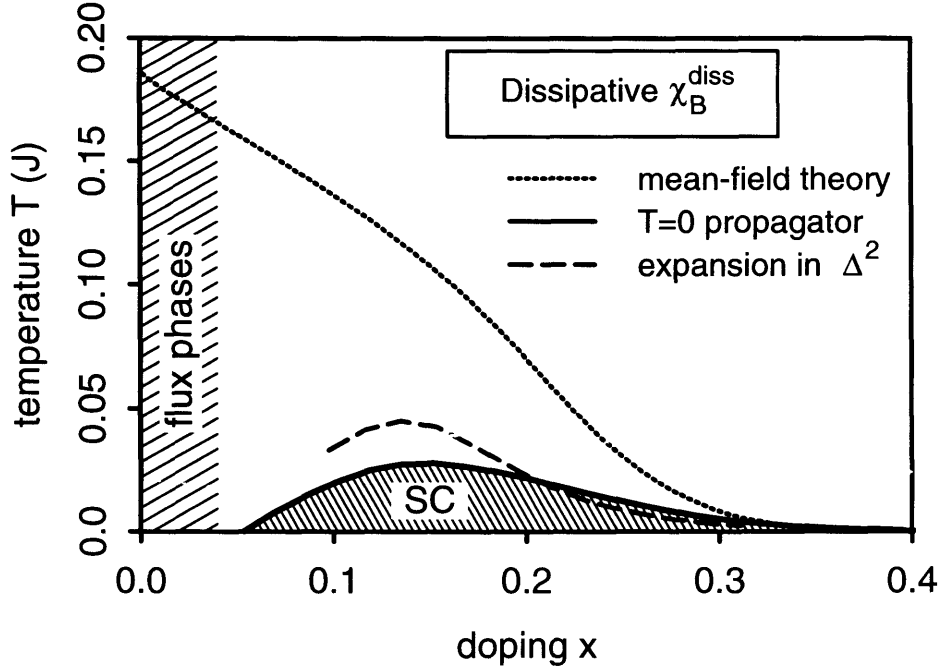


Figure 4-3: The phase-diagram of the t - J model in the doping-temperature plane for $t/J = 3$, using the dissipative model for the susceptibility χ_B^{diss} . The solid line for $T_c(x)$ uses $T = 0$ expressions for the propagator $\Pi_F(\nu)$, while the dashed line is obtained by expanding $\text{Im}\Pi_F(\nu)$ and $\text{Re}\Pi_F(\nu)$ in Δ_0^2 . The $T = 0$ approximation for the propagator (solid line) is more appropriate, because of the large first-order jump in Δ_0 at the transition. In the underdoped case the susceptibility χ_B^{diss} is relatively small at the transition, so this model predicts a direct transition from a strange metal to a superconducting phase. Note that in this phase diagram the transition temperature $T_c(x)$ is much lower than in Fig. 4-2. This is directly related to the fact that in the dissipative model Bose condensation occurs at a much lower temperature than if one uses χ_B^0 or χ_B^{SC} (see Fig. 4-4). For large doping $x \gtrsim 0.35$ the gauge field becomes so stiff, that the transition line $T_c(x)$ approaches $T_c^0(x)$ (dotted line).

We will now discuss how fluctuations alter the mean-field results mentioned above. We will restrict our analysis to Gaussian fluctuations of the phase a_{ij} of the RVB-order parameter ξ_{ij} , which is a massless Goldstone-mode. The field a_{ij} is called a gauge field, because the Hamiltonian (4.2) is invariant under the local gauge transformation [23]

$$\begin{aligned}
f_{i\sigma} &\longrightarrow f_{i\sigma} e^{i\theta_i} \\
b_i &\longrightarrow b_i e^{i\theta_i} \\
a_{ij} &\longrightarrow a_{ij} + \theta_i - \theta_j
\end{aligned}
\tag{4.4}$$

We will chose to work in the Coulomb gauge $\nabla \cdot \mathbf{a} = 0$, in which case the gauge-field propagator $\Pi_{\mu\nu}(q) = (\delta_{\mu\nu} - p_\mu p_\nu / p^2) \Pi(q)$ is purely transverse. Here we defined $\mu_\mu = 2 \sin q_\mu / 2$ to take the lattice structure into account. The Lagrange multiplier field λ_i can be considered as the time component of the gauge field [23, 35]. In this paper we will simply replace $i\lambda_i$ by its saddlepoint value μ_B , which will serve as the chemical potential of the bosons. The gauge field couples to both the fermions and the bosons, so one expects that both the d -wave pairing-line and the Bose-condensation line in Fig. 4-1 will be affected by the fluctuating gauge field [35]. While the main topic of this paper concerns the coupling of the fermions to the gauge field, this problem cannot be addressed without considering the coupling of the bosons to the gauge field as well.

The coupling of the bosons to the gauge field is a strong-coupling problem in the physically interesting case of $t/J > 1$, and is therefore difficult to analyze. This was illustrated by a diagrammatic analysis of Ioffe and Kalmeyer [39], who calculated the lowest-order gauge-field correction to the diamagnetic susceptibility χ_B . They showed that this correction becomes very large if one approaches the Bose-condensation temperature T_{BE}^0 , at which point the perturbative analysis becomes unreliable. The problem has also been treated by a renormalization group analysis [8] and by path-integration methods, assuming that $\text{Re}\Pi(q) \propto q^2$. It was pointed out that the fluctuating gauge field tends to reduce the projected area of Feynman

paths, so that the path-integral is dominated by almost retracing paths [36]. Wheatley and co-workers [41, 42, 43] did a further analysis of the path-integral formulation, by making the rather drastic approximation of relating the problem to one where the bosons couple to a dissipative bath. This problem of non-interacting bosons coupled to a heat bath with a damping time τ_0 can be solved exactly. For strong coupling, i.e. for $\tau_0^{-1} \gg k_B T$, the boson susceptibility χ_B is given by [43]

$$\chi_B = \frac{\tau_0 x}{\pi m_B^2}. \quad (4.5)$$

It is tempting to identify τ_0^{-1} with the transport scattering rate of the bosons by the gauge field, which is given in Born approximation by $\tau_0^{-1} \simeq k_B T / 4m_B \chi$. If we further follow Wheatley *et al.* and replace χ by the free fermion expression $\chi_F^0 = 1/(12\pi m_F)$, we obtain

$$\chi_B^{\text{diss}} \simeq \frac{2\chi_F^0 T_{\text{BE}}^0}{\pi^2 T}. \quad (4.6)$$

We will refer to this result as the *dissipative* model. Note that χ_B^{diss} diverges only as T^{-1} , as opposed to the exponential growth of χ_B^0 given by Eq. (4.3).

We believe that Eq. (4.6) grossly overestimates the effect of the gauge-field fluctuations for at least the following reason. The susceptibility χ that controls the strength of the gauge-field fluctuations is the sum $\chi_F + \chi_B$, where χ_B should be treated self-consistently. Note that this self-consistency is missing in Eq. (4.6), because χ was simply replaced by χ_F . As χ_B grows τ_0^{-1} is reduced so that the dissipation crosses over to the weak-coupling limit, and Eq. (4.5) no longer applies. We have carried out a self-consistent calculation of χ_B , where we used the full solution of the susceptibility valid for arbitrary τ_0 . The resulting self-consistent χ_B^{SC} is shown in Fig. 4-4. A recent analysis based on self-retracing Feynman paths yields qualitatively the same results [9].

The value of χ_B^{SC} (solid line) lies between χ_B^0 (dotted line) and χ_B^{diss} (dashed line), and diverges exponentially below a temperature which is a fraction of T_{BE}^0 . In the absence of a full theory, we believe that χ_B^{SC} is a reasonable guess of the behavior of the boson susceptibility, which we can use in the interim. We have to keep in mind

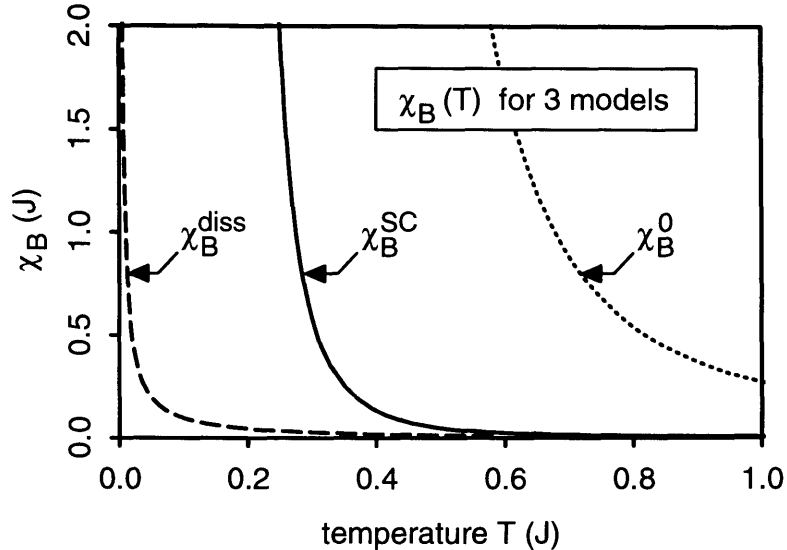


Figure 4-4: The boson susceptibility $\chi_B(T)$ for three different models for a doping $x = 0.07$. The fact that $\chi_B(T)$ increases rapidly at low temperatures indicates that the bosons effectively condense into a superfluid state below a certain crossover temperature. The dotted line is the mean-field value χ_B^0 , given by Eq. (4.3). The dashed line represents the dissipative model for χ_B^{diss} , given by Eq. (4.6), which we believe grossly overestimates the effectiveness of the gauge field to suppress Bose condensation. The solid line is the self-consistent dissipative χ_B^{SC} , which takes into account that a large χ_B stiffens the gauge field. In the absence of a full theory χ_B^{SC} is a reasonable guess for the behavior of the susceptibility $\chi_B(T)$. We however believe that at low doping χ_B^{SC} underestimates the suppression of Bose condensation.

however that at low doping χ_B^{SC} is probably too large, because the self-consistent dissipative model assumes that $\Pi_B(q) = \chi_B q^2$ [43], while in reality $\Pi_B(q)$ levels off to $\rho_S = x/m_B$ for large q . This means that when ρ_S is small the self-consistent dissipative model underestimates the gauge-field fluctuations for large regions of \mathbf{q} space, resulting in a susceptibility χ_B^{SC} that is too large.

In this paper we have carried out the calculation of the phase diagram using all three different choices for χ_B . For reasons to be explained below, it turns out that χ_B^0 and χ_B^{SC} yield practically indistinguishable phase boundaries for the onset of superconductivity. That result is shown in Fig. 4-2. For completeness the phase boundary using χ_B^{diss} is shown in Fig. 4-3.

The main result of this paper is that *quantum* fluctuations of the gauge field are very effective in suppressing the pairing between fermions. In fact, the suppression is

so effective that the spin-gap phase (region II in Fig. 4-1) is destroyed completely, and only a direct transition to a d -wave pairing state remains. The transition temperature T_c is reduced compared to the mean-field value T_c^0 , and T_c vanishes completely at low doping. The result of our numerical calculation of T_c is shown in Figs. 4-2 and 4-3. Before going into any technical details, we give a qualitative discussion of the physics behind this suppression. The coupling of the fermions to the gauge field is very much analogous to the coupling of electrons to an electromagnetic field, except that the magnitude of the dimensionless coupling constant is very different. The dimensionless coupling constant is very small for an electromagnetic gauge field, but of order unity in the t - J model. It is known that in metals the low-lying excitations associated with a fluctuating gauge field give rise to a large negative contribution to the free energy, so that the specific heat in three dimensions varies as $T \log T$ [60]. In ordinary metals this is a small effect because it is proportional to v_F^2/c^2 , and has not yet been observed. This small factor is absent in the t - J model, which makes these fluctuations very important. In two dimensions the specific heat varies as $T^{2/3}$, implying a free energy term F_{gauge} proportional to $T^{5/3}$. The importance of the gauge-field contribution to the free energy has been pointed out by Hlubina *et al.* [55], who showed that the contribution from the transverse gauge-field fluctuations, together with the longitudinal gauge-field fluctuations, brings the mean-field free energy much closer to that given by high temperature expansions. Unlike the transverse mode, the longitudinal mode does not give rise to singular corrections at low temperatures, because it is screened. We will therefore ignore the longitudinal contribution to the free energy in what follows below.

In a pairing state a gap Δ opens up in the fermion spectrum. This introduces a gap in the gauge-field excitation spectrum as well, so that gauge-field modes with frequencies less than 2Δ do not contribute to the free energy, resulting in a net free energy cost. We can estimate the free energy cost δF_{gauge} by replacing the temperature cutoff in F_{gauge} by Δ , resulting in $\delta F_{\text{gauge}} \propto \Delta^{5/3}$. On the other hand the BCS-like free energy gain from pairing is proportional to Δ^2 , so that δF_{gauge} always dominates, at least for small enough Δ . This situation will change when the boson susceptibility

becomes so large that the bosons effectively condense into a superfluid state. In that case the gauge field becomes effectively massive, with a stiffness equal to the superfluid density $\rho_S \simeq x$ of the bosons, due to the Anderson-Higgs mechanism. The gauge field is then so stiff that F_{gauge} is no longer dominating, and its role in suppressing fermion pairing disappears. We expect then a direct transition to a superconducting phase with d -wave pairing between physical electrons.

This qualitatively explains the phase diagrams shown in Figs. 4-2 and 4-3, which were obtained by a detailed numerical calculation to be described in the rest of the paper. We see in Figs. 4-2 and 4-3 that in contrast to the mean-field solution, T_c now vanishes for sufficiently low doping $x \lesssim 0.05$. For larger doping the stiffness of the gauge field increases and it becomes less effective in suppressing pairing. Therefore for large doping $x \gtrsim 0.2$ the transition line $T_c(x)$ is close to the mean field line $T_c^0(x)$, as one can see in Figs. 4-2 and 4-3. At low doping the phase diagram now describes a direct transition from a metallic phase to a superconducting state, by-passing the spin-gap phase. This implies that we have to look beyond the single layer t - J model for an explanation of the spin-gap phase in bi-layer materials, in agreement with the analysis of Millis and Monien mentioned earlier [59]. In the overdoped region $x \gtrsim 0.2$ we expect a direct transition from a Fermi-liquid phase, i.e. a phase in which the bosons are Bose condensed, to a superconducting state.

Another consequence of our numerical analysis is that we expect the transition to be first-order, with a relatively large jump of Δ . Of course, in practice the transition will be rounded off by phase fluctuations of the pairing field Δ_{ij} , which are not considered in this analysis. Therefore the calculation presented here should be considered as a calculation of the mean-field T_c as far as two dimensional fluctuations in the pairing field Δ_{ij} are concerned.

In the remainder of this paper we will describe the details of our calculation of F_{gauge} and its dependence on Δ_0 . In section 4.3 we derive a formal expression for the free energy $F_{\text{gauge}}(\Delta_0)$, which will be analyzed in two limiting cases in sections 4.3.1 and 4.3.2. We present our numerical analysis in section 4.4. This numerical analysis takes several important aspects of the t - J model into account, that we did not discuss

so far. For instance, an important role is played by the d -wave symmetry of the gap function $\Delta(\mathbf{k})$ and the non-spherical Fermi surface. These anisotropies have a large effect on the free energy F_{gauge} , and are taken fully into account in our numerical analysis described in section 4.4.

4.3 The gauge-field contribution to $F(\Delta_0)$ in the presence of a gap

We now present a detailed calculation of the gauge-field contribution to the free energy in the presence of pairing between the fermions. In the presence of a gauge field the onset of pairing is still determined by minimizing the total free energy $F_{\text{tot}}(\Delta_0)$, analogous to BCS-theory. However, the total free energy will now have a contribution from the gauge field as well [55]. We note that the free energy is a gauge invariant quantity, and is free of the singularities that plague quantities that are not gauge invariant, such as the fermion Green function [38]. This is why we choose to analyze $F_{\text{tot}}(\Delta_0)$, rather than a diagrammatic study of the pairing amplitude in the presence of a gauge field.

We will calculate $F_{\text{tot}}(\Delta_0)$ using the following procedure. First we integrate over the matter fields $f_{i\sigma}$ and b_i , which leads to an effective action $S_{\text{eff}} = \beta F_{\text{MF}}(\Delta_0) + S_{\text{gauge}}[a]$, where

$$\begin{aligned}
F_{\text{MF}}(\Delta_0) &= \frac{3J}{4}\xi^2 + \frac{4}{3J}\Delta_0^2 - 2T \int \frac{d^2\mathbf{k}}{(2\pi)^2} \log(\cosh(E_k/2T)) \\
&\quad + T \int \frac{d^2\mathbf{k}}{(2\pi)^2} \log(1 - e^{-\Omega_k/T}) \\
S_{\text{gauge}}[a] &= \frac{T}{2} \sum_{i\nu_n} \int \frac{d^2\mathbf{q}}{(2\pi)^2} \Pi_{\mu\nu}(\mathbf{q}, i\nu_n) a_q^\mu a_{-q}^\nu.
\end{aligned} \tag{4.7}$$

The dispersion relations $E_k = \sqrt{\epsilon_k^2 + \Delta_k^2}$ for the fermions and Ω_k for the bosons are given by

$$\Omega_k = 2t\xi(\cos k_x + \cos k_y) - \mu_B;$$

$$\begin{aligned}\epsilon_{\mathbf{k}} &= \frac{3J\xi}{4}(\cos k_x + \cos k_y) - \mu_F; \\ \Delta_{\mathbf{k}} &= \Delta_0(\cos k_x - \cos k_y).\end{aligned}\tag{4.8}$$

Finally we obtain the total free energy $F_{\text{tot}}(\Delta_0) = F_{\text{MF}}(\Delta_0) + F_{\text{gauge}}(\Delta_0)$, by integrating over the gauge field in the action $S_{\text{gauge}}[a]$. By distorting the contour integral and noting that the analytical continuation of $\log \Pi(\mathbf{q}, i\nu_n)$ has a branch-cut along the real axis, one finds that the contribution of the gauge field to the free energy can be written as

$$F_{\text{gauge}}(\Delta_0) = \int \frac{d^2q}{(2\pi)^2} \int_0^\infty \frac{d\nu}{2\pi} [2n_B(\nu) + 1] \arctan \left(\frac{\text{Im } \Pi(q, \nu + i\delta, \Delta_0)}{\text{Re } \Pi(q, \nu + i\delta, \Delta_0)} \right), \tag{4.9}$$

where $n_B(\nu) = (e^{\nu/k_B T} - 1)^{-1}$ is the Bose-occupation number. For $\Delta_0 = 0$, Eq. (4.9) is equivalent to the expression written down by Hlubina *et al.* [55]. Notice that while Hlubina *et al.* needed a regularization scheme to keep F_{gauge} finite, we avoided the infinite constant by taking the analytical continuation $i\nu_n \rightarrow \nu + i\delta$.

The opening of a gap Δ_0 will mostly affect the fermionic contribution to the total gauge-field propagator $\Pi = \Pi_F + \Pi_B$. In the normal state Π_F has the form $\Pi_F(\mathbf{q}, \nu) = \chi_F p^2 - i\gamma_F(\mathbf{q})\nu/p$, where we defined $p_\mu = 2 \sin q_\mu/2$ to take the lattice structure of the t - J model into account. The fermion susceptibility χ_F is given by

$$\chi_F = -\frac{1}{12} \int \frac{d^2k}{(2\pi)^2} \frac{\partial^2 \epsilon_k}{\partial k_x^2} \frac{\partial^2 \epsilon_k}{\partial k_y^2} f'(\epsilon_k).\tag{4.10}$$

Notice that χ_F is negative for the t - J model for any doping $x \lesssim 0.5$, which indicates that the uniform phase $\xi_{ij} = \xi$ is unstable towards flux phases close to half-filling [7]. Away from half-filling the uniform phase regains its stability, because the sum $\chi = \chi_F + \chi_B$ becomes positive as soon as the density of bosons is sufficiently large. The damping parameter $\gamma_F(\mathbf{q})$ is a finite number which depends on the direction of \mathbf{q} , and for the t - J model close to half-filling $\gamma_F(\mathbf{q})$ is small in the $(1, 0)$ -direction, but strongly enhanced in the $(1, 1)$ -direction.

When a gap Δ_0 opens up the propagator $\Pi_F(\mathbf{q}, \nu)$ will be modified, which will

change the free energy F_{gauge} in Eq. (4.9). The most obvious change in the propagator is that $\Pi_F(q=0)$ becomes massive with a mass proportional to Δ_0^2 . This is responsible for the Meissner effect in ordinary superconductors. The effect of this mass term on the free energy has been discussed earlier by Halperin *et al.* [61] in the context of a fluctuating electromagnetic field in a BCS superconductor. Their work was a classical calculation, based on a Ginzburg-Landau free energy. They argued that this mass term in $\text{Re}\Pi_F$ gives rise to an additional term in the free energy, that is non-analytic in Δ^2 . This implies that the superconducting transition must be a first-order transition.

We are more interested in the question how the total free energy is influenced by *quantum* fluctuations of the gauge field. We therefore need to know how a nonzero gap modifies the propagator $\Pi_F(\nu)$ at *finite* frequencies. We first consider $\Pi_F(\nu)$ in the normal state, i.e. without a gap. To get a simple estimate of $F_{\text{gauge}}(\Delta_0=0)$ we consider first for simplicity an isotropic band structure, in which case $\Pi_F(q, \nu+i\delta) = \chi_F q^2 - ik_F \nu/q$ for $\nu < k_F q/m_F$. We further concentrate on the *quantum fluctuations* in Eq. (4.9), i.e. $\nu > k_B T$, so that $2n_B + 1$ may be replaced by unity. In the normal state we approximate F_{gauge} by

$$F_{\text{gauge}}(\Delta_0=0) \simeq - \int \frac{d^2 q}{(2\pi)^2} \int_{k_B T}^{k_F q/m_F} \frac{d\nu}{2\pi} \arctan\left(\frac{k_F \nu}{\chi q^3}\right). \quad (4.11)$$

This is a large negative quantity, which is finite because \mathbf{q} is restricted to the first Brillouin zone. We are interested in how this quantity depends on the lower cut-off $k_B T$ in the frequency integral. For small frequencies $\nu \ll \chi k_F^2$ the q integration can be done first, which yields a factor proportional to $(k_F \nu/\chi)^{2/3}$. The ν integration then yields a large negative term plus a $T^{5/3}$ correction due to the lower cut-off at $k_B T$.

When a gap Δ opens up both the real and imaginary part of the propagator are modified, and in general $\text{Im}\Pi_F(\nu)$ and $\text{Re}\Pi_F(\nu)$ become very complicated functions of the frequency ν , especially when the gap $\Delta(\mathbf{k})$ is anisotropic. Before studying the general case, we will first consider the simpler case of an isotropic gap at $T=0$. In that case the propagator is modified by the gap as follows.

- Low-lying gauge-field modes with $\nu < 2\Delta$ are undamped, i.e. $\text{Im } \Pi_F = 0$ for $\nu < 2\Delta$ (at $T = 0$). In ordinary superconductors this is responsible for the anomalous skin effect [62, 63].
- The real part of $\Pi_F(q, \nu)$ is enhanced, which stiffens the gauge field.

We now see that this change in $\text{Im } \Pi_F(\nu)$ and $\text{Re } \Pi_F(\nu)$ gives rise to a huge cost in the free energy. From the discussion following Eq. (4.11) we learned that in the normal state all gauge-field modes give a negative contribution to the free energy $F_{\text{gauge}}(\Delta = 0)$. When an isotropic gap $\Delta \gg T$ opens up the gauge-field modes with frequencies $\nu < 2\Delta$ do not contribute to the free energy anymore. The ν integral in Eq. (4.11) is now cut-off by Δ instead of $k_B T$, so that a free energy cost of $\Delta^{5/3}$ results. This free energy cost is in general much larger than the free energy gain coming from $F_{\text{MF}}(\Delta)$, which is proportional to Δ^2 . This implies that due to low-lying gauge-field fluctuations it is not favorable anymore to open up a gap Δ , and hence the superconducting transition temperature will be suppressed.

We now turn to the calculation of $\text{Im } \Pi_F(\nu)$ and $\text{Re } \Pi_F(\nu)$ in the general case of an anisotropic gap $\Delta(\mathbf{k})$ at finite temperatures. The calculation is analogous to the calculation of the complex conductivity in a BCS superconductor, which was first performed by Mattis and Bardeen [62, 63], and by Abrikosov and Gorkov [64]. Their results were originally meant for an s -wave gap $\Delta(\mathbf{k}) = \Delta$, but it is a straightforward exercise to generalize these expressions to the anisotropic case of a d -wave gap $\Delta(\mathbf{k})$ [65]. We will do our calculations in the extreme anomalous limit (i.e. $1/q$ much larger than the coherence length), which is the appropriate limit in our case. In this limit one obtains

$$\begin{aligned}
\text{Im } \Pi_F(\mathbf{q}, \nu) &= -\frac{\gamma_F(\mathbf{q})}{q} \left[\int_{|\Delta|, |\Delta'|-\nu}^{\infty} + \int_{-\infty}^{-|\Delta|, -|\Delta'|-\nu} + \theta(\nu - |\Delta| - |\Delta'|) \int_{|\Delta'|-\nu}^{-|\Delta|} \right] \\
&\quad \times (f(E) - f(E + \nu)) \left| \frac{E(E + \nu) + \Delta\Delta'}{[E^2 - \Delta^2]^{\frac{1}{2}} [(E + \nu)^2 - \Delta'^2]^{\frac{1}{2}}} \right| dE \quad (4.12) \\
\text{Re } \Pi_F(\mathbf{q}, \nu) &= \frac{\gamma_F(\mathbf{q})}{q} \int dE \left[-\frac{E(E + \nu) + \Delta\Delta'}{[\Delta^2 - E^2]^{\frac{1}{2}} [(E + \nu)^2 - \Delta'^2]^{\frac{1}{2}}} f(E + \nu) \right]
\end{aligned}$$

$$+ \frac{E(E + \nu) + \Delta\Delta'}{[\Delta'^2 - E^2]^{\frac{1}{2}}[(E + \nu)^2 - \Delta^2]^{\frac{1}{2}}} f(-E - \nu) \Big] \text{sign}(E + \nu), \quad (4.13)$$

where $\Delta = \Delta_0 \varphi_{\mathbf{k}+\mathbf{q}/2}$ and $\Delta' = \Delta_0 \varphi_{\mathbf{k}-\mathbf{q}/2}$ ($\varphi_{\mathbf{k}} = \cos k_x - \cos k_y$). Here we must choose \mathbf{k} such that $\mathbf{k} \pm \mathbf{q}/2$ are on the Fermi surface, so that Δ and Δ' are completely determined by \mathbf{q} . The lower limit in the first integral in Eq. (4.12) is the maximum of $|\Delta|$ and $|\Delta'| - \nu$. Similarly the integrals in Eq. (4.13) are restricted to those values of E , for which the arguments of the square roots are positive. For $\Delta = \Delta'$ the Eqs. (4.12) and (4.13) reduce to the expressions given by Mattis and Bardeen [62]. At $T = 0$ only the last integral in Eq. (4.12) survives, and therefore $\text{Im } \Pi_F$ is only nonzero for $\nu > |\Delta| + |\Delta'|$.

In principle we would like to solve for $F_{\text{gauge}}(\Delta_0)$, by combining Eqs. (4.9), (4.12) and (4.13). However, doing this while taking full account of the anisotropic d -wave gap and the non-spherical Fermi surface is a complex numerical problem. Instead we will study two limiting cases for the propagator $\Pi_F(\nu, \Delta, \Delta')$. We will first consider the zero temperature limit (i.e. $T \ll \Delta_0$), which is the simplest case to understand from a physical point of view. We will later consider the opposite limit $\Delta_0 \ll T$, to study the possibility of a second-order transition.

4.3.1 The propagator at $T = 0$

The objective of this section is to give an estimate of $F_{\text{gauge}}(\Delta_0)$, using zero temperature expressions for $\text{Im } \Pi_F(\nu)$ and $\text{Re } \Pi_F(\nu)$. The dependence of $\text{Im } \Pi_F(\nu)$ and $\text{Re } \Pi_F(\nu)$ on the gap Δ_0 at $T = 0$ is shown in Figs. 4-5 and 4-6, for various values of $\Delta'/\Delta = \Delta(\mathbf{k}-\mathbf{q}/2)/\Delta(\mathbf{k}+\mathbf{q}/2)$. For $q \rightarrow 0$ one always has $\Delta'/\Delta \simeq 1$, and $-\text{Im}\Pi_F(\nu)$ is suppressed for all ν , even for $\nu > |\Delta| + |\Delta'|$. However for large q it is possible that $\Delta\Delta' < 0$, in which case $-\text{Im } \Pi_F(\nu)$ is actually *enhanced* for $\nu > |\Delta| + |\Delta'|$. This is an important point to make, because this means that while scattering processes that involve a small momentum transfer are pair-breaking, scattering processes with a large momentum transfer can have exactly the opposite effect. The dependence of $\text{Re } \Pi_F(\nu)$ on Δ_0 shows a similar behavior (see Fig. 4-6), in the sense that $\text{Re } \Pi_F(\nu)$

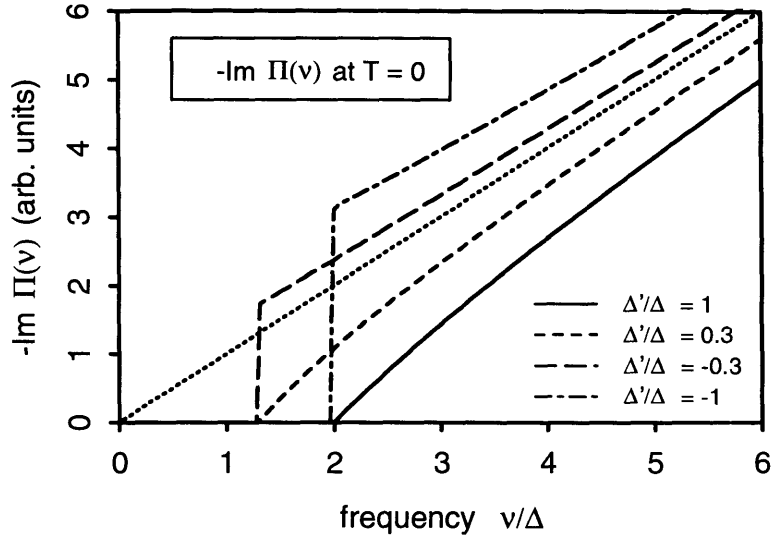


Figure 4-5: This figure shows $\text{Im } \Pi_F(\nu)$ at $T = 0$ for $\Delta'/\Delta = 1, 0.3, -0.3$ and -1 . Notice that there is no absorption for $\nu < |\Delta| + |\Delta'|$. For $\nu > |\Delta| + |\Delta'|$ it depends on the relative sign of Δ and Δ' whether $\text{Im } \Pi_F(\nu)$ is enhanced or suppressed by the gap. The dotted line is the normal state ($\Delta = 0$) value.

in Eq. (4.13) is positive when $\Delta\Delta' > 0$ and negative when $\Delta\Delta' < 0$.

We will initially ignore the anisotropy of the gap, which is a valid assumption as long as the important momenta \mathbf{q} are small compared to the size of the Brillouin zone. The most important feature of $\text{Im } \Pi_F(\nu, \Delta_0)$ is then that $\text{Im } \Pi_F(\nu) = 0$ for $\nu < 2\Delta_0$, so that gauge-field modes with $\nu < 2\Delta_0$ do not contribute to $F_{\text{gauge}}(\Delta_0)$ in Eq. (4.9) anymore. A crude estimate of $F_{\text{gauge}}(\Delta_0) - F_{\text{gauge}}(0)$ is therefore given by the contribution to $F_{\text{gauge}}(0)$ of the “missing” gauge-field modes with $\nu < 2\Delta_0$. For $T > T_{\text{BE}}$ we can use $\text{Re } \Pi_F(q) \simeq \chi q^2$, so that we can do the \mathbf{q} -integration in Eq. (4.9) by scaling:

$$\begin{aligned}
F_{\text{gauge}}(\Delta_0) - F_{\text{gauge}}(0) &\simeq \int_0^{2\Delta_0} \frac{d\nu}{2\pi} \coth\left(\frac{\nu}{2T}\right) \int \frac{d^2q}{(2\pi)^2} \arctan\left(\frac{\gamma_F \nu}{\chi q^3}\right) \\
&\sim \int_0^{2\Delta_0} d\nu \coth\left(\frac{\nu}{2T}\right) \left(\frac{\gamma_F \nu}{\chi}\right)^{2/3} \\
&\sim \left(\frac{\gamma_F}{\chi}\right)^{2/3} \Delta_0^{5/3}.
\end{aligned} \tag{4.14}$$

Note that $F_{\text{gauge}}(\Delta_0) \sim \Delta_0^{5/3}$ is non-analytic in Δ_0^2 , so that the pairing transition must

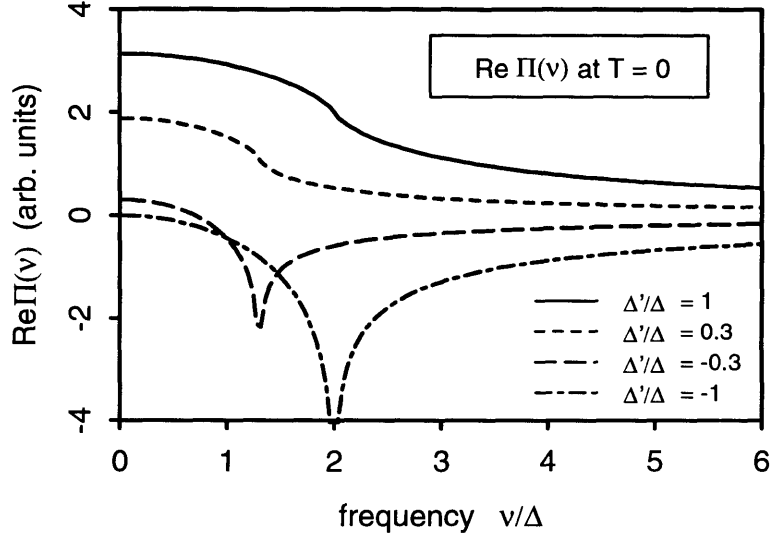


Figure 4-6: This figure shows $\text{Re } \Pi_F(\nu)$ at $T = 0$ for $\Delta'/\Delta = 1, 0.3, -0.3$ and -1 . Similar to the case of $\text{Im } \Pi_F(\nu)$ it depends on the relative sign of Δ and Δ' whether $\text{Re } \Pi_F(\nu)$ is positive or negative.

be a first-order transition in this approximation. More importantly, $F_{\text{gauge}}(\Delta_0) - F_{\text{gauge}}(0)$ is always much larger than $F_{\text{MF}}(\Delta_0)$ for any Δ_0 , as long as $\chi \sim 1/(24\pi m_B)$ remains small. This implies that the opening of a gap will never happen for $T > T_{\text{BE}}$.

However, for $T < T_{\text{BE}}$ the susceptibility $\chi \simeq \chi_B$ will increase rapidly, which will lower $F_{\text{gauge}}(\Delta_0)$ in Eq. (4.14) significantly. In fact, if χ_B becomes much larger than $1/m_B = 2\xi t$, the approximation $\text{Re } \Pi_B(q) \simeq \chi_B q^2$ is only valid for very small q . Instead $\text{Re } \Pi_B(q)$ levels off to $\text{Re } \Pi_B(q) \simeq \rho_S$ for $\chi q^2 \gtrsim \rho_S$, where $\rho_S \simeq x/m_B$ is the superfluid density of holons. The fact that $\text{Re } \Pi_B(q)$ becomes massive below T_{BE} implies that we cannot assume anymore that the dominant momenta q are small in the integral (4.9) for $F_{\text{gauge}}(\Delta_0)$. That means that for $T < T_{\text{BE}}$ the anisotropy of the d -wave gap $\Delta(\mathbf{k})$ will start to play an important role. This decreases the pair-breaking effects of the gauge field, because as pointed out in the beginning of this section, modes with a large momentum \mathbf{q} actually *favor* pairing. The reason for this is that $\Delta(\mathbf{k} + \mathbf{q}/2)$ and $\Delta(\mathbf{k} - \mathbf{q}/2)$ can have opposite signs if \mathbf{q} is large enough.

The consequences of this for the phase diagram are that the gauge field suppresses pairing very strongly at low doping, but for large doping the pair-breaking effects of the gauge field will be less pronounced, because the gauge field is in that case stiffened

by a large superfluid density ρ_S .

4.3.2 The propagator for $\Delta_0 \ll T$

In the previous section we used a zero temperature expression for the gauge-field propagator. The fact that the free energy varied as $F_{\text{gauge}}(\Delta_0) \sim \Delta_0^{5/3}$ for $T > T_{\text{BE}}$ implied that the superconducting transition had to be a first-order transition in that approximation. It is an interesting question whether the transition can become second-order if we would use a finite temperature expression for $\text{Im}\Pi_F(\nu)$ and $\text{Re}\Pi_F(\nu)$. To address this question we will assume that $\Delta_0 \ll T$, and expand the propagator in powers of Δ_0^2 by writing $\Pi(\Delta_0) \simeq \Pi(\Delta_0 = 0) + \Delta_0^2 \partial\Pi/\partial\Delta_0^2$. We can then use this expansion to find $F_{\text{gauge}}(\Delta_0)$ for $\Delta_0 \ll T$. Using Eqs. (4.12) and (4.13) one can show that in the limit $\Delta_0 \rightarrow 0$, $\partial\Pi_F/\partial\Delta_0^2$ has the following functional form:

$$\lim_{\Delta_0 \rightarrow 0} \frac{\partial}{\partial\Delta_0^2} \Pi_F(\mathbf{q}, \nu) = \frac{\gamma_F(\mathbf{q})}{q\nu} \left[h_R\left(\frac{\nu}{T}\right) + i h_I\left(\frac{\nu}{T}\right) \right]; \quad (4.15)$$

$$h_I\left(\frac{\nu}{T}\right) = \frac{1}{2} \mathcal{P} \int_{-\infty}^{\infty} dx \left(\frac{x}{x} + \frac{\varphi}{1+x} \right)^2 \left[\frac{1}{2} - f(\nu) - f(x\nu) + f((1+x)\nu) \right]; \quad (4.16)$$

$$h_R\left(\frac{\nu}{T}\right) = \varphi\varphi' \tanh\left(\frac{\nu}{2T}\right) + \frac{\nu}{8T} (\varphi^2 + \varphi'^2) \left(1 - \tanh^2\left(\frac{\nu}{2T}\right) \right). \quad (4.17)$$

Notice that we have to use a finite temperature expression for $\partial\Pi_F/\partial\Delta_0^2$, because $h_I(\nu/T)$ diverges logarithmically for $T \rightarrow 0$. For $\varphi\varphi' > 0$ h_I and h_R are always positive, but for $\varphi\varphi' < 0$ h_I and h_R can become negative. This shows explicitly that scattering processes with a large momentum transfer (for which $\varphi\varphi' < 0$) are not necessarily pair-breaking. We will later take this into account in our numerical calculations, but we will ignore the anisotropy of the gap in the simple estimates that follow below.

We can now use the expressions for $h_I(\nu/T)$ and $h_R(\nu/T)$ to evaluate $\partial F_{\text{gauge}}/\partial\Delta_0^2$,

which according to Eq. (4.9) can be written as

$$\left. \frac{\partial F_{\text{gauge}}}{\partial \Delta_0^2} \right|_{\Delta=0} = \int \frac{d^2 q}{(2\pi)^2} \int_0^\infty \frac{d\nu}{2\pi} \frac{\gamma_F}{q\nu} \coth\left(\frac{\nu}{2T}\right) \frac{h_I(\nu/T)\text{Re } \Pi - h_R(\nu/T)\text{Im } \Pi}{(\text{Re } \Pi)^2 + (\text{Im } \Pi)^2}. \quad (4.18)$$

It is instructive to estimate $\partial F_{\text{gauge}}/\partial \Delta_0^2$, assuming that $\text{Re } \Pi \simeq \chi q^2$, which is a valid assumption above the Bose-condensation temperature T_{BE} . The calculation is similar to the calculation of $F_{\text{gauge}}(\Delta_0)$ in Eq. (4.14). The q -integration in Eq. (4.18) can again be done by scaling, and one obtains

$$\frac{\partial F_{\text{gauge}}}{\partial \Delta_0^2} \sim \left(\frac{\gamma_F}{\chi}\right)^{2/3} \int_0^\infty \frac{d\nu}{\nu^{4/3}} \coth\left(\frac{\nu}{2T}\right) \tilde{h}\left(\frac{\nu}{T}\right), \quad (4.19)$$

where $\tilde{h}(\nu/T)$ is a linear combination of the functions $h_I(\nu/T)$ and $h_R(\nu/T)$. The frequency integral in Eq. (4.19) diverges at $\nu \rightarrow 0$, because $h_R(\nu/T)$ is linear in ν/T for $\nu \rightarrow 0$. This implies that a second-order transition is impossible for $T > T_{\text{BE}}$.

We will now analyze Eq. (4.19) for a small finite gap Δ_0 . One can repeat the calculations that led to Eq. (4.19) for a nonzero gap $\Delta_0 \ll T$, by noticing that a nonzero gap Δ_0 essentially introduces a lower cut-off in the frequency integral in Eq. (4.19). This cut-off is due to the fact that the expansion in Eq. (4.15) is only valid for $\nu \gg 2\Delta$, and the expansion clearly breaks down for $\nu < 2\Delta$. Using this cut-off one can now evaluate the frequency integral in Eq. (4.19), which gives

$$\frac{\partial F_{\text{gauge}}}{\partial \Delta_0^2} \sim \left(\frac{\gamma_F}{\chi}\right)^{2/3} \frac{1}{\Delta_0^{1/3}}. \quad (4.20)$$

This is the same functional form for $F_{\text{gauge}}(\Delta_0)$ as obtained in Eq. (4.14), where we used a zero temperature expression for the propagator $\Pi(\nu, \Delta_0)$. The conclusion is again that the superconducting transition has to be first-order for $T > T_{\text{BE}}$.

As before, the arguments that led to $\partial F_{\text{gauge}}/\partial \Delta_0^2 \sim \Delta_0^{-1/3}$ have to be modified if a superfluid density ρ_S develops for $T < T_{\text{BE}}$. If one replaces $\text{Re } \Pi(q) = \chi q^2$ by $\text{Re } \Pi(\nu) = \rho_S$ one finds that the expression for $\partial F_{\text{gauge}}/\partial \Delta_0^2$ in Eq. (4.18) converges, even for $\Delta_0 \rightarrow 0$. This makes it in principle possible to have a second-order transition

for $T < T_{\text{BE}}$, if ρ_S is sufficiently large. Considering that the pair-breaking effect of the gauge field diminishes as the superfluid density increases, we expect that the first-order jump of Δ_0 at the transition becomes smaller as ρ_S increases, and the transition might become second-order if ρ_S is sufficiently large.

These arguments assumed that there is a true superfluid state for the holons, i.e. $\text{Re } \Pi_B(q) = \rho_S$ for $q \rightarrow 0$. However, we discussed in section 4.2 that the interaction of the bosons with the gauge field can lead to the dissipative susceptibility χ_B in Eq. (4.6), that increases according to a Curie-law $\chi_B \sim 1/T$ [43], instead of diverging exponentially below T_{BE}^0 . In that case there is no true superfluid state anymore, which means that even at low temperatures $\text{Re } \Pi_B(q)$ varies like χq^2 for small momenta q . This implies that $F_{\text{gauge}}(\Delta_0)$ will still vary like $\Delta_0^{5/3}$ for a sufficiently small gap Δ_0 . Therefore we will always find a first-order transition if we use the Curie-like expression for χ_B in Eq. (4.6).

4.4 Numerical analysis of $F_{\text{gauge}}(\Delta_0)$

We did a numerical analysis of $F_{\text{tot}}(\Delta_0)$, using the expression for $F_{\text{gauge}}(\Delta_0)$ in Eq. (4.9), and assuming a d -wave symmetry for the gap $\Delta(\mathbf{k})$. We used mean-field expressions for the RVB-order parameter ξ , the susceptibility χ_F and the damping parameter $\gamma_F(\mathbf{q})$, and we carefully took the diamond-like shape of the Fermi surface into account. As mentioned after Eq. (4.10), χ_F is actually negative for the t - J model (for doping $x \lesssim 0.5$), and $\gamma_F(\mathbf{q})$ is highly anisotropic due to the non-spherical shape of the Fermi surface. The value of the order parameter ξ depends on x and T , and decreases rapidly if the doping x becomes very small. We minimized the total free energy $F_{\text{tot}}(\Delta_0)$ with respect to Δ_0 , and the onset of superconductivity is determined by the temperature T_c at which $F_{\text{tot}}(\Delta_0)$ has its global minimum at a nonzero value of Δ_0 .

The most challenging part of this numerical calculation is to find expressions for $\text{Im } \Pi_F(\nu, \Delta, \Delta')$ and $\text{Re } \Pi_F(\nu, \Delta, \Delta')$, that take into account that the d -wave gap $\Delta = \Delta_0 \varphi_{k_{\pm} q/2}$ is anisotropic around the Fermi surface. As pointed out after Eq.

(4.13) this anisotropy of the gap has the feature that processes with a large momentum transfer \mathbf{q} tend to *favor* pair-breaking, because $\Delta\Delta'$ can become negative for large \mathbf{q} . The anisotropy of the gap is very important for the numerical values that one obtains for the suppression of $T_c(x)$, and can definitely not be ignored. We performed the numerical calculation in the two limiting cases that we discussed in sections 4.3.1 and 4.3.2. In the first case we used zero temperature expressions for $\text{Im } \Pi_F(\nu, \Delta, \Delta')$ and $\text{Re } \Pi_F(\nu, \Delta, \Delta')$, which is a good approximation when $\Delta_0 \gg T$. In the second case we expanded $\text{Im } \Pi_F$ and $\text{Re } \Pi_F$ in Δ_0^2 , which is a good approximation when $\Delta_0 \ll T$. For $\nu > |\Delta| + |\Delta'|$ we used the functions $h_I(\nu/T)$ and $h_R(\nu/T)$ as defined in Eqs. (4.16) and (4.17). This expansion fails for $\nu < |\Delta| + |\Delta'|$, in which case we used a high temperature expression for the propagator instead.

To take the effect of Bose condensation into account we used a parametrization of $\text{Re } \Pi_B(q)$, which interpolates between the limits $\text{Re } \Pi_B(q) \simeq \chi_B q^2$ (for $q \rightarrow 0$) and $\text{Re } \Pi_B(q) \simeq x/m_B$ (for large q). For χ_B we used the three possibilities discussed in section 4.2: (i) the mean-field expression χ_B^0 in Eq. (4.3); (ii) the dissipative expression χ_B^{diss} in Eq. (4.5); (iii) the self-consistent dissipative χ_B^{SC} shown in Fig. 4-4.

The result of our numerical analysis is shown in the phase diagrams in Fig. 4-2 (using the mean-field χ_B^0) and Fig. 4-3 (using the dissipative χ_B^{diss}). The phase-diagrams show that $T_c(x)$ is indeed strongly suppressed compared to the mean-field transition temperature $T_c^0(x)$ (dotted line), especially at low doping. The solid line represents $T_c(x)$ if one uses $T = 0$ expressions for the propagator, as discussed in section 4.3.1, and the dashed line is the result for $T_c(x)$ if one assumes $\Delta_0 \ll T$, as discussed in section 4.3.2. These two approximations for the propagator give results that are qualitatively similar. One has to compare the first-order jump in Δ_0 at $T_c(x)$ with $T_c(x)$ itself to decide which approximation is more appropriate.

In Fig. 4-2 the first-order jump in Δ_0 is small for large doping so that the dashed line is appropriate, whereas for small doping the jump in Δ_0 becomes so large that the solid line is more appropriate. The line indicated with diamonds, which interpolates between the dashed line and the solid line, is our best guess of what the correct phase boundary is. We re-iterate that the need to use two different approximations for the

propagator (represented by the dashed line and the solid line) is purely technical, due to the limitation of our computational abilities. Note that the superconducting transition temperature goes to zero at a finite doping near $x = 0.05$. This is not too surprising, because the gauge field becomes unstable towards a flux phase for $x \simeq 0.04$ and hence the strength of the gauge-field fluctuations diverges in the vicinity of this point. At higher doping the transition temperature $T_c(x)$ approaches the mean-field transition line $T_c^0(x)$, because the gauge field becomes very stiff as the superfluid density $\rho_S \simeq x/m_B$ increases.

When we repeat the calculation using χ_B^{SC} the result is indistinguishable from Fig. 4-2. The reason is clear from Fig. 4-4 by observing that for $x \simeq 0.07$ the self-consistent χ_B^{SC} is exponentially large for $T \lesssim 0.2J$. Because the phase boundary is at a much lower temperature, the bosons have essentially Bose condensed at the transition, whether one uses χ_B^0 or χ_B^{SC} . This model therefore predicts a Fermi liquid in a temperature range just above T_c , even in the underdoped case. This aspect of the model may be in disagreement with experiments, and we believe that this is related to the fact that in the underdoped case $x < 0.1$ the self-consistent dissipative model underestimates the effectiveness of the gauge field to suppress Bose condensation.

For completeness we show in Fig. 4-3 the phase diagram using the dissipative model χ_B^{diss} . Note that the suppression of $T_c(x)$ is much larger than in Fig. 4-2. The first-order jump in Δ_0 is large at the transition, so that the solid line, which uses the approximation $\Delta_0 \gg T$, will be close to the correct answer for $T_c(x)$. According to Fig. 4-4, χ_B^{diss} is still relatively small at the transition temperature for $x = 0.07$, so that the dissipative model predicts a direct transition from a strange metal phase into a superconducting phase at low doping. The fact that in the dissipative model the gauge field is still massless at T_c is the reason why $T_c(x)$ is suppressed more strongly in Fig. 4-3 than in Fig. 4-2. As explained in section 4.2 we believe that this dissipative model grossly overestimates the effectiveness of the gauge field in suppressing T_c . We therefore think that the phase diagram in Fig. 4-2 is closer to the truth than the phase diagram in Fig. 4-3. In the underdoped case $x < 0.1$ the true answer will lie somewhere in between Fig. 4-2 and Fig. 4-3, because at low doping the

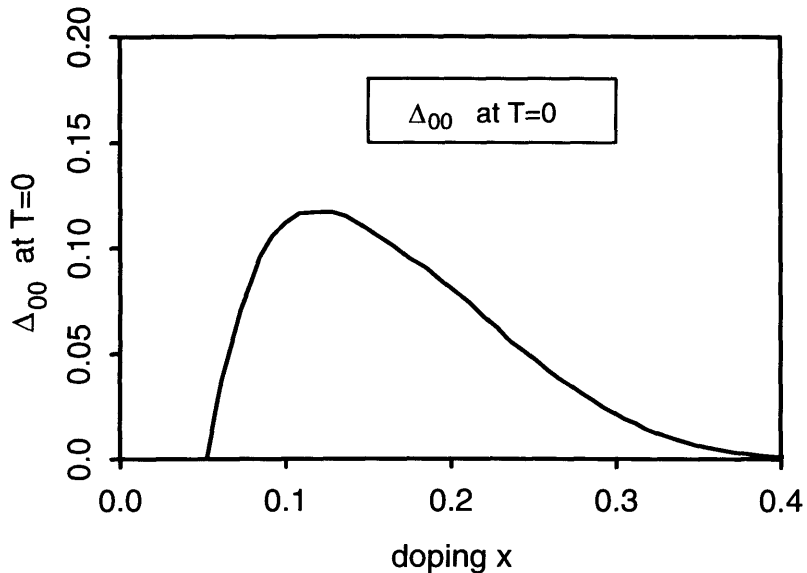


Figure 4-7: This figure shows $\Delta_{00}(x)$, the gap at $T = 0$. By comparing this to $T_c(x)$ in Figs. 4-2 and 4-3 we find that the ratio $2\Delta_{00}/T_c$ is approximately 3 if one uses the mean-field χ_B^0 (or the self-consistent χ_B^{SC}), and approximately 8 if one uses the dissipative χ_B^{diss} . This should be compared to the mean-field d -wave value of $2\Delta_{00}/T_c^0 \simeq 2.6$, which does not include any gauge field fluctuations. We believe that in the underdoped case the true value of $2\Delta_{00}/T_c$ is significantly larger than 3, because at low doping the self-consistent χ_B^{SC} underestimates the effectiveness of the gauge field to suppress Bose condensation.

self-consistent model underestimates the effectiveness of the gauge field in suppressing Bose condensation.

As pointed out earlier in section 4.2 the first-order jump in Δ_0 will be rounded off by phase fluctuations of the pairing field Δ_{ij} . Taking this in consideration the interpretation of our numerical results should be that the gap Δ_0 increases very rapidly below T_c , much faster than according to BCS theory. Our numerical results indicate that this rapid increase in Δ_0 will be more pronounced in the underdoped case $x \lesssim 0.1$.

In Fig. 4-7 we show a plot of $\Delta_{00}(x)$, where $\Delta_{00}(x)$ is the gap at $T = 0$. Remark that $\Delta_{00}(x)$ is independent of the particular model for χ_B , because the bosons are condensed at $T = 0$ for all three models. As expected the function $\Delta_{00}(x)$ has essentially the same shape as $T_c(x)$. We are mostly interested in the ratio $2\Delta_{00}(x)/T_c(x)$, which is a constant according to BCS theory. For a d -wave gap without a gauge field we find that this ratio to be approximately equal to 2.6. If we include the gauge field

this ratio is enhanced, depending on the model that one uses to determine $T_c(x)$. If we use the dissipative χ_B^{diss} the ratio is strongly enhanced to $2\Delta_{00}/T_c \simeq 8$, but if we use the mean-field χ_B^0 or the self-consistent χ_B^{SC} this ratio is only slightly enhanced to $2\Delta_{00}/T_c \simeq 3$. Because we believe that at low doping χ_B^{SC} underestimates the importance of gauge-field fluctuations, we expect that the correct value of $2\Delta_{00}(x)/T_c(x)$ will be significantly larger than 3 in the underdoped case $x < 0.1$.

4.5 Conclusions

We analyzed the pair-breaking effects of the gauge field, by studying the contribution from the gauge field to the total free energy. This contribution $F_{\text{gauge}}(\Delta_0)$ depends on Δ_0 , because a nonzero gap Δ_0 modifies the gauge-field propagator, and therefore changes the free energy. We showed that $F_{\text{gauge}}(\Delta_0) \sim \Delta_0^{5/3}$, which implies that the superconducting transition must be first-order, if one ignores fluctuations in the pairing field itself.

Our numerical calculations, that took into account that the gap $\Delta(\mathbf{k})$ has a d -wave symmetry around the Fermi surface, showed that there is indeed a strong suppression of superconductivity by the gauge field. The value of the boson susceptibility χ_B , which indicates whether the holons are condensed or not, played an important role in the suppression of $T_c(x)$. We used several models for χ_B , and in all cases we found that superconductivity only survives in an intermediate range of doping $0.05 \lesssim x \lesssim 0.35$. The maximum critical temperature occurs near $x = 0.15$. These numerical results are in qualitative agreement with the well-known phase-diagram of the high- T_c copper-oxides.

One of our predictions is that the experimentally observed “spin-gap phase” cannot be due to pairing of spinons within the plane, because those Cooper pairs are broken by the fluctuating gauge field. We also predict that the nature of the superconducting transition is significantly altered by the gauge field, especially in the underdoped case. The signature for this is that the magnitude of the gap Δ_0 increases very rapidly below T_c . Moreover, we expect that in the underdoped case the ratio

$2\Delta_{00}/T_c$, where Δ_{00} is the gap at $T = 0$, will be significantly larger than what one would obtain from BCS theory.

Acknowledgements

This work was done in collaboration with Patrick A. Lee [10]. The work was supported by the NSF through the Material Research Laboratory under Grant No. DMR-90-22933.

Chapter 5

Spin-gap formation in bi-layer cuprates due to enhanced inter-layer pairing

5.1 Introduction

Since the early days of high- T_c superconductivity physicists have focused on the copper-oxide planes to explain the unusual properties of the high- T_c cuprates. A widely accepted point of view is that the structure between the CuO_2 planes can be considered as a charge reservoir, whose only role is to fix a certain charge density in the CuO_2 planes. Consequently many theoretical models for the cuprates, such as the t - J model and the Hubbard model, are actually models for a *single* CuO_2 plane, ignoring the exchange coupling between the layers. This is appropriate for single-layer materials such as $\text{La}_{2-x}\text{Sr}_x\text{CuO}_4$, where the inter-layer coupling is frustrated because the CuO_2 layers are shifted relative to each other. However, this is not the case for bi-layer materials such as YBCO, because the two CuO_2 planes in each bi-layer are directly on top of each other, giving rise to an unfrustrated exchange coupling between the two planes.

Experiments indicate that there is a significant difference between the physical properties of single-layer materials and the properties of multi-layer materials. For

instance, it is well known that the superconducting transition temperature is in general higher for compounds that have more CuO_2 planes in a unit cell. Another difference is that in multi-layer materials such as $\text{YBa}_2\text{Cu}_3\text{O}_{6.6}$ one observes a *spin gap* in experiments that probe the spin degrees of freedom of the electrons [66, 67, 68]. This spin-gap phase is observed at low doping and survives well above the superconducting transition temperature. According to a recent analysis of the experimental data [59], the spin-gap phase is only observed in multi-layer materials but not in single-layer materials. It is then plausible that the spin gap is directly related to the pairing of electrons on nearby CuO_2 planes [59, 69].

Before considering a model for coupled CuO_2 planes, we will first briefly discuss the physics of a single CuO_2 plane. A single CuO_2 plane can be described by the t - J model [13], which has been studied extensively in previous articles using the slave-boson-gauge field approach [10, 33, 34, 35, 36, 37, 54]. In this approach the physical electrons are split into fermions and bosons [sometimes called *spinons* and *holons*], that interact with each other via a fluctuating gauge field. The superconducting phase is the phase in which the fermions have formed Cooper pairs, while the bosons are Bose condensed at the same time. It was suggested that the spin-gap phase corresponds to the situation in which the fermions have formed Cooper pairs, but the bosons are not Bose condensed yet [33, 34, 35, 58, 70]. In a recent article we showed that this picture is modified significantly by the fluctuating gauge field, which is very effective in destroying the formation of Cooper pairs at low doping [10]. As a result the superconducting transition temperature is suppressed at low doping and the spin-gap phase disappears completely. After including the pair-breaking effects of the gauge field the superconducting phase diagram that we obtained corresponds very well with the actual phase diagram of the single-layer high- T_c cuprates. We conclude that the two-dimensional t - J model is successful in explaining the phase diagram of single-layer cuprates, but is not able to explain certain features of multi-layer materials, such as the spin-gap phase.

In this paper we consider a model for two coupled CuO_2 planes, where each plane is described by the two-dimensional t - J model. In addition we include a small antifer-

romagnetic spin interaction between the two planes of the form $J_{\perp}^0 \sum_i \mathbf{S}_i^{(1)} \cdot \mathbf{S}_i^{(2)}$. This model is similar to a model studied by Millis and Monien [59]. The antiferromagnetic inter-layer coupling is responsible for the fact that close to half filling the spins on nearby CuO_2 planes are locked in an antiparallel orientation. Experimentalists have not been able to determine the exact value of J_{\perp}^0 , but Tranquada *et al.* and Shamoto *et al.* have reported a lower limit of 8 meV for J_{\perp}^0 [66, 68]. Because the inter-plane coupling is much smaller than the in-plane coupling one would naively expect that the inter-plane coupling is completely irrelevant for the pairing mechanism of the high- T_c cuprates. We will argue however, that due to strong antiferromagnetic spin correlations the *effective* inter-plane coupling $J_{\perp}^{\text{eff}}(\mathbf{r})$ is strongly enhanced, and extends over a coherence length of several lattice spacings. The picture that we have in mind is that the spins in each plane are correlated in patches that consist of several spins, so that effectively there is a coupling of correlated patches of spins on adjacent planes. This is clearly a much stronger coupling than the original coupling of single spins. The method that we use to take the antiferromagnetic correlation of the spins into account is the random-phase approximation (RPA).

Our main conclusion is that the enhanced inter-plane coupling $J_{\perp}^{\text{eff}}(\mathbf{r})$ leads to strongly enhanced pairing between fermions on different planes, described by the inter-plane order parameter $\Delta_{\perp}(\mathbf{r}_{ij}) = \langle f_{i\uparrow}^{(1)} f_{j\downarrow}^{(2)} - f_{i\downarrow}^{(1)} f_{j\uparrow}^{(2)} \rangle$. The possibility of inter-plane pairing has been discussed earlier by Altshuler and Ioffe [69]. We find that due to the antiferromagnetic spin correlations the order parameter $\Delta_{\perp}(\mathbf{r}_{ij})$ extends over a coherence length of several lattice spacings. Our calculations show that the inter-plane gap $\Delta_{\perp}(\mathbf{k})$ has an extended *s*-wave symmetry (without nodes), and is peaked at the corners of the Fermi surface. This should be contrasted to the in-plane gap $\Delta_{\parallel}(\mathbf{k})$, which has a *d*-wave symmetry with nodes at four points on the Fermi surface.

We propose that the inter-plane gap $\Delta_{\perp}(\mathbf{k})$ is responsible for the observed spin-gap phase in multi-layer cuprates, which had been suggested earlier by Millis and Monien [59]. An objection against their work has been that J_{\perp}^0 is much too small to explain the spin gap in $\text{YBa}_2\text{Cu}_3\text{O}_{6.6}$. We avoided this problem with the argument that at low doping J_{\perp}^{eff} is strongly enhanced by antiferromagnetic correlations. This

leaves the question why we cannot apply the same argument to create a spin gap using the *in-plane* coupling $J_{\parallel}^{\text{eff}}$, which is still larger than the inter-plane coupling J_{\perp}^{eff} . This is partly explained by the fact that J_{\perp}^{eff} is much more enhanced than $J_{\parallel}^{\text{eff}}$. However, for a complete answer we have to go beyond mean-field theory, and discuss the pair-breaking effects of the gauge field in the t - J model. In a previous paper we showed that at low doping the in-plane gap $\Delta_{\parallel}(\mathbf{k})$ is destroyed by gauge field fluctuations [10], so that the in-plane pairing can not give rise to a spin-gap phase. We expect that the gauge field is less effective in destroying the inter-plane gap $\Delta_{\perp}(\mathbf{k})$. This difference, which will be discussed in greater detail in Sec. 5.5, can be understood as follows. The pair-breaking effect of a gauge field is related to the question whether or not a gap Δ breaks the gauge symmetry in the system. In the case of an in-plane gap $\Delta_{\parallel}(\mathbf{k})$ the gauge symmetry is completely broken, while in the case of an inter-plane gap $\Delta_{\perp}(\mathbf{k})$ there is still a gauge symmetry left in the system, corresponding to a massless out-of-phase gauge-field mode. As a result the inter-plane gap $\Delta_{\perp}(\mathbf{k})$ can survive above the Bose-condensation temperature, explaining the spin-gap phase in multi-layer cuprates.

5.2 RPA analysis of two coupled CuO_2 planes

In this paper we study a system of two coupled CuO_2 planes, which is a simple model for a bi-layer high- T_c cuprate such as YBCO. We describe each individual plane with the two-dimensional t - J model, and in addition we include an antiferromagnetic spin coupling between the electrons on neighboring planes. This gives the Hamiltonian [66, 59, 71]

$$H = H_{t-J_{\parallel}}^{(1)} + H_{t-J_{\parallel}}^{(2)} + J_{\perp}^0 \sum_i \mathbf{S}_i^{(1)} \cdot \mathbf{S}_i^{(2)}, \quad (5.1)$$

where $H_{t-J}^{(n)}$ is the usual t - J Hamiltonian on plane n ($n = 1$ or 2), and $\mathbf{S}_i^{(n)} = c_{i\alpha}^{(n)\dagger} \boldsymbol{\sigma}_{\alpha\beta} c_{i\beta}^{(n)}$ is the spin operator of the electron $c_{i\alpha}^{(n)\dagger}$ at site i on plane n . Notice that we did not include any inter-layer hopping in the Hamiltonian in Eq. (5.1). We will return to address this issue in Sec. 5.7. Typical values for the parameters t , J_{\parallel}^0

and J_{\perp}^0 are

$$\begin{aligned}
t &\simeq 0.4 \text{ eV}; \\
J_{\parallel}^0 &\simeq 0.12 \text{ eV}; \\
J_{\perp}^0 &\gtrsim 0.01 \text{ eV}.
\end{aligned}
\tag{5.2}$$

The exact value of the inter-layer exchange J_{\parallel}^0 is still unknown, but a lower limit of 8 meV has been reported by Tranquada *et al.* and Shamoto *et al.* [66, 68]. This lower limit was obtained by studying the (absence of) optical spin-wave modes in undoped cuprates in neutron scattering experiments.

At low doping the motion of the electrons on each plane is controlled by the few empty sites. In order to take this physics into account we will employ the slave-boson approach, in which the original electron operator $c_{i\sigma}^{\dagger}$ is replaced by $f_{i\sigma}^{\dagger} b_i$, where $f_{i\sigma}^{\dagger}$ is a fermion operator carrying the spin of the electron, and b_i is a boson operator that keeps track of the empty sites, carrying the charge of the electron [7, 15, 17, 18]. In the slave-boson approach the t - J_{\parallel} Hamiltonian takes the form

$$H_{t-J_{\parallel}} = -t \sum_{\langle i,j \rangle} (f_{i\sigma}^{\dagger} b_i b_j^{\dagger} f_{j\sigma} + \text{c.c.}) + J_{\parallel}^0 \sum_{\langle i,j \rangle} (\mathbf{S}_i \cdot \mathbf{S}_j - \frac{1}{4} n_i n_j), \tag{5.3}$$

where $\mathbf{S}_i = f_{i\alpha}^{\dagger} \boldsymbol{\sigma}_{\alpha\beta} f_{i\beta}$ is the spin of the electron on site i .

We will use a Hubbard-Stratonovich transformation to decouple the various terms in this Hamiltonian. The interaction term $\mathbf{S}_i \cdot \mathbf{S}_j$ can be decoupled in various different channels. The most common decoupling is in the particle-hole channel by writing

$$\mathbf{S}_i \cdot \mathbf{S}_j = -\frac{1}{2} (f_{i\sigma}^{\dagger} f_{j\sigma}) (f_{j\sigma}^{\dagger} f_{i\sigma}) - \frac{1}{4} n_i n_j + \frac{1}{2} n_i. \tag{5.4}$$

This decoupling gives rise to terms of the form $\xi_{ij} f_{i\sigma}^{\dagger} f_{j\sigma}$ in the Hamiltonian, where ξ_{ij} is a tight-binding like resonating-valence-bond (RVB) order parameter [13]. The disadvantage of this decoupling is that it does not take the antiferromagnetic correlations of the spins into account explicitly. In order to take the antiferromagnetic

correlations into account it is more appropriate to keep terms of the form $\mathbf{S}_i \cdot \mathbf{S}_j$ in the Hamiltonian, which can be treated perturbatively to include the effect of the spin correlations [72]. In order to avoid double counting we write the Hamiltonian in Eq. (5.3) as

$$H_{t-J_{\parallel}} = H_{t-\frac{1}{2}J_{\parallel}} + \frac{1}{2}J_{\parallel}^0 \sum_{\langle i,j \rangle} \left(\mathbf{S}_i \cdot \mathbf{S}_j - \frac{1}{4}n_i n_j \right), \quad (5.5)$$

and treat the first term using an RVB mean-field ξ_{ij} and the second term using RPA. This admittedly *ad hoc* decomposition will affect the numerical factors in our results, but not the qualitative conclusions. We decouple $H_{t-\frac{1}{2}J_{\parallel}}$ in the particle-hole channel to obtain

$$\begin{aligned} H_{t-\frac{1}{2}J_{\parallel}} &= \frac{1}{4}J_{\parallel}^0 \sum_{\langle i,j \rangle} \left[|\xi_{ij}|^2 - \xi_{ij} \left(f_{i\sigma}^{\dagger} f_{j\sigma} + \frac{4t}{J_{\parallel}} b_i^{\dagger} b_j \right) - \text{c.c.} \right] \\ &\quad + \frac{4t^2}{J_{\parallel}} \sum_{\langle i,j \rangle} b_i^{\dagger} b_j b_j^{\dagger} b_i. \end{aligned} \quad (5.6)$$

At this point the analysis is still exact if one integrates over all configurations of the RVB field $\xi_{ij}(\tau)$. In the mean-field approximation the field ξ_{ij} is replaced by its saddlepoint

$$\xi = \left\langle f_{i\sigma}^{\dagger} f_{j\sigma} + \frac{4t}{J_{\parallel}} b_i^{\dagger} b_j \right\rangle. \quad (5.7)$$

The total Hamiltonian for the fermionic degrees of freedom then takes the form

$$H = \sum_{\mathbf{k}} \epsilon_{\mathbf{k}} \left(f_{\mathbf{k}\sigma}^{(1)\dagger} f_{\mathbf{k}\sigma}^{(1)} + f_{\mathbf{k}\sigma}^{(2)\dagger} f_{\mathbf{k}\sigma}^{(2)} \right) + H_{\text{I}}, \quad (5.8)$$

where $\epsilon_{\mathbf{k}} = -\frac{1}{2}J_{\parallel}^0 \xi (\cos k_x + \cos k_y) - \mu_F$. The interaction Hamiltonian H_{I} is given by

$$\begin{aligned} H_{\text{I}} &= \frac{1}{2} \sum_{\langle i,j \rangle, n, n'} J_{nn'}^0(\mathbf{r}_{ij}) \mathbf{S}_i^{(n)} \cdot \mathbf{S}_j^{(n')} \\ &= \frac{1}{2} \sum_{\mathbf{q}, n, n'} J_{nn'}^0(\mathbf{q}) \mathbf{S}_{\mathbf{q}}^{(n)} \cdot \mathbf{S}_{-\mathbf{q}}^{(n')}, \end{aligned} \quad (5.9)$$

where $J_{nn}^0(\mathbf{q}) = \tilde{J}_{\parallel}^0(\mathbf{q}) = J_{\parallel}^0(\cos q_x + \cos q_y)$ and $J_{nn'}^0(\mathbf{q}) = \tilde{J}_{\perp}^0(q_z) = J_{\perp}^0 e^{iq_z d}$, and d denotes the distance between the two planes. It is convenient to write H_{I} explicitly

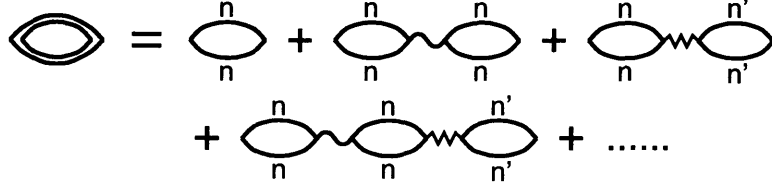


Figure 5-1: The renormalized susceptibility $\chi^{\text{RPA}}(q)$ in the RPA approximation. In each individual bubble the fermion can be either on plane $n = 1$ or on plane $n' = 2$. The wavy line denotes the in-plane exchange $\mathbf{S}_i^{(n)} \cdot \mathbf{S}_j^{(n)}$, and the jagged line denotes the inter-plane exchange $\mathbf{S}_i^{(n)} \cdot \mathbf{S}_i^{(n')}$. We show that due to antiferromagnetic correlations $\chi^{\text{RPA}}(q)$ has strong incommensurate peaks at $\mathbf{q} = \mathbf{Q}_{\text{AF}}$.

in terms of the fermion operators $f_{\mathbf{k}\sigma}^{(n)}$:

$$H_{\text{I}} = \frac{1}{4} \sum_{\mathbf{q}, n, n'} J_{nn'}^0(\mathbf{q}) \begin{pmatrix} \uparrow\uparrow \\ \downarrow\downarrow \\ \uparrow\downarrow \\ \downarrow\uparrow \end{pmatrix}_{\mathbf{q}, n} \begin{bmatrix} \frac{1}{2} & \frac{1}{2} & 0 & 0 \\ \frac{1}{2} & \frac{1}{2} & 0 & 0 \\ 0 & 0 & 1 & 0 \\ 0 & 0 & 0 & 1 \end{bmatrix} \begin{pmatrix} \uparrow\uparrow \\ \downarrow\downarrow \\ \uparrow\downarrow \\ \downarrow\uparrow \end{pmatrix}_{-\mathbf{q}, n'}, \quad (5.10)$$

where $(\uparrow\uparrow)_{\mathbf{q}, n}$ denotes $\sum_{\mathbf{k}} f_{\mathbf{k}+\mathbf{q}/2, \uparrow}^{(n)\dagger} f_{\mathbf{k}-\mathbf{q}/2, \uparrow}^{(n)}$.

We will use a random-phase approximation to analyze the antiferromagnetic correlations induced by the terms in H_{I} . We will first calculate the dynamic spin susceptibility $\chi(q)$ [where q denotes $(\mathbf{q}, q_z, i\omega_n)$], which contains all the information about spin correlations. Within RPA, $\chi^{\text{RPA}}(q)$ is given by a sum over the strings of bubbles shown in Fig. 5-1. The susceptibility is actually an 8 by 8 matrix, because at each vertex of a bubble the fermion can be either on plane 1 or on plane 2, and in addition there are four possible spin combinations at each vertex ($\uparrow\uparrow$, $\downarrow\downarrow$, $\uparrow\downarrow$ or $\downarrow\uparrow$). We can safely suppress the spin indices, because every power of the 4 by 4 spin matrix in Eq. (5.10) yields the same matrix again. This leaves us with simple 2 by 2 matrices, where the index denotes whether the fermion is on plane 1 or 2. The susceptibility is then given by the matrix sum

$$\chi^{\text{RPA}}(q) = \chi^0(q) \sum_{m=0}^{\infty} \left(-\frac{1}{4} \mathbf{J}^0(q) \chi^0(q) \right)^m, \quad (5.11)$$

where $\chi^0(q)$ is the contribution of a single bubble. The matrix $\mathbf{J}^0(q)$ is given by

$$\mathbf{J}^0(q) = \begin{bmatrix} \tilde{J}_{\parallel}^0(q) & \tilde{J}_{\perp}^0(q) \\ \tilde{J}_{\perp}^0(q)^* & \tilde{J}_{\parallel}^0(q) \end{bmatrix}. \quad (5.12)$$

Evaluating the matrix sum in Eq. (5.11) gives

$$\begin{aligned} \chi^{\text{RPA}} &= \chi^0 \begin{bmatrix} 1 + \frac{1}{4}\chi^0 \tilde{J}_{\parallel}^0 & \frac{1}{4}\chi^0 \tilde{J}_{\perp}^0 \\ \frac{1}{4}\chi^0 \tilde{J}_{\perp}^{0*} & 1 + \frac{1}{4}\chi^0 \tilde{J}_{\parallel}^0 \end{bmatrix}^{-1} \\ &= \frac{\chi^0}{(1 + \frac{1}{4}\chi^0 \tilde{J}_{\parallel}^0)^2 - |\frac{1}{4}\chi^0 \tilde{J}_{\perp}^0|^2} \begin{bmatrix} 1 + \frac{1}{4}\chi^0 \tilde{J}_{\parallel}^0 & -\frac{1}{4}\chi^0 \tilde{J}_{\perp}^0 \\ -\frac{1}{4}\chi^0 \tilde{J}_{\perp}^{0*} & 1 + \frac{1}{4}\chi^0 \tilde{J}_{\parallel}^0 \end{bmatrix}. \end{aligned} \quad (5.13)$$

This expression is only valid if the eigenvalues of the matrix $\frac{1}{4}\chi^0(q)\mathbf{J}^0(q)$ are smaller than 1. Putting $i\omega_n = 0$ this leads to the inequality

$$\chi^0(\mathbf{q}) < \frac{4}{J_{\perp}^0 - J_{\parallel}^0(\cos q_x + \cos q_y)} \quad (5.14)$$

At intermediate doping this inequality is usually satisfied. However, at low doping $\chi^0(\mathbf{q})$ is enhanced at the nesting vector $\mathbf{Q}_{\text{AF}} \simeq (\pi, \pi)$, so that at sufficiently low doping the inequality breaks down for $\mathbf{q} \simeq \mathbf{Q}_{\text{AF}}$. This indicates that at low doping the system becomes unstable against a long-range Néel order with $\langle \mathbf{S} \rangle \neq 0$.

We analyzed $\chi^{\text{RPA}}(\mathbf{q})$ numerically using the parameters $t/J_{\parallel}^0 = 3$ and $J_{\perp}^0/J_{\parallel}^0 = 0.2$. We found that for these parameters the AF instability occurs at a doping $x \simeq 0.08$. We are mostly interested in the regime close to the AF instability, i.e. $x \gtrsim 0.08$, which is characterized by strong (incommensurate) peaks in the renormalized susceptibility $\chi^{\text{RPA}}(q)$ at the nesting vector $\mathbf{q} = \mathbf{Q}_{\text{AF}} \simeq (\pi, \pi \pm 2x)$. This feature of $\chi^{\text{RPA}}(\mathbf{q})$ has been studied extensively by Tanamoto and co-workers for a generalized t - J model that included next-nearest neighbor hopping terms to simulate the band structure of different cuprates [72]. Their analysis was for a single CuO_2 plane, and did therefore not include any inter-plane interactions. They emphasized that the critical doping x_c at which the AF instability occurs depends strongly on the details of the band

structure.

The physical susceptibility that one measures in neutron scattering experiments is proportional to $\sum_{n,n'} \langle n' | \chi | n \rangle$, which gives

$$\chi_{\text{phys}}^{\text{RPA}}(\mathbf{q}, q_z, i\omega_n) = \left[\frac{\cos^2(\frac{1}{2}q_z d)}{1 + \frac{1}{4}\chi^0(\tilde{J}_{\parallel}^0(\mathbf{q}) + J_{\perp}^0)} + \frac{\sin^2(\frac{1}{2}q_z d)}{1 + \frac{1}{4}\chi^0(\tilde{J}_{\parallel}^0(\mathbf{q}) - J_{\perp}^0)} \right] \chi^0(\mathbf{q}, i\omega_n). \quad (5.15)$$

Here we used that $\tilde{J}_{\perp}^0(q_z) = J_{\perp}^0 e^{iq_z d}$. This expression shows that $\chi_{\text{phys}}^{\text{RPA}}(\mathbf{q}, q_z)$ has a modulation as a function of q_z with a period $2\pi/d$. The maxima occur at $q_z = \pi/d \pmod{2\pi/d}$ and the minima at $q_z = 0 \pmod{2\pi/d}$. This modulation is especially pronounced close to the AF instability with $\mathbf{q} \simeq \mathbf{Q}_{\text{AF}}$. In that case the maxima can be significantly larger than the minima. This corresponds well with the neutron scattering experiments of Tranquada *et al*, who measured $\chi''(\mathbf{Q}_{\text{AF}}, q_z)$ as a function of q_z [66]. They indeed observed a modulation of period $2\pi/d$, with maxima at $q_z = \pm\pi/d$ that were approximately twice the value of the minimum at $q_z = 0$.

We will now use the expression for $\chi^{\text{RPA}}(q)$ in Eq. (5.13) to calculate the effective spin-spin interaction, that we denote by $J_{\parallel}^{\text{eff}}(\mathbf{q})$ and $J_{\perp}^{\text{eff}}(\mathbf{q}, q_z)$. Within RPA the effective interaction can be written in matrix notation as

$$\mathbf{J}^{\text{eff}} = \mathbf{J}^0 - \frac{1}{4}\mathbf{J}^0 \chi^{\text{RPA}} \mathbf{J}^0, \quad (5.16)$$

where the 2 by 2 matrices \mathbf{J}^0 and χ^{RPA} are given by Eqs. (5.12) and (5.13). Evaluating the matrix products gives

$$J_{\parallel}^{\text{eff}}(\mathbf{q}) = \frac{\tilde{J}_{\parallel}^0(\mathbf{q}) \left(1 + \frac{1}{4}\chi^0 \tilde{J}_{\parallel}^0(\mathbf{q})\right) - \frac{1}{4}\chi^0 J_{\perp}^0{}^2}{\left(1 + \frac{1}{4}\chi^0 \tilde{J}_{\parallel}^0(\mathbf{q})\right)^2 - \left(\frac{1}{4}\chi^0 J_{\perp}^0\right)^2}; \quad (5.17)$$

$$\tilde{J}_{\perp}^{\text{eff}}(\mathbf{q}, q_z) = \frac{J_{\perp}^0}{\left(1 + \frac{1}{4}\chi^0 \tilde{J}_{\parallel}^0(\mathbf{q})\right)^2 - \left(\frac{1}{4}\chi^0 J_{\perp}^0\right)^2} e^{iq_z d}. \quad (5.18)$$

Note that $\tilde{J}_{\perp}^{\text{eff}}$ always has the form $\tilde{J}_{\perp}^{\text{eff}}(\mathbf{q}, q_z) = J_{\perp}^{\text{eff}}(\mathbf{q}) e^{iq_z d}$. Close to the AF instability $J_{\parallel}^{\text{eff}}(\mathbf{q})$ and $J_{\perp}^{\text{eff}}(\mathbf{q})$ are both strongly peaked at the nesting vector $\mathbf{q} = \mathbf{Q}_{\text{AF}}$, and the width of this peak is related to the correlation length r_0 over which the spins are Néel

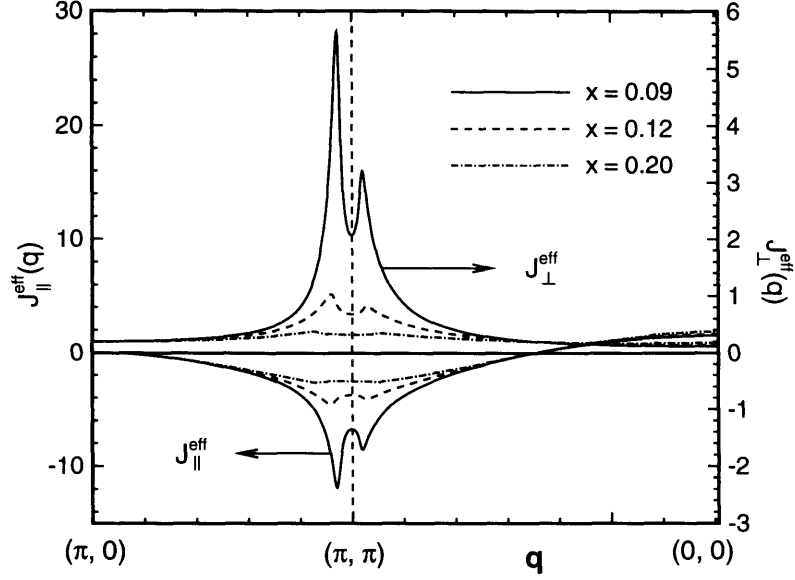


Figure 5-2: The effective in-plane coupling $J_{\parallel}^{\text{eff}}(\mathbf{q})$ (left axis) and the effective inter-plane coupling $J_{\perp}^{\text{eff}}(\mathbf{q})$ (right axis) for various values of the doping x . The right axis is blown up by a factor of 5 in order to show the features of $J_{\perp}^{\text{eff}}(\mathbf{q})$ more clearly. Close to the AF instability at $x_c = 0.08$, $J_{\parallel}^{\text{eff}}(\mathbf{q})$ and $J_{\perp}^{\text{eff}}(\mathbf{q})$ have strong incommensurate peaks at $\mathbf{Q}_{\text{AF}} \simeq (\pi, \pi \pm 0.19)$. These peaks fade away at higher dopings $x \gg x_c$. Notice that for $x \rightarrow x_c$ the inter-plane coupling $J_{\perp}^{\text{eff}}(\mathbf{Q}_{\text{AF}})$ is more enhanced than $J_{\parallel}^{\text{eff}}(\mathbf{Q}_{\text{AF}})$. As a result J_{\perp}^{eff} and $J_{\parallel}^{\text{eff}}$ become comparable in strength, even though initially $J_{\perp}^0 \ll J_{\parallel}^0$.

ordered. Let us first study Eqs. (5.17) and (5.18) in the important limit $J_{\perp}^0 \ll J_{\parallel}^0$. In that case $J_{\parallel}^{\text{eff}}$ is enhanced by a factor $(1 + \frac{1}{4}\chi^0 \tilde{J}_{\parallel}^0)^{-1}$, while J_{\perp}^{eff} is enhanced by the *square* of this factor. We conclude that for $\mathbf{q} \simeq \mathbf{Q}_{\text{AF}}$, $J_{\perp}^{\text{eff}}(\mathbf{q})$ is much stronger enhanced by antiferromagnetic correlations than $J_{\parallel}^{\text{eff}}(\mathbf{q})$. It is interesting to note however, that $J_{\perp}^{\text{eff}}(\mathbf{q})$ will never exceed $|J_{\parallel}^{\text{eff}}(\mathbf{q})|$, assuming that $J_{\perp}^0 < |\tilde{J}_{\parallel}^0(\mathbf{q})|$. In the limit $\frac{1}{4}\chi^0(\mathbf{q})(\tilde{J}_{\parallel}^0(\mathbf{q}) - J_{\perp}^0) \rightarrow -1$, J_{\perp}^{eff} approaches $J_{\parallel}^{\text{eff}}(\mathbf{q})$, even if J_{\perp}^0 was initially much smaller than \tilde{J}_{\parallel}^0 . This implies that close to the AF instability J_{\perp}^{eff} and $J_{\parallel}^{\text{eff}}$ are approximately equal in strength.

We analyzed $J_{\parallel}^{\text{eff}}(\mathbf{q})$ and $J_{\perp}^{\text{eff}}(\mathbf{q})$ numerically using the parameters $t/J_{\parallel}^0 = 3$ and $J_{\perp}^0/J_{\parallel}^0 = 0.2$. We focused in particular on doping slightly above the critical doping $x_c \simeq 0.08$ at which the AF instability occurs. In Fig. 5-2 we show plots of $J_{\parallel}^{\text{eff}}(\mathbf{q})$ and $J_{\perp}^{\text{eff}}(\mathbf{q})$ for $x = 0.09$, $x = 0.12$ and $x = 0.20$. The three curves show that close to the AF instability there are strongly pronounced incommensurate peaks at

$\mathbf{Q}_{\text{AF}} \simeq (\pi, \pi \pm 2x)$. By analyzing the width of the peak we find that for $x = 0.09$ the correlation length r_0 is roughly 3 lattice spacings, i.e. $r_0/a \simeq 3$. These peaks fade away when the doping is much higher than x_c . Notice that for $x = 0.09$, $J_{\perp}^{\text{eff}}(\mathbf{q})$ is much smaller than $J_{\parallel}^{\text{eff}}(\mathbf{q})$ over most of the Brillouin zone, but close to the incommensurate peaks $J_{\perp}^{\text{eff}}(\mathbf{q})$ is more strongly enhanced than $J_{\parallel}^{\text{eff}}(\mathbf{q})$, so that the $J_{\perp}^{\text{eff}}(\mathbf{q})$ and $J_{\parallel}^{\text{eff}}(\mathbf{q})$ become comparable in strength at $\mathbf{q} \simeq \mathbf{Q}_{\text{AF}}$. This means that the inter-plane coupling can not be ignored when the spins of the electrons exhibit strong antiferromagnetic correlations.

5.3 Inter-plane pairing

In the previous section we showed that the inter-plane coupling $J_{\perp}^{\text{eff}}(\mathbf{q})$ is strongly enhanced around $\mathbf{q} \simeq \mathbf{Q}_{\text{AF}}$ due to antiferromagnetic correlations. We will now show that this enhanced coupling leads to inter-plane pairing at a much higher energy scale than before. The physical picture that we have in mind is that the spins on both planes form patches of correlated spins, so that the system can create extended Cooper pairs that consist of patches of spins on one plane that pair up with corresponding patches of spins on the other plane. This inter-plane pairing is characterized by the order parameter $\Delta_{\perp}(\mathbf{r}_{ij}) = \langle f_{i\uparrow}^{(1)} f_{j\downarrow}^{(2)} - f_{i\downarrow}^{(1)} f_{j\uparrow}^{(2)} \rangle$.

Consider the Hamiltonian in Eq. (5.8), but with the bare in-plane and inter-plane couplings J_{\parallel}^0 and J_{\perp}^0 replaced by the effective couplings $J_{\parallel}^{\text{eff}}$ and J_{\perp}^{eff} . Each of these interaction terms can be written in the form

$$J_{nn'}^{\text{eff}}(\mathbf{r}_{ij}) \left(\mathbf{S}_i^{(n)} \cdot \mathbf{S}_j^{(n')} - \frac{1}{4} n_i n_j \right) = -\frac{1}{2} J_{nn'}^{\text{eff}}(\mathbf{r}_{ij}) \left(f_{i\uparrow}^{(n)\dagger} f_{j\downarrow}^{(n')\dagger} - f_{i\downarrow}^{(n)\dagger} f_{j\uparrow}^{(n')\dagger} \right) \left(f_{j\downarrow}^{(n')} f_{i\uparrow}^{(n)} - f_{j\uparrow}^{(n')} f_{i\downarrow}^{(n)} \right). \quad (5.19)$$

The coupling constants $J_{nn'}^{\text{eff}}(\mathbf{r}_{ij})$ are the Fourier transforms of the functions $J_{\parallel}^{\text{eff}}(\mathbf{q})$ and $J_{\perp}^{\text{eff}}(\mathbf{q})$ in Eqs. (5.17) and (5.18). The terms in Eq. (5.19) can be decoupled in the particle-particle channel by defining a Hubbard-Stratonovich field $\Delta_{ij}^{(nn')}$ on the

bond (i, j) , under the condition that $J_{nn'}(\mathbf{r}_{ij}) > 0$. This gives the Hamiltonian

$$H = \sum_{\mathbf{k}, n} \epsilon_{\mathbf{k}} f_{\mathbf{k}\sigma}^{(n)\dagger} f_{\mathbf{k}\sigma}^{(n)} + \frac{1}{2} \sum'_{(in, jn')} J_{nn'}^{\text{eff}}(\mathbf{r}_{ij}) \times \left[\left| \Delta_{ij}^{nn'} \right|^2 - \Delta_{ij}^{nn'*} \left(f_{i\uparrow}^{(n)} f_{j\downarrow}^{(n')} - f_{i\downarrow}^{(n)} f_{j\uparrow}^{(n')} \right) - \text{c.c.} \right], \quad (5.20)$$

where the indices n and n' denote plane 1 or 2. The prime in \sum' denotes that the sum is only over the bonds (i, j) for which $J_{nn'}(\mathbf{r}_{ij}) > 0$. This means that for $J_{\parallel}^{\text{eff}}(\mathbf{r}_{ij})$ we only include bonds (i, j) with i and j on different sublattices, while for $J_{\perp}^{\text{eff}}(\mathbf{r}_{ij})$ we only include bonds (i, j) with i and j on the same sublattice. At the mean-field level the fields $\Delta_{ij}^{nn'}$ are replaced by their saddlepoints, i.e. constant values that minimize the total free energy. Assuming that $\Delta_{ij}^{nn'} = \Delta_{nn'}(\mathbf{r}_{ij})$ is real, we can write the Hamiltonian in momentum space in the matrix form

$$H = \sum_{\mathbf{k}} \begin{pmatrix} f_{\mathbf{k}\uparrow}^{(1)} \\ f_{-\mathbf{k}\downarrow}^{(1)\dagger} \\ f_{\mathbf{k}\uparrow}^{(2)} \\ f_{-\mathbf{k}\downarrow}^{(2)\dagger} \end{pmatrix}^{\dagger} \begin{bmatrix} \epsilon_{\mathbf{k}} & \Delta_{\parallel} & 0 & \Delta_{\perp} \\ \Delta_{\parallel} & -\epsilon_{\mathbf{k}} & \Delta_{\perp} & 0 \\ 0 & \Delta_{\perp} & \epsilon_{\mathbf{k}} & \Delta_{\parallel} \\ \Delta_{\perp} & 0 & \Delta_{\parallel} & -\epsilon_{\mathbf{k}} \end{bmatrix} \begin{pmatrix} f_{\mathbf{k}\uparrow}^{(1)} \\ f_{-\mathbf{k}\downarrow}^{(1)\dagger} \\ f_{\mathbf{k}\uparrow}^{(2)} \\ f_{-\mathbf{k}\downarrow}^{(2)\dagger} \end{pmatrix} + \sum'_{\mathbf{r}} \left[J_{\parallel}^{\text{eff}}(\mathbf{r}) \Delta_{\parallel}(\mathbf{r})^2 + J_{\perp}^{\text{eff}}(\mathbf{r}) \Delta_{\perp}(\mathbf{r})^2 \right], \quad (5.21)$$

where

$$\epsilon_{\mathbf{k}} = -\frac{1}{2} \xi J_{\parallel}^0 (\cos k_x + \cos k_y) - \mu_F; \quad (5.22)$$

$$\Delta_{\parallel}(\mathbf{k}) = \sum'_{\mathbf{r}} \cos(\mathbf{k} \cdot \mathbf{r}) J_{\parallel}^{\text{eff}}(\mathbf{r}) \Delta_{\parallel}(\mathbf{r}); \quad (5.23)$$

$$\Delta_{\perp}(\mathbf{k}) = \sum'_{\mathbf{r}} \cos(\mathbf{k} \cdot \mathbf{r}) J_{\perp}^{\text{eff}}(\mathbf{r}) \Delta_{\perp}(\mathbf{r}). \quad (5.24)$$

The sum $\sum'_{\mathbf{r}}$ denotes a sum over bonds, which means that \mathbf{r} and $-\mathbf{r}$ should be counted only once and $\mathbf{r} = 0$ is counted half. The Hamiltonian in Eq. (5.21) can easily be diagonalized, which gives the quasi-particle energy dispersion

$$E_{\pm}(\mathbf{k}) = \sqrt{\epsilon_{\mathbf{k}}^2 + \Delta_{\pm}(\mathbf{k})^2}; \quad (5.25)$$

$$\Delta_{\pm}(\mathbf{k}) = \Delta_{\parallel}(\mathbf{k}) \pm \Delta_{\perp}(\mathbf{k}). \quad (5.26)$$

The order parameters $\Delta_{\parallel}(\mathbf{r})$ and $\Delta_{\perp}(\mathbf{r})$ are determined by the condition that the free energy is at a local minimum. The free energy is given by

$$F = \sum_{\mathbf{r}}' \left[J_{\parallel}^{\text{eff}}(\mathbf{r}) \Delta_{\parallel}(\mathbf{r})^2 + J_{\perp}^{\text{eff}}(\mathbf{r}) \Delta_{\perp}(\mathbf{r})^2 \right] - 2T \sum_{s=\pm} \int \frac{d^2k}{(2\pi)^2} \log [\cosh(E_s(\mathbf{k})/2T)]. \quad (5.27)$$

Putting $\partial F / \partial \Delta^{nn'}(\mathbf{r}) = 0$ for all $\Delta^{nn'}(\mathbf{r})$, we obtain the following set of self-consistency equations:

$$\Delta_{nn'}(\mathbf{r}) = \sum_{s=\pm 1} \int \frac{d^2k}{(2\pi)^2} \cos(\mathbf{k} \cdot \mathbf{r}) \left(\frac{s^{n-n'} \Delta_s(\mathbf{k})}{E_s(\mathbf{k})} \right) \tanh \left(\frac{E_s(\mathbf{k})}{2T} \right). \quad (5.28)$$

This set of self-consistency equations has in general several solutions, depending on the symmetry that one chooses for the order parameter, i.e. the relative signs of the order parameters $\Delta_{nn'}(\mathbf{r})$ on different bonds \mathbf{r} . Close to half filling one can find the most favorable symmetry of the order parameter, by studying the free energy in Eq. (5.27) in the limit $\Delta_{nn'}(\mathbf{r}) \rightarrow 0$. This gives

$$F(\Delta) - F(0) = \sum_{\mathbf{r}}' \left[J_{\parallel}^{\text{eff}}(\mathbf{r}) \Delta_{\parallel}(\mathbf{r})^2 + J_{\perp}^{\text{eff}}(\mathbf{r}) \Delta_{\perp}(\mathbf{r})^2 \right] - \int \frac{d^2k}{(2\pi)^2} \left[\Delta_{\parallel}(\mathbf{k})^2 + \Delta_{\perp}(\mathbf{k})^2 \right] \frac{\tanh(\epsilon_{\mathbf{k}}/2T)}{\epsilon_{\mathbf{k}}}. \quad (5.29)$$

The gain in free energy is largest if all the terms in the expression for $\Delta_{nn'}(\mathbf{k})$ in Eqs. (5.23) and (5.24) add constructively for the momenta \mathbf{k} that give the largest contribution to the integral in Eq. (5.29). Close to half filling the momentum integral in Eq. (5.29) is dominated by the \mathbf{k} vectors at the four corners of the Fermi surface, i.e. the points $\mathbf{k} = (\pm\pi, 0)$ and $\mathbf{k} = (0, \pm\pi)$, because close to half filling the density of states diverges at those four points. At the corner $\mathbf{k} = (\pi, 0)$ the gap $\Delta_{nn'}(\mathbf{k})$ is

given by

$$\Delta_{nn'}(\pi, 0) = \sum_{\mathbf{r}}' (-1)^{r_x} J_{nn'}(\mathbf{r}) \Delta_{nn'}(\mathbf{r}). \quad (5.30)$$

Because the summation $\sum_{\mathbf{r}}'$ is only over vectors \mathbf{r} for which $J_{nn'}(\mathbf{r})$ is positive, the terms in Eq. (5.30) add constructively if we let the sign of $\Delta_{nn'}(\mathbf{r})$ alternate depending on whether r_x and r_y are even or odd. We will measure r_x and r_y in units of the lattice constant a . To be more explicit, the gain in free energy is largest if we choose

$$\Delta_{\parallel}(\mathbf{r}) = \begin{cases} > 0 & \text{for } r_x \text{ even and } r_y \text{ odd;} \\ < 0 & \text{for } r_x \text{ odd and } r_y \text{ even;} \\ = 0 & \text{for } r_x + r_y \text{ even;} \end{cases} \quad (5.31)$$

$$\Delta_{\perp}(\mathbf{r}) = \begin{cases} > 0 & \text{for } r_x \text{ and } r_y \text{ even;} \\ < 0 & \text{for } r_x \text{ and } r_y \text{ odd;} \\ = 0 & \text{for } r_x + r_y \text{ odd.} \end{cases} \quad (5.32)$$

Notice that $\Delta_{\parallel}(r_x, r_y) = -\Delta_{\parallel}(r_y, r_x)$ and $\Delta_{\perp}(r_x, r_y) = +\Delta_{\perp}(r_y, r_x)$. This implies that $\Delta_{\perp}(\mathbf{k})$ has an extended s -wave symmetry [i.e., $\Delta_{\perp}(\mathbf{k}) = \Delta_{\perp}(\mathbf{k}_{\perp})$ for $\mathbf{k}_{\perp} = (k_y, k_x)$], while $\Delta_{\parallel}(\mathbf{k})$ has an extended d -wave symmetry [i.e., $\Delta_{\parallel}(\mathbf{k}) = -\Delta_{\parallel}(\mathbf{k}_{\perp})$]. The prefix “extended” indicates that $\Delta_{\perp}(\mathbf{k})$ and $\Delta_{\parallel}(\mathbf{k})$ can be anisotropic around the Fermi surface, with peaks at the corners $(\pm\pi, 0)$ and $(0, \pm\pi)$. This should be contrasted to a *pure* s -wave symmetry [$\Delta_{\perp}(\mathbf{k}) = \text{constant}$] or a *pure* d -wave symmetry [$\Delta_{\parallel}(\mathbf{k}) \propto \cos k_x - \cos k_y$].

We can now explain why superconductivity is enhanced when the effective coupling $J^{\text{eff}}(\mathbf{r})$ extends over several lattice spacings. Suppose that $J^{\text{eff}}(\mathbf{r})$ falls off over a correlation length r_0 , for example $J^{\text{eff}}(\mathbf{r}) = J^0 e^{-r/r_0}$. In that case there are of the order of r_0^2 terms $\Delta(\mathbf{r})$ that add constructively in the expression for the gap $\Delta(\mathbf{k})$ in Eq. (5.30) for $\mathbf{k} = (\pm\pi, 0)$ or $(0, \pm\pi)$. Therefore the second term in the free energy in Eq. (5.29), which corresponds to a *gain* of free energy, is essentially enhanced by a factor r_0^4 . On the other hand the first term in Eq. (5.29), which corresponds to a *cost* of free energy, is only enhanced by a factor r_0^2 . We therefore obtain a net gain of free energy which becomes larger and larger if the correlation length r_0 increases. As a

result superconductivity is enhanced. We would like to emphasize that our arguments for the behavior of $\Delta_{\parallel}(\mathbf{k})$ and $\Delta_{\perp}(\mathbf{k})$ are only valid close to half filling, and under the condition that $T \ll J$ and $\Delta(\mathbf{k}) \ll J$. These conditions are needed to make sure that the momentum integrals in Eqs. (5.28) and (5.29) are dominated by the corners of the Fermi surface. Away from half filling the corners of the Fermi surface become progressively less important, and therefore superconductivity will not be as strongly enhanced in that case.

From this point on we will focus on the order parameter $\Delta_{\perp}(\mathbf{r})$, and ignore $\Delta_{\parallel}(\mathbf{r})$. The motivation for this is twofold. The first reason is that the inter-plane order parameter Δ_{\perp} is more efficient in taking advantage of the antiferromagnetic correlations than Δ_{\parallel} , which is partly due to the fact that $J_{\perp}^{\text{eff}}(\mathbf{q})$ is stronger peaked at $\mathbf{q} = \mathbf{Q}_{\text{AF}}$ than $J_{\parallel}^{\text{eff}}(\mathbf{q})$, as we explained after Eq. (5.18). But our main motivation for ignoring Δ_{\parallel} is that the gauge field is very effective in destroying the in-plane gap $\Delta_{\parallel}(\mathbf{k})$ at low doping [10]. This is the region we are interested in, because the spin-gap phase is observed at low doping. We anticipate that the gauge field is less effective in destroying the inter-plane gap $\Delta_{\perp}(\mathbf{k})$, which we will discuss in more detail in Sec. 5.5.

5.4 Numerical analysis of inter-plane pairing

The numerical results presented in this section are meant for underdoped cuprates in the spin-gap phase. Within our model this corresponds to the situation in which Δ_{\perp} is finite, but $\Delta_{\parallel} = 0$. We solved the self-consistency equations for $\Delta_{\perp}(\mathbf{r})$ in Eq. (5.28), using the RPA-enhanced inter-plane coupling $J_{\perp}^{\text{eff}}(\mathbf{r})$ that we calculated in Sec. 5.2. We performed the calculations at a doping $x = 0.085$, which is close to the AF instability at $x \simeq 0.08$. In this calculation we assumed $J_{\perp}^0 = 0.2 J_{\parallel}^0$. For this amount of doping $J_{\perp}^{\text{eff}}(\mathbf{r})$ falls off over a correlation length of approximately 3 to 4 lattice spacings, which is quite typical for high- T_c cuprates in the spin-gap phase.

In Fig. 5-3 we show a plot of $(-1)^{r_x} \Delta_{\perp}(\mathbf{r})$ versus $|\mathbf{r}|$ for the discrete set of bonds on which $\Delta_{\perp}(\mathbf{r})$ is defined, i.e. $r_x + r_y$ is even. Note that $\Delta_{\perp}(\mathbf{r})$ falls off over a coherence length of approximately 3 to 4 lattice spacings, and that $\Delta_{\perp}(\mathbf{r})$ is positive on the

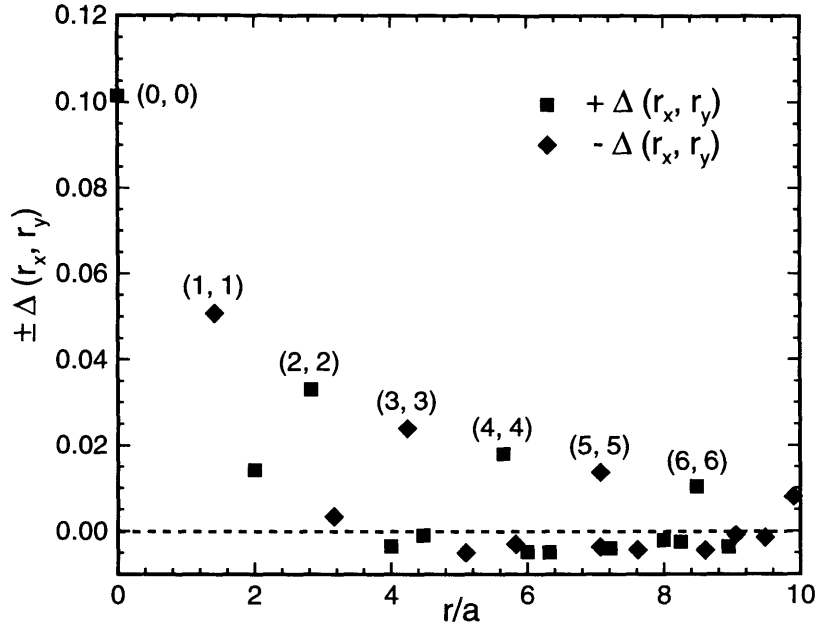


Figure 5-3: The pairing order parameter $\Delta_{\perp}(\mathbf{r})$ for $x = 0.085$. Due to the antiferromagnetic correlations $\Delta_{\perp}(\mathbf{r})$ is also nonzero for $\mathbf{r} \neq 0$, and $\Delta_{\perp}(\mathbf{r})$ decays over a correlation length of approximately 3-4 lattice spacings. Notice that $\Delta_{\perp}(\mathbf{r})$ alternates sign from one sublattice to the next, as indicated by the squares ($+\Delta_{\perp}$) and the diamonds ($-\Delta_{\perp}$). Also notice that $\Delta_{\perp}(\mathbf{r})$ is relatively strong along the diagonals $r_x = \pm r_y$. This implies that in momentum space $\Delta_{\perp}(\mathbf{k})$ is enhanced around the diamond-shaped Fermi surface.

sublattice with r_x even [denoted by squares], and negative on the sublattice with r_x odd [denoted by diamonds]. This alternating sign was anticipated in the previous section in Eq. (5.32). Also notice that $|\Delta_{\perp}(\mathbf{r})|$ is relatively large on the diagonal $\mathbf{r} = (j, j)$, which means that in momentum space $\Delta_{\perp}(\mathbf{k})$ will be enhanced along the diamond defined by $k_x \pm k_y = \pm\pi$.

In Fig. 5-4 we show a two-dimensional plot of $\Delta_{\perp}(\mathbf{k})$ in momentum space. Observe that $\Delta_{\perp}(\mathbf{k})$ is indeed enhanced at the Fermi surface, and that $\Delta_{\perp}(\mathbf{k})$ is especially large at the four corners of the Fermi surface. This anisotropy of $\Delta_{\perp}(\mathbf{k})$ is easier to see in Fig. 5-5, which shows a plot of $\Delta_{\perp}(\mathbf{k})$ around the Fermi surface for three different values of doping. Note that $\Delta_{\perp}(\mathbf{k})$ has an (extended) s -wave symmetry without nodes, and that the anisotropy of $\Delta_{\perp}(\mathbf{k})$ is quite pronounced for $x = 0.085$, but less pronounced for $x = 0.09$ and $x = 0.10$. Let us first look at the results for $x = 0.085$ (solid line). At the corners of the Fermi surface the value of $\Delta_{\perp}(\mathbf{k})$

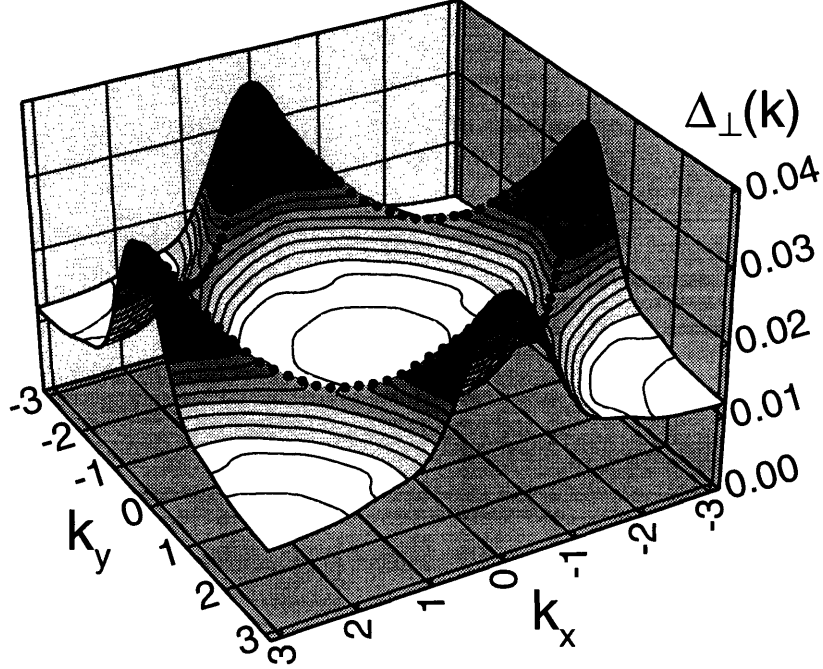


Figure 5-4: A contour plot of the gap $\Delta_{\perp}(\mathbf{k})$ for $x = 0.085$ and $J_{\perp}^0 = 0.2 J_{\parallel}^0$. The diamond-like Fermi surface is indicated by the black dotted line. Notice that the gap $\Delta_{\perp}(\mathbf{k})$ has an extended s -wave symmetry, with peaks at the four corners $\mathbf{k} = (\pm\pi, 0)$ and $\mathbf{k} = (0, \pm\pi)$, and without nodes. At the corners of the Fermi surface the gap is approximately $\Delta_{\perp}(\mathbf{k}) \simeq 0.032 J_{\parallel}^{\text{eff}} \simeq 4$ meV. Also notice that $\Delta_{\perp}(\mathbf{k})$ is significantly larger at the Fermi surface than in the middle of the Brillouin zone.

is approximately $0.032 J_{\parallel}^0 \simeq 4$ meV. In the middle of the Fermi surface the gap is approximately two third of this value. We also calculated the pairing transition temperature T_P^{\perp} at $x = 0.085$, which gave the result $T_P^{\perp} \simeq 0.016 J_{\parallel}^0$, which is of the order of 20 K. We emphasize that these numbers depend strongly on the specific values of the parameters in the model, and how close the doping is to the critical value x_c . Although the magnitude of the gap $\Delta_{\perp}(\mathbf{k})$ is still too small, we believe it is plausible to identify the spin gap observed in $\text{YBa}_2\text{Cu}_3\text{O}_{6.6}$ with $\Delta_{\perp}(\mathbf{k})$, and the spin-gap phase transition with T_P^{\perp} . In Fig. 5-5 we also show $\Delta_{\perp}(\mathbf{k})$ for a slightly higher doping $x = 0.09$ and $x = 0.10$. Notice that further away from the critical doping $x_c = 0.08$ the magnitude of $\Delta_{\perp}(\mathbf{k})$ decreases rapidly, and the anisotropy of $\Delta_{\perp}(\mathbf{k})$ is less pronounced as well. This result shows that the antiferromagnetic correlations are essential to make inter-layer pairing possible at a reasonably high energy scale.

In the RPA treatment the antiferromagnetic correlations are tied to the band

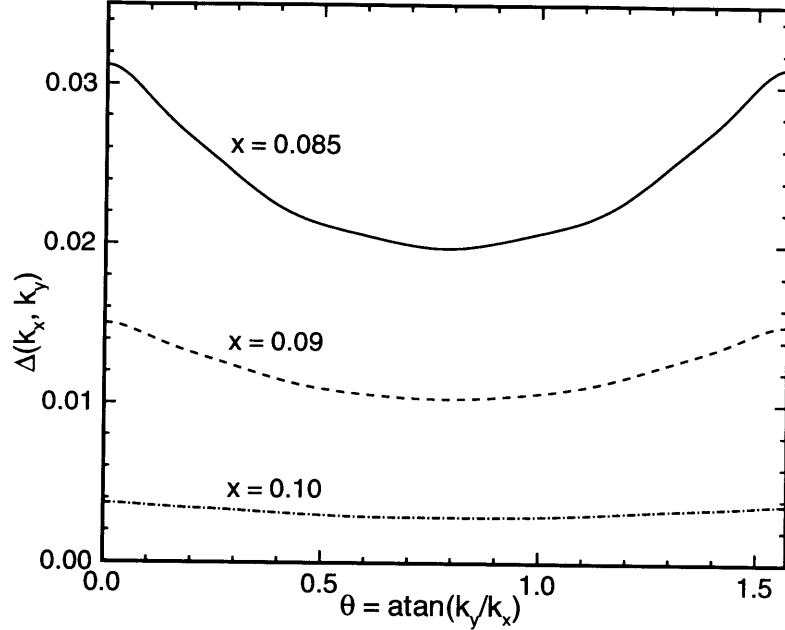


Figure 5-5: The inter-plane gap $\Delta_{\perp}(\mathbf{k})$ around the Fermi surface for $x = 0.085$, $x = 0.09$ and $x = 0.10$. The gap $\Delta_{\perp}(\mathbf{k})$ has an extended s -wave symmetry, and is anisotropic around the Fermi surface, with peaks at the corners of the Fermi surface. This anisotropy is quite pronounced for $x = 0.085$, which is close to the AF instability at $x_c = 0.08$. At the corners of the Fermi surface the gap is approximately $0.032J_{\parallel}^{\text{eff}} \simeq 4$ meV for $x = 0.085$. For higher doping $x = 0.09$ and $x = 0.10$ the amplitude of the gap decreases rapidly, and the anisotropy almost disappears. The conclusion is that the antiferromagnetic correlations are essential for the enhancement of $\Delta_{\perp}(\mathbf{k})$.

structure in a way that may not be quantitatively correct. To study the dependence of the gap Δ_{\perp} on the correlation length r_0 and the coupling constant J_{\perp}^0 , we consider an effective inter-plane pairing parametrized by

$$J_{\perp}^{\text{eff}}(\mathbf{r}) = J_{\perp}^0 (-1)^{i+j} e^{-r/r_0}, \quad (5.33)$$

where $\mathbf{r}/a = (i, j)$, and r_0 should be interpreted as the correlation length of the antiferromagnetic correlations. The dependence of the gap on the coupling constant J_{\perp}^0 is shown in Fig. 5-6, which is a logarithmic plot of $\Delta_{\perp}^{\text{max}}$ versus $(J_{\perp}^0)^{-1}$. We defined $\Delta_{\perp}^{\text{max}}$ as the value of $\Delta_{\perp}(\mathbf{k})$ at the corner of the Fermi surface. We did the calculations for a correlation length $r_0 \rightarrow 0$ [\square], $r_0 = 3$ [\triangle], and $r_0 = 6$ [∇]. The case $r_0 \rightarrow 0$ is the situation when $J_{\perp}^{\text{eff}}(\mathbf{r})$ and $\Delta_{\perp}(\mathbf{r})$ are only nonzero for $\mathbf{r} = 0$, which corresponds to a pure s -wave symmetry. Observe that the data points lie on straight lines with

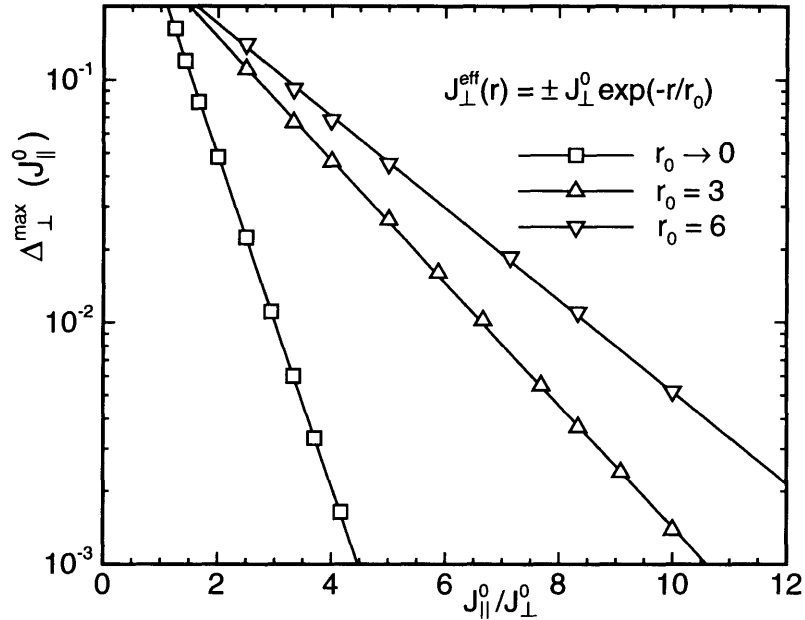


Figure 5-6: A logarithmic plot of the gap Δ_{\perp}^{\max} at the corner of the Fermi surface as a function of the inter-plane coupling constant $(J_{\perp}^0)^{-1}$. In this calculation we assumed that the effective coupling is given by $J_{\perp}^{\text{eff}}(\mathbf{r}) = \pm J_{\perp}^0 \exp(-r/r_0)$, and we fixed the doping at $x = 0.09$. We performed the calculations for a correlation length $r_0 = 3$ [Δ] and $r_0 = 6$ [∇], and compared the results with an “on-site” interaction, which corresponds with $r_0 \rightarrow 0$ [\square]. The straight lines show that Δ_{\perp}^{\max} depends exponentially on $(J_{\perp}^0)^{-1}$. The functional form is given in Eq. (5.34). Notice that for $r_0 = 3$ the slope of the line is 2.7 times smaller than for $r_0 \rightarrow 0$, and that therefore $\Delta_{\perp}^{\max}(r_0 = 3) \gg \Delta_{\perp}^{\max}(r_0 \rightarrow 0)$. The finite correlation length has the effect of enhancing J_{\perp}^0 by a factor of 2.7.

different slopes. We conclude that $\Delta_{\perp}^{\max}(\mathbf{k})$ has the functional form

$$\Delta_{\perp}^{\max} \simeq \begin{cases} 1.14 J_{\parallel}^0 \exp(-1.56 J_{\parallel}^0/J_{\perp}^0) & \text{for } r_0/a \rightarrow 0; \\ 0.48 J_{\parallel}^0 \exp(-0.58 J_{\parallel}^0/J_{\perp}^0) & \text{for } r_0/a = 3; \\ 0.41 J_{\parallel}^0 \exp(-0.44 J_{\parallel}^0/J_{\perp}^0) & \text{for } r_0/a = 6. \end{cases} \quad (5.34)$$

This BCS-like functional form is not surprising, because $\Delta_{\perp}(\mathbf{k})$ is determined in a way that is very similar to BCS theory. Notice however that the coefficients Eq. (5.34) change dramatically when the correlation length r_0/a increases from 0 to 3. For $r_0/a \gtrsim 3$ these coefficients do not change much anymore, because the system can only take advantage of very long correlation lengths if there is perfect nesting of the Fermi surface. This calculation was done at a finite doping $x = 0.09$, and thus the

nesting is not perfect. First consider the coefficient in the exponent, which drops from 1.56 to 0.58 when r_0/a increases from 0 to 3. The physical explanation for this is that when patches of spins cooperate to form extended Cooper pairs, J_{\perp}^0 gets effectively renormalized by a factor which increases with r_0/a . This renormalized J'_{\perp} is the coupling constant that enters the exponent in Eq. (5.34), i.e. $J'_{\perp} = \frac{1.56}{0.58} J_{\perp}^0 \sim 3J_{\perp}^0$ for $r_0/a = 3$. Now consider the prefactor in Eq. (5.34), which is proportional to J_{\parallel}^0 . In BCS theory this prefactor would be equal to the Debye frequency, which provides a cutoff in the energy integrations. In the calculation that led to Eq. (5.34) there was no cutoff in the energy integrations, so the Debye frequency is replaced by J_{\parallel}^0 , the overall energy scale. If the correlation length r_0 increases an effective energy cutoff is introduced, because $\Delta_{\perp}(\mathbf{k})$ becomes anisotropic with peaks that have a width proportional to a/r_0 . Therefore the “Debye frequency” J_{\parallel}^0 gets replaced by roughly $(a/r_0)J_{\parallel}^0$. We would like to mention that this calculation did not take any frequency dependence of $J^{\text{eff}}(\mathbf{q}, \omega)$ into account. Millis and Monien argued that the frequency dependence of $J^{\text{eff}}(\mathbf{q}, \omega)$ introduces another cutoff in the energy integrations, of the order of $(a/r_0)^2 J_{\parallel}^0$ [59, 73], and is therefore more important than the cutoff provided by the momentum dependence of $J^{\text{eff}}(\mathbf{q}, \omega)$. This argument does not modify the coefficients in the exponents in Eq. (5.34), and thus $\Delta_{\perp}^{\text{eff}}$ is still strongly enhanced when the correlation length increases.

5.5 Pair-breaking effects of the gauge field

We have argued in a previous paper that for a single CuO_2 plane a fluctuating gauge field destroys the in-plane pairing order parameter Δ_{\parallel} above the Bose-condensation temperature T_{BE} [10]. This explains the absence of a spin-gap phase in single-layer materials. In this section we will argue that the gauge field is not as effective in destroying the inter-plane order parameter Δ_{\perp} , so that the spin-gap can survive in multi-layer materials.

In the previous sections we discussed a mean-field approximation of the t - J model. To go beyond mean-field theory we will now introduce a gauge field, that takes a

$$\begin{aligned}\Pi_{\parallel}(\mathbf{q}) &= \text{---} \overset{n}{\circlearrowleft} \text{---} \text{---} \overset{n}{\circlearrowright} \text{---} + \text{---} \overset{n}{\circlearrowleft} \text{---} \overset{n}{\circlearrowright} \text{---} \\ \Pi_{\perp}(\mathbf{q}) &= \text{---} \overset{n}{\circlearrowleft} \text{---} \overset{n'}{\circlearrowright} \text{---} \text{---} \end{aligned}$$

Figure 5-7: The diagrams for the gauge field propagators $\Pi_{\parallel}(q)$ and $\Pi_{\perp}(q)$. The indices n and n' indicate plane 1 or plane 2 (and $n \neq n'$). The propagator $\Pi_{\perp}(q)$ is only nonzero if there is a coupling between the two planes. In Sec. 5.5 we show that the in-phase propagator $\Pi_{+} = \Pi_{\parallel} + \Pi_{\perp}$ becomes massive when an inter-plane gap Δ_{\perp} opens up, while the out-of-phase propagator $\Pi_{-} = \Pi_{\parallel} - \Pi_{\perp}$ remains massless.

certain class of fluctuations around the mean-field result into account. The gauge field is the phase of the RVB-order parameter

$$\xi_{ij} = \xi e^{ia_{ij}}, \quad (5.35)$$

where ξ is given by Eq. (5.7). We refer to other papers for a more comprehensive discussion of the properties of this gauge field a_{ij} [10, 23, 33, 34, 35, 54]. In our model for two CuO_2 planes there are two gauge field modes per unit cell, because each plane has its own gauge field, denoted by $a_{ij}^{(1)}$ and $a_{ij}^{(2)}$. Suppose that the two planes are coupled by a nonzero inter-plane order parameter Δ_{\perp} , as described by the Hamiltonian in Eq. (5.21). In that case the two gauge field modes are coupled as well, and the total gauge field action has the form

$$S[a] = \frac{T}{2} \sum_{\mathbf{q}} \left(\delta_{\alpha\beta} - \frac{q_{\alpha}q_{\beta}}{q^2} \right) \begin{pmatrix} a_{\mathbf{q}}^{(1)\alpha} \\ a_{\mathbf{q}}^{(2)\alpha} \end{pmatrix}^{\dagger} \begin{bmatrix} \Pi_{\parallel}(q) & \Pi_{\perp}(q) \\ \Pi_{\perp}(q) & \Pi_{\parallel}(q) \end{bmatrix} \begin{pmatrix} a_{\mathbf{q}}^{(1)\beta} \\ a_{\mathbf{q}}^{(2)\beta} \end{pmatrix}, \quad (5.36)$$

where q denotes $(\mathbf{q}, i\nu_n)$ and $i\nu_n$ is a Matsubara frequency. The propagators $\Pi_{\parallel}(q)$ and $\Pi_{\perp}(q)$ are given by the diagrams in Fig. 5-7. Notice that $\Pi_{\perp}(q) = 0$ when $\Delta_{\perp} = 0$, because in that case the two planes are uncoupled, and thus the diagram in Fig. 5-7(b) vanishes. The eigenmodes of the action in Eq. (5.36) are the *in-phase* mode $a_{\mathbf{q}}^{(+)} \equiv (a_{\mathbf{q}}^{(1)} + a_{\mathbf{q}}^{(2)})/\sqrt{2}$ and the *out-of-phase* mode $a_{\mathbf{q}}^{(-)} \equiv (a_{\mathbf{q}}^{(1)} - a_{\mathbf{q}}^{(2)})/\sqrt{2}$. We will

denote the propagators of these two eigenmodes by $\Pi_{\pm}(q) \equiv \Pi_{\parallel}(q) \pm \Pi_{\perp}(q)$.

In order to decide whether the combined effect of the two gauge field modes is pair breaking or not, one has to calculate the total free energy of each gauge field mode, and study whether the free energy increases or not when a gap Δ_{\perp} opens up. This is outside the scope of this paper, and we will instead limit ourselves to qualitative arguments why it is less costly to have an inter-plane gap Δ_{\perp} than to have an in-plane gap Δ_{\parallel} . Our qualitative argument is based on the fact that in the case of inter-plane pairing one of the two gauge field modes remains massless, while in the case of in-plane pairing both modes become massive. The fact that a certain mode becomes massive is generally an indication that this mode is pair breaking.

Evaluating the diagrams in Fig. 5-7 in the presence of an inter-plane gap $\Delta_{\perp}(\mathbf{k})$ gives

$$\Pi_{\pm}(\mathbf{q}, i\nu_n) = C + 2T \sum_{i\omega_n} \int \frac{d^2k}{(2\pi)^2} \left(\hat{\mathbf{q}} \times \frac{\partial \epsilon}{\partial \mathbf{k}} \right) \left(\hat{\mathbf{q}} \times \frac{\partial \epsilon'}{\partial \mathbf{k}} \right) \frac{\epsilon \epsilon' - \omega_n \omega'_n \pm \Delta \Delta'}{(\omega_n^2 + E^2)(\omega'_n{}^2 + E'^2)}, \quad (5.37)$$

where $i\omega'_n = i\omega_n - i\nu_n$; $\epsilon, \epsilon' = \epsilon_{k \pm q/2}$; $\Delta, \Delta' = \Delta_{\perp}(\mathbf{k} \pm \mathbf{q}/2)$; and $E = \sqrt{\epsilon^2 + \Delta^2}$. The first term in Eq. (5.37) is a constant given by the first diagram in Fig. 5-7(a), which is equal to

$$C = 2T \sum_{i\omega_n} \int \frac{d^2k}{(2\pi)^2} \frac{\partial^2 \epsilon_k}{\partial \mathbf{k}^2} \frac{\epsilon_k}{E_k^2 + \omega_n^2}. \quad (5.38)$$

For $\Delta = 0$ this constant C exactly cancels the second term in Eq. (5.37) for $\mathbf{q} \rightarrow 0$ and $i\nu_n = 0$. Thus the gauge field is massless in the normal state. Note that the functional form of the in-phase propagator $\Pi_{+}(q)$ is similar to the BCS expression for the propagator of the electromagnetic gauge field in the presence of a gap [65], except that the coupling constants are very different. It is very well known that this propagator becomes massive when a gap opens up, i.e. $\Pi_{+}(0, 0) \propto \Delta_{\perp}^2$, which is responsible for the Meissner effect in BCS superconductors.

The out-of-phase mode $a_q^{(-)}$, on the other hand, has a propagator $\Pi_{-}(q)$ with a different coherence factor, proportional to $\epsilon \epsilon' - \omega_n \omega'_n - \Delta \Delta'$. One can easily check that due to the minus sign in the coherence factor the second term in Eq. (5.37) exactly cancels the constant C in Eq. (5.38) in the limit $\mathbf{q} \rightarrow 0$ and $i\nu_n = 0$, even when

$\Delta \neq 0$. In other words, the out-of-phase propagator $\Pi_-(q)$ remains massless when an inter-layer gap opens up. The physical reason why the out-of-phase mode $a_q^{(-)}$ remains massless is related to gauge invariance. Without pairing the Hamiltonian is invariant under the local gauge transformation

$$f_{j\sigma}^{(n)} \longrightarrow e^{i\varphi_j^{(n)}} f_{j\sigma}^{(n)} \quad (5.39)$$

$$a_{ij}^{(n)} \longrightarrow a_{ij}^{(n)} - \varphi_i^{(n)} + \varphi_j^{(n)}. \quad (5.40)$$

A finite gap Δ generally breaks this gauge invariance, which implies that the gauge field mode becomes massive. This is usually referred to as the Higgs mechanism. In order to see what happens to the out-of-phase gauge field mode $a_q^{(-)}$, we only consider gauge transformations that satisfy $\varphi_i^{(1)} = -\varphi_i^{(2)}$. One immediately observes that the inter-plane order parameter $\Delta_\perp = \langle f_{i\uparrow}^{(1)} f_{i\downarrow}^{(2)} - f_{i\downarrow}^{(1)} f_{i\uparrow}^{(2)} \rangle$ is invariant under this class of gauge transformations. The Higgs mechanism does not apply because the gauge invariance is not broken, and therefore the out-of-phase gauge field mode $a_q^{(-)}$ remains massless.

For a more detailed analysis of the pair-breaking effects of the gauge field modes $a^{(+)}$ and $a^{(-)}$, one has to study the contribution of the gauge field to the free energy, given by [10, 55]

$$\begin{aligned} F_{\text{gauge}}^{(\pm)} &= T \sum_{\mathbf{q}, \nu_n} \log \Pi_\pm(\mathbf{q}, i\nu_n) \\ &= \sum_{\mathbf{q}} \int_0^\infty \frac{d\nu}{2\pi} [2n_B(\nu) + 1] \arctan \left(\frac{\text{Im} \Pi_\pm(\mathbf{q}, \nu + i\delta)}{\text{Re} \Pi_\pm(\mathbf{q}, \nu + i\delta)} \right). \end{aligned} \quad (5.41)$$

In the normal state the gauge field gives a rather large negative contribution to the free energy. It has been shown that the free energy from free fermions and bosons is much too large, and that the negative contribution from the transverse and longitudinal gauge fluctuations yields a free energy which is in much better agreement with high-temperature expansions [55].

Let us now ask what happens when a gap opens up in the fermion spectrum. We can calculate $F_{\text{gauge}}^{(\pm)}(\Delta)$ by substituting the propagator $\Pi_\pm(\mathbf{q}, \nu, \Delta)$ into Eq. (5.41).

Let us first consider $F_{\text{gauge}}^{(+)}(\Delta)$. For $\Delta \neq 0$ a gap appears in $\text{Im } \Pi_{\pm}(\mathbf{q}, \nu)$, eliminating the contribution of modes with $\nu < 2\Delta$. For $\nu > 2\Delta$, $-(\text{Im } \Pi_{+}/\text{Re } \Pi_{+})$ is still suppressed compared to its normal state value, causing a significant increase in $F_{\text{gauge}}^{(+)}(\Delta)$. It was shown in Ref. [10] that $F_{\text{gauge}}^{(+)}(\Delta) \propto \Delta^{5/3}$ if $T > T_{\text{BE}}$. This cost in free energy is so large that it destroys the possibility of fermion pairing for $T > T_{\text{BE}}$, thereby eliminating the spin-gap phase in single-layer cuprates.

The story is quite different for $F_{\text{gauge}}^{(-)}(\Delta)$. Again a gap appears in $\text{Im } \Pi_{-}(\mathbf{q}, \nu)$, but for $\nu > 2\Delta$ the coherence factor in Eq. (5.37) is such that $-(\text{Im } \Pi_{-}/\text{Re } \Pi_{-})$ is actually *enhanced* [10], which overwhelms the loss of free energy from frequencies $\nu < 2\Delta$. Considering that $F_{\text{gauge}}^{(-)}(\Delta)$ decreases when a gap opens up, we conclude that the gauge field mode $a_q^{(-)}$ is pair enhancing. The pair-enhancing nature of $a_q^{(-)}$ can also be understood in another way. The fermions on the two planes couple to the $a^{(-)}$ mode with opposite charge, so that the exchange of an $a^{(-)}$ mode leads to an attraction, analogous to what happens in the t - t' - J model [31, 75]. In our case we expect that the effects of the $a_q^{(+)}$ and $a_q^{(-)}$ gauge fluctuations largely cancel each other, so that the mean-field treatment of inter-plane pairing may be quite reliable. As a result it is likely that over a certain temperature range the in-plane gap $\Delta_{\parallel}(\mathbf{k})$ is completely destroyed by gauge field fluctuations, while the inter-plane gap $\Delta_{\perp}(\mathbf{k})$ still survives. This region can be identified with the spin-gap phase.

5.6 NMR-relaxation rates

Experiments on $\text{YBa}_2\text{Cu}_3\text{O}_{6.6}$ show that quantities that probe the spin-degrees of freedom of the system, such as the NMR-relaxation rate, the echo-decay rate, and the Knight shift, are strongly reduced below a certain crossover temperature. In this section we will show that our model can reproduce the unusual temperature dependence of these quantities. The two main ingredients to obtain our results are the presence of strong antiferromagnetic correlations, and the opening of a spin gap Δ_{\perp} due to the pairing of fermions on adjacent CuO_2 planes. We will mainly focus on the calculation of the NMR-relaxation rate $(T_1 T)^{-1}$, whose temperature dependence

contains information about both the magnitude of the spin gap and the presence of antiferromagnetic correlations.

The NMR-relaxation rate is directly related to the susceptibility according to the formula

$$\frac{1}{T_1 T} = \frac{1}{\mu_B^2 \hbar} \sum_{\mathbf{q}} F(\mathbf{q}) \lim_{\omega \rightarrow \infty} \frac{\chi''_{\text{phys}}(\mathbf{q}, \omega)}{\omega}. \quad (5.42)$$

The form factor $F(\mathbf{q})$ depends on the direction of the magnetic field, and whether one probes the copper sites or the oxygen sites. Following Millis *et al.* and Monien *et al.* [76, 77], the form factors are given by

$$\begin{aligned} {}^{63}F_{\parallel}(\mathbf{q}) &= \frac{3}{8} [A_{\parallel} + 2B(\cos q_x a + \cos q_y a)]^2 + \frac{3}{8} [A_{\perp} + 2B(\cos q_x a + \cos q_y a)]^2 \\ {}^{63}F_{\perp}(\mathbf{q}) &= \frac{3}{4} [A_{\perp} + 2B(\cos q_x a + \cos q_y a)]^2 \\ {}^{17}F(\mathbf{q}) &= \frac{3}{2} C^2 (1 + \cos q_x a), \end{aligned} \quad (5.43)$$

where “63” denotes the ${}^{63}\text{Cu}$ site, and “17” denotes the ${}^{17}\text{O}$ site. The constants A_{\parallel} , A_{\perp} and C are approximately equal to [77]

$$\begin{aligned} A_{\parallel} &= -4B, \\ A_{\perp} &= 0.84B, \\ C &= 1.68B, \end{aligned} \quad (5.44)$$

and $B \simeq 40.8 \text{ kOe}/\mu_B$. The main feature of these form factors is that ${}^{17}F(\mathbf{q})$ vanishes at $\mathbf{q} = (\pi, \pi)$, while ${}^{63}F_{\parallel}(\mathbf{q})$ has its maximum at $\mathbf{q} = (\pi, \pi)$. This implies that the relaxation rate on the copper sites will be strongly enhanced due to antiferromagnetic correlations, while this enhancement will not be seen in $({}^{17}T_1 T)^{-1}$.

In order to find $(T_1 T)^{-1}$ we will use the RPA approximation to calculate the susceptibility $\chi_{\text{phys}}(\mathbf{q}, \omega)$. Within the RPA approximation one can express $\chi_{\text{phys}}^{\text{RPA}}$ in terms of the bare susceptibility $\chi^0(\mathbf{q}, \omega)$, similar to the expression in Eq. (5.15). The only difference is that we now have a finite spin gap $\Delta_{\perp}(\mathbf{k})$ coupling the two planes, which implies that the bare susceptibility $\chi^0(\mathbf{q}, \omega)$ is now a 2 by 2 matrix instead of a number. Following the derivation of Eq. (5.15), and replacing χ^0 by a 2 by 2 matrix

χ^0 at each step, we obtain

$$\chi_{\text{phys}}(\mathbf{q}, q_z, \omega) = \left[\frac{\cos^2(\frac{1}{2}q_z d)}{1 + J_+ \chi_+} + \frac{\sin^2(\frac{1}{2}q_z d)}{1 + J_- \chi_-} \right] \chi_+(\mathbf{q}, \omega), \quad (5.45)$$

where

$$\begin{aligned} \chi_{\pm} &= \chi_{\parallel}^0 \pm \chi_{\perp}^0, \\ J_{\pm} &= J_{\parallel} \pm J_{\perp}. \end{aligned} \quad (5.46)$$

[For $\chi_+ = \chi_- = \chi^0$ this reduces to the expression in Eq. (5.15).] The susceptibilities χ_{\pm} are determined by evaluating a single fermion bubble, which gives [65, 78]

$$\begin{aligned} \chi_{\pm}(\mathbf{q}, \omega + i\delta) &= \int \frac{d^2k}{(2\pi)^2} \frac{1}{2} \left[l_{\pm}^2 \frac{f(E') - f(E)}{E - E' + \omega + i\Gamma} + \right. \\ &\quad \left. p_{\pm}^2 \frac{1 - f(E') - f(E)}{E + E' + \omega + i\Gamma} \right] + [\omega + i\Gamma \rightarrow -(\omega + i\Gamma)], \end{aligned} \quad (5.47)$$

where $\epsilon = \epsilon_{\mathbf{k}+q/2}$, $\epsilon' = \epsilon_{\mathbf{k}-q/2}$, and $E = \sqrt{\epsilon^2 + \Delta^2}$. The coherence factors l_{\pm}^2 and p_{\pm}^2 are defined by

$$\begin{aligned} l_{\pm}^2 &= \frac{1}{2} \left(1 + \frac{\epsilon\epsilon' \pm \Delta\Delta'}{EE'} \right), \\ p_{\pm}^2 &= \frac{1}{2} \left(1 - \frac{\epsilon\epsilon' \pm \Delta\Delta'}{EE'} \right). \end{aligned} \quad (5.48)$$

In BCS theory one only obtains the “plus” coherence factors l_+^2 and p_+^2 [65]. In our case the “minus” coherence factors l_-^2 and p_-^2 are due to the fact that the pairing is between fermions on different planes, which can be in-phase or out-of-phase with each other.

We included a finite scattering rate Γ in the expression for χ_{\pm} [78], in order to remove a logarithmic singularity in $\chi_{\pm}''(\mathbf{q}, \omega)/\omega$ in the limit $\omega \rightarrow 0$. In conventional superconductors this logarithmic singularity, cut-off by a small scattering rate $\Gamma \ll T$, is responsible for the Hebel-Slichter peak in $(T_1 T)^{-1}$ just below the pairing transition temperature. For the cuprates it is well-known that there is an anomalously large scattering rate Γ , which can be a sizable fraction of the temperature T . Within our treatment of the t - J model this scattering rate is due to strong gauge-field fluctuations [35]. The large value of Γ implies that the Hebel-Slichter peak will be significantly smaller in the cuprates than in conventional superconductors.

Before presenting our numerical results, we will first discuss the value of the gap $\Delta_{\perp}(\mathbf{k})$ that enters the calculation of $\chi_{\pm}(\mathbf{q}, \omega)$. The gap Δ_{\perp} has to be quite large in order to identify Δ_{\perp} with the temperature scale below which $(T_1 T)^{-1}$ decreases, which happen at about 150 K for underdoped $\text{YBa}_2\text{Cu}_3\text{O}_{6.6}$. As was discussed in Secs. 5.3 and 5.4, the inter-plane gap $\Delta_{\perp}(\mathbf{k})$ is strongly enhanced by the antiferromagnetic correlations in underdoped cuprates. Within our RPA treatment we can only obtain a sufficiently large value for $\Delta(\mathbf{k})$ if the doping is very close to the critical doping $x_c \simeq 0.08$ at which the antiferromagnetic instability occurs. However, experiments show that the antiferromagnetic correlations remain rather strong over a wide range of doping. Unfortunately the RPA approximation is not powerful enough to capture this physics. We will therefore in this section use a value of Δ_{\perp} that fits the observed temperature dependence of $(T_1 T)^{-1}$, keeping in mind that the antiferromagnetic correlations are responsible for such a large value of the gap. Although $\Delta_{\perp}(\mathbf{k})$ is anisotropic around the Fermi surface, this anisotropy does not play an important role in the calculations below. The reason for this is that the expression for $(T_1 T)^{-1}$ is dominated by wave vectors $\mathbf{q} \simeq \mathbf{Q}_{\text{AF}}$, and the integrand for $\chi_{\pm}(\mathbf{Q}_{\text{AF}}, 0)$ is only large when $\mathbf{k} + \frac{1}{2}\mathbf{Q}_{\text{AF}}$ and $\mathbf{k} - \frac{1}{2}\mathbf{Q}_{\text{AF}}$ are both on the Fermi surface. This condition is only satisfied when $\mathbf{k} \pm \frac{1}{2}\mathbf{Q}_{\text{AF}} = \pm \frac{1}{2}\mathbf{Q}_{\text{AF}}$. Thus we can safely put $\Delta_{\perp} = \Delta_{\perp}(\frac{1}{2}\mathbf{Q}_{\text{AF}})$ in the calculation of $(T_1 T)^{-1}$. Notice that it is important that $\Delta_{\perp}(\mathbf{k})$ has an (extended) *s*-wave symmetry, because $\Delta_{\perp}(\frac{1}{2}\mathbf{Q}_{\text{AF}})$ would nearly vanish if $\Delta_{\perp}(\mathbf{k})$ had a *d*-wave symmetry.

We will now discuss the temperature dependence of the gap $\Delta_{\perp}(T)$. The most straightforward approximation would be to assume that Δ_{\perp} is a mean-field order parameter with a BCS-like temperature dependence. In that case $\Delta_{\perp}(T) = 0$ for $T > T_P$, and $\Delta_{\perp}(T)$ increases with an infinite slope just below T_P , as is shown in the insert in Fig. 5-8. However, this BCS picture assumes that there is a long coherence length, so that Δ_{\perp} can be interpreted as a long-range order parameter. As was pointed out by McMillan [79], this is not the appropriate picture if there is a relatively short coherence length, which is clearly the case for cuprates in the spin-gap phase. If the coherence length is small the long-range order parameter $\langle \Delta_{\perp}(\mathbf{r}) \rangle$ vanishes, and

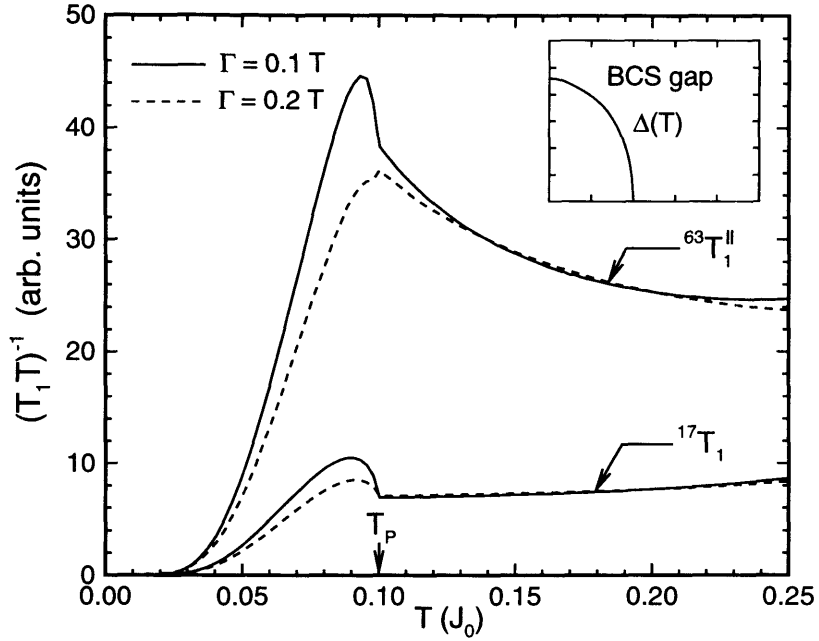


Figure 5-8: The NMR-relaxation rate $(T_1T)^{-1}$ on the copper and the oxygen sites for two values of the scattering rate Γ . This calculation uses a BCS-like temperature dependence for the spin-gap $\Delta_{\perp}(T)$. The Hebard-Slichter peak gets less pronounced when Γ increases. For $T > T_P$ the relaxation rate $({}^{63}T_1^{\parallel}T)^{-1}$ rises when T decreases, while $({}^{17}T_1T)^{-1}$ remains constant. This rise in $({}^{63}T_1^{\parallel}T)^{-1}$ is due to antiferromagnetic correlations. Notice that there is a sharp change in behavior for $T < T_P$ and $T > T_P$, which is not observed in experiments.

instead one should identify the gap with the *local* order parameter $\langle |\Delta_{\perp}(\mathbf{r})|^2 \rangle$. Thus we are not dealing with a true gap, but with a *pseudo* gap. This implies that there is not a sharp transition at which the gap disappears, because above the mean-field transition temperature the local orderparameter $\langle |\Delta_{\perp}(\mathbf{r})|^2 \rangle$ remains nonzero. This is indicated by the insert in Fig. 5-9, which shows a tail in the pseudo gap Δ_{\perp} for $T > T_P^0$. For most purposes this tail in $\Delta_{\perp}(T)$ is not very important, because it will be washed out by thermal fluctuations. However, the tail in $\Delta_{\perp}(T)$ will have a significant effect on the Hebel-Slichter peak in $(T_1T)^{-1}$, which will be smeared out if the gap $\Delta_{\perp}(T)$ is smoothly varying instead of dropping down to zero at $T = T_P$. This can explain the absence of a Hebel-Slichter peak for the high- T_c cuprates at the onset of the spin-gap phase.

In Fig. 5-8 we show plots of the NMR-relaxation rate $(T_1T)^{-1}$ on the copper and the oxygen sites for various values of the scattering rate Γ . This calculation assumes

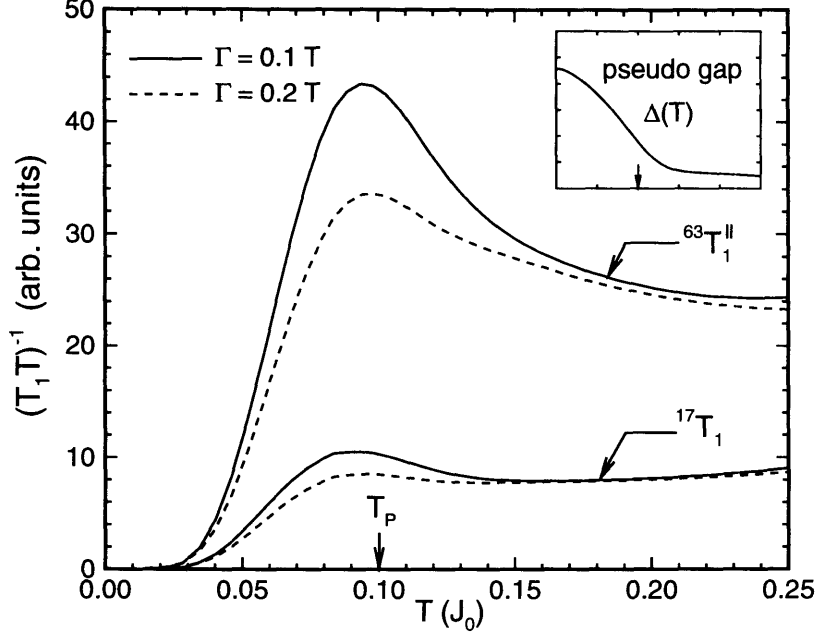


Figure 5-9: The NMR-relaxation rate $(T_1T)^{-1}$ on the copper and the oxygen sites, using a pseudo-gap $\Delta_{\perp}(T)$ which has a finite tail for $T > T_P^0$, as is shown in the inset. The main difference with Fig. 5-8 is that the Hebard-Slichter peak gets smeared out over a wider range of temperature. As a result $(T_1T)^{-1}$ varies smoothly as a function of temperature, which agrees well with measurements on underdoped $\text{YBa}_2\text{Cu}_3\text{O}_{6.6}$.

a BCS-like behavior for the gap $\Delta_{\perp}(T)$, and T_P is chosen to be equal to $0.1J$. For small values of the scattering rate Γ the Hebel-Slichter peak is quite pronounced, but the size of this peak gets smaller and smaller when Γ increases. However, even for a large value of Γ one still observes a drastic change in the behavior of $(T_1T)^{-1}$ when T crosses the transition temperature T_P . Also notice that for $T > T_P$, $(^{63}\text{T}_1T)^{-1}$ increases when T decreases, while $(^{17}\text{T}_1T)^{-1}$ remains almost constant. The reason for this difference is that the form factor $^{63}F(\mathbf{q})$ is finite at $\mathbf{q} = (\pi, \pi)$, while $^{17}F(\mathbf{q})$ vanishes at $\mathbf{q} = (\pi, \pi)$ according to Eq. (5.43). Therefore only the copper sites can take full advantage of the enhancement of $\chi''_{\text{phys}}(\mathbf{q}, \omega)$ for $\mathbf{q} \simeq \mathbf{Q}_{\text{AF}}$, which becomes stronger and stronger at lower temperatures.

In Fig. 5-9 we again show $(T_1T)^{-1}$ as a function of temperature, but this time we assumed that $\Delta_{\perp}(T)$ has a finite tail for $T \gtrsim T_P^0$, as is shown in the inset. The main difference between Figs. 5-8 and 5-9 is that the tail in $\Delta_{\perp}(T)$ smears out the Hebel-Slichter peak. As a result the temperature dependence of $(T_1T)^{-1}$ in Fig. 5-9 is

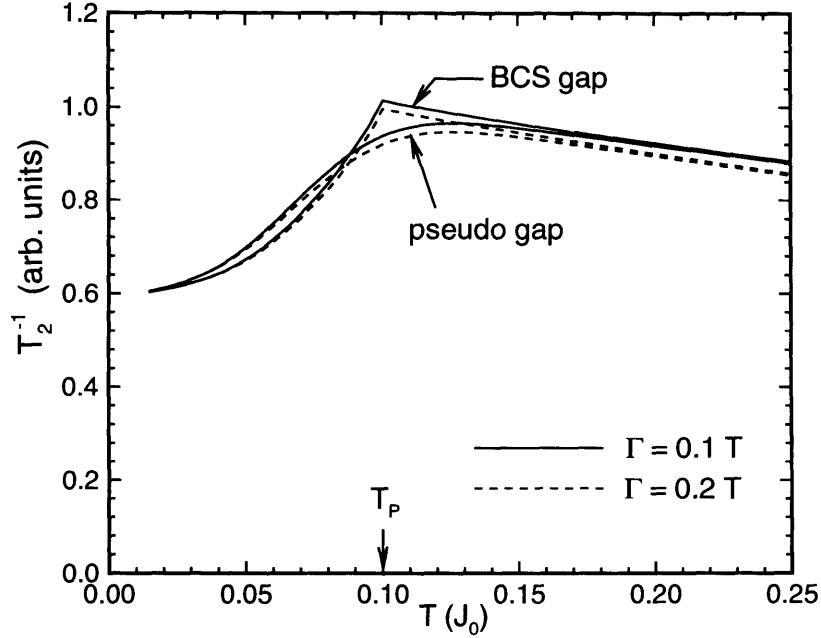


Figure 5-10: The echo-decay rate T_2^{-1} as a function of temperature for two values of the scattering rate Γ . The dashed lines assume a BCS-like temperature dependence of the spin-gap $\Delta_{\perp}(T)$, and the solid lines assume a pseudo-gap behavior. The tail in the pseudo-gap removes the singular behavior of T_2^{-1} at $T = T_P$. Changing the value of Γ does not have a significant effect on the behavior of T_2^{-1} .

smooth over the entire temperature range, which agrees much better with experiments than the plots in Fig. 5-8. As explained earlier in this section, we think that a tail in the pseudo gap $\Delta_{\perp}(T)$ is closer to the truth than a BCS-like behavior of $\Delta_{\perp}(T)$.

We now turn to the calculation of the spin echo-decay rate rate T_2^{-1} , which has been measured experimentally by Takigawa [80]. It is given theoretically by [81]

$$\frac{1}{T_2} \propto \left(\sum_{\mathbf{q}} \chi_{\text{phys}}(\mathbf{q}, 0)^2 \right)^{1/2}. \quad (5.49)$$

In Fig. 5-10 we plot T_2^{-1} versus temperature for various values of the scattering rate Γ . Notice that in contrast to Figs. 5-8 and 5-9, introducing a finite Γ does not modify T_2^{-1} significantly. Comparing the solid lines and the dashed lines we see that a tail in the pseudo-gap $\Delta_{\perp}(T)$ smears out the singular behavior of T_2^{-1} at $T = T_P^0$. Notice that for $T > T_P^0$, the echo-decay rate T_2^{-1} increases upon lowering T , which is due to antiferromagnetic correlations. This resembles the temperature dependence of

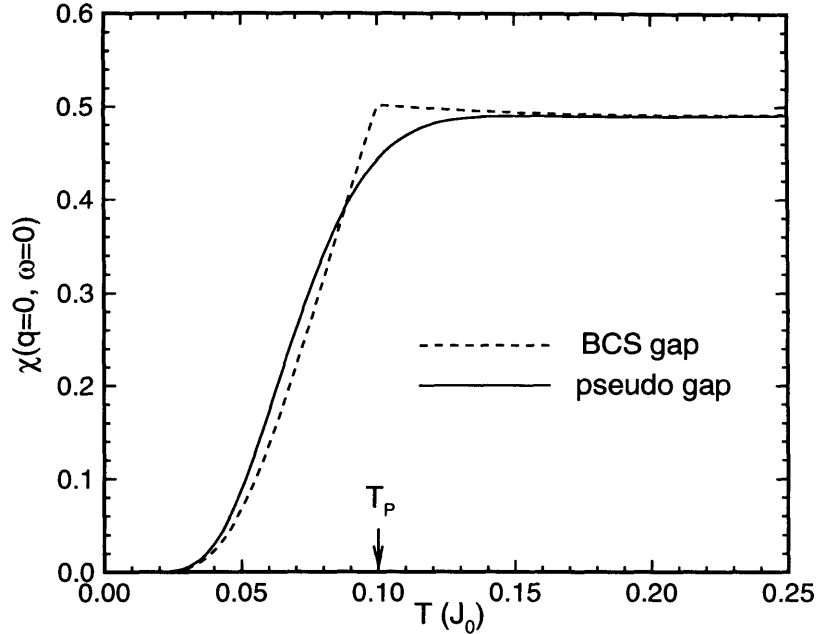


Figure 5-11: The Knight shift as a function of temperature. In this calculation we used $\Gamma = 0$. The dashed line assumes a BCS-like temperature dependence of the spin-gap $\Delta_{\perp}(T)$, and the solid line assumes a pseudo-gap behavior. The Knight shift decays exponentially when $T \lesssim \Delta_{\perp}(T)$.

$({}^{63}\text{T}_1 T)^{-1}$ in Fig. 5-9. However, for $T < T_P^0$ the temperature dependences of $(T_1 T)^{-1}$ and T_2^{-1} are very different, because $(T_1 T)^{-1}$ vanishes exponentially for $T \rightarrow 0$, while T_2^{-1} remains finite.

For completeness we show in Fig. 5-11 the temperature dependence of the Knight shift, which is proportional to $\chi_{\text{phys}}(\mathbf{q} \rightarrow 0, \omega = 0)$. This quantity essentially probes the density of states around the Fermi surface, and vanishes exponentially when a spin-gap opens up. We conclude that our calculation of T_1^{-1} , T_2^{-1} and $\chi_{\text{phys}}(0, 0)$ exhibits spin-gap behavior qualitatively similar to experiments, and that in order to explain the onset of the spin gap at $150 \text{ K} \simeq 0.1 J_{\parallel}^0$, a spin gap of the order $\Delta_{\perp} \simeq 0.2 J_{\parallel}^0$ is required.

5.7 Discussion

In this paper we studied a model for two CuO_2 planes, coupled with a small antiferromagnetic inter-plane interaction $J_{\perp}^0 \sum_i \mathbf{S}_i^{(1)} \cdot \mathbf{S}_i^{(2)}$. This model is relevant for

multi-layered high- T_c cuprates, that have two (or more) CuO_2 planes in a unit cell.

Using a random-phase approximation we showed that close to half filling the susceptibility $\chi_{nn'}^{\text{RPA}}(\mathbf{q}, q_z)$ is strongly peaked at the nesting vector $\mathbf{q} \simeq \mathbf{Q}_{\text{AF}}$, due to short-ranged antiferromagnetic correlations of the spins in each plane. Our expression for $\chi^{\text{RPA}}(\mathbf{q}, q_z)$ explains the strong modulations as a function of q_z that have been observed in neutron scattering experiments for underdoped cuprates [66]. Within the same RPA analysis we showed that the effective coupling constants $J_{\parallel}^{\text{eff}}(\mathbf{r})$ and $J_{\perp}^{\text{eff}}(\mathbf{r})$ are also strongly enhanced by antiferromagnetic correlations. As a result $J_{\parallel}^{\text{eff}}(\mathbf{r})$ and $J_{\perp}^{\text{eff}}(\mathbf{r})$ can extend over several lattice spacings. Close to the AF instability $J_{\parallel}^{\text{eff}}$ and J_{\perp}^{eff} become comparable in strength, because $J_{\perp}^{\text{eff}}(\mathbf{q})$ is stronger enhanced than $J_{\parallel}^{\text{eff}}(\mathbf{q})$ for $\mathbf{q} \simeq \mathbf{Q}_{\text{AF}}$.

Due to the fact that the inter-plane coupling $J_{\perp}^{\text{eff}}(\mathbf{r})$ is longer ranged, the system can form Cooper pairs that consist of fermions that are separated by several lattice spacings, characterized by the order parameter $\Delta_{\perp}(\mathbf{r})$. We solved the self-consistency equations for the order parameters $\Delta_{\perp}(\mathbf{r})$, and found that the inter-plane pairing is indeed strongly enhanced by the antiferromagnetic correlations. An interesting aspect is that the gap $\Delta_{\perp}(\mathbf{k})$ has an extended s -wave symmetry without nodes. A similar treatment of the in-plane pairing would lead to a gap $\Delta_{\parallel}(\mathbf{k})$ with an extended d -wave symmetry with nodes at four points on the Fermi surface. The gap $\Delta_{\perp}(\mathbf{k})$ is enhanced close to the Fermi surface, and is in particular large at the corners of the Fermi surface. How much can we trust the numbers that come out of this calculation? First of all the value of the gap is quite sensitive on the exact value of the parameters of the model. One also has to keep in mind that the RPA approximation is a gross oversimplification when the system is close to an AF instability. We can however state that our results are in qualitative agreement with the observed spin gap in underdoped $\text{YBa}_2\text{Cu}_3\text{O}_{6.6}$.

We propose that the enhanced inter-plane pairing provides a mechanism for the observed spin-gap phase in multi-layer cuprates. To support this we argued that the gauge field, which destroys the in-plane gap Δ_{\parallel} in a single CuO_2 plane close to half filling, is less effective in destroying the inter-plane gap Δ_{\perp} . The physical

argument for this is that the out-of-phase mode $a_q^{(-)} = (a_q^{(1)} - a_q^{(2)})/\sqrt{2}$ remains massless when the inter-plane gap $\Delta_{\perp}(\mathbf{k})$ opens up. This implies that the gauge field mode $a_q^{(-)}$ is not pair breaking. A more detailed calculation in Ref. [10] of the free energy of a gauge field indicates that the gauge field mode $a_q^{(-)}$ actually *favors* pairing, and will partly cancel the pair-breaking effects of the in-phase gauge field mode $a_q^{(+)} = (a_q^{(1)} + a_q^{(2)})/\sqrt{2}$. The physical consequence of this is that at low doping the inter-plane gap $\Delta_{\perp}(\mathbf{k})$ can survive at a higher temperature than the in-plane gap $\Delta_{\parallel}(\mathbf{k})$. This makes it possible that inter-plane pairing is responsible for the observed spin-gap phase in multi-layer cuprates.

Our model is able to explain the unusual temperature dependence of several physical quantities that are related to the spin susceptibility. We calculated the NMR-relaxation rate $(T_1T)^{-1}$, using a value of the inter-plane gap Δ_{\perp} that corresponds with the observed spin gap in underdoped $\text{YBa}_2\text{Cu}_3\text{O}_{6.6}$. Our numerical result show that at high temperatures $(^{63}\text{T}_1T)^{-1}$ increases when T decreases, while $(^{17}\text{T}_1T)^{-1}$ remains almost constant. Below the pairing transition temperature T_P , $(^{63}\text{T}_1T)^{-1}$ and $(^{17}\text{T}_1T)^{-1}$ both decrease rapidly. The Hebel-Slichter peak is reduced by the assumption of a pseudo-gap behavior and the presence of inelastic scattering, presumably due to gauge field fluctuations. The physical reason why there is a pseudo gap instead of the usual BCS gap, is because there is a rather short coherence length, so that the gap should be interpreted as a *local* order parameter [79], which does not undergo any sharp transitions.

So far we have ignored any inter-layer hopping of the form $t_{\perp}c_{i\sigma}^{(1)\dagger}c_{i\sigma}^{(2)}$. From the analog of Eq. (5.3) it is clear that ignoring t_{\perp} is reasonable provided that $xt_{\perp} < J_{\perp}$. If this is violated we expect inter-layer pairing to be suppressed, but we have not studied this quantitatively. Not enough is known about t_{\perp} and J_{\perp} , but our guess is that xt_{\perp} and J_{\perp} are comparable. However, even a small t_{\perp} will lead to coherence between bosons on the two planes immediately below T_{BE} , so that the fermion pairing becomes genuine superconducting pairing between electrons on the two layers.

The possibility of inter-plane pairing has interesting consequences for the symmetry of the superconducting gap in bi-layer materials. In Fig. 5-12 we show a

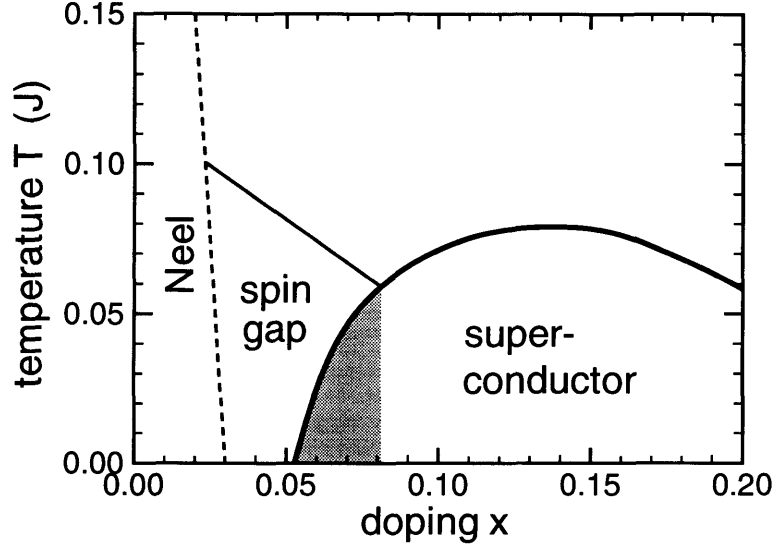


Figure 5-12: A schematic phase diagram for bi-layer cuprates. We predict that the spin-gap phase is due to inter-layer fermion pairing, enhanced by antiferromagnetic correlations. Below the superconducting transition (thick solid line) the s -wave inter-plane pairing and the d -wave in-plane pairing coexist. We expect that for underdoped samples $\Delta_{\perp}(\mathbf{k})$ dominates over $\Delta_{\parallel}(\mathbf{k})$, giving rise to a nodeless superconducting state, indicated by the shaded region. At higher doping the four nodes of a d -wave superconductor are split into eight nodes.

schematic phase diagram for these materials, in which the thick solid line denotes the onset of superconductivity. At low temperatures the in-plane d -wave and the inter-plane s -wave pairing will co-exist, giving rise to a quasi-particle dispersion $E(\mathbf{k}) = (\epsilon(\mathbf{k})^2 + \Delta_{\pm}(\mathbf{k})^2)^{1/2}$, where $\Delta_{\pm}(\mathbf{k}) = \Delta_{\perp}(\mathbf{k}) \pm \Delta_{\parallel}(\mathbf{k})$. If Δ_{\perp} is indeed as large as 150 K, as the experiments seem to indicate, it is likely that for underdoped materials $\Delta_{\perp} > |\Delta_{\parallel}|$ for all \mathbf{k} , which implies that the superconducting gap is nodeless. This is indicated by the shaded region in Fig. 5-12. As doping is increased, Δ_{\perp} decreases rapidly with the loss of antiferromagnetic correlations, and we crossover to a superconducting state with nodes. We expect that in fully doped systems the d -wave order parameter Δ_{\parallel} dominates, but as long as Δ_{\perp} remains finite the four nodes for a conventional d -wave superconductor will be split into eight nodes.

Acknowledgements

This work was done in collaboration with Patrick A. Lee [12]. We would like to thank Andy Millis for helpful discussions. The work was supported by the NSF through the Material Research Laboratory under Grant No. DMR-90-22933.

Appendix A

Decoupling of $\mathbf{S}_i \cdot \mathbf{S}_j$

We like to discuss a recipe that helps to decide how to decouple the four-fermion term $\mathbf{S}_i \cdot \mathbf{S}_j$ into the different channels [30]. By means of a Hubbard-Stratonovich transformation any four-fermion term $f_i^\dagger f_i f_j^\dagger f_j$ can be decoupled into either “exchange” terms of the form $f_i^\dagger f_j$, “pairing” terms of the form $f_i f_j$, or “direct” terms of the form $f_i^\dagger f_i$. We like to take advantage of the freedom one has in taking combinations of these three decouplings.

The idea is to write

$$\mathbf{S}_i \cdot \mathbf{S}_j = \hat{v}_E + \hat{v}_P + \hat{v}_D, \quad (\text{A.1})$$

and to use introduce Hubbard-Stratonovich fields to decouple \hat{v}_E , \hat{v}_P and \hat{v}_D into, respectively, exchange, pairing and direct terms. The way to determine $\hat{v}_{E,P,D}$ is to require that decoupling $\hat{v}_P + \hat{v}_D$ into exchange terms will not generate terms already generated by \hat{v}_E . A similar condition is imposed on $\hat{v}_D + \hat{v}_E$ and $\hat{v}_E + \hat{v}_P$. These three conditions can be viewed as self-consistency conditions for the decoupling into the three terms $\hat{v}_{E,P,D}$.

To implement the above recipe, we take $\hat{v}_{E,P,D}$ of the form

$$\hat{v}_{E,P,D} = \sum_{k=0}^3 c_{E,P,D}^k (f_{i\alpha}^\dagger \sigma_{\alpha\beta}^k f_{i\beta}) (f_{j\alpha'}^\dagger \sigma_{\alpha'\beta'}^k f_{j\beta'}) \quad (\text{A.2})$$

(σ^k are Pauli matrices and σ^0 is the identity matrix). We specify a priori that we

want to end up with a decomposition that contains exchange terms of the specific form $f_{i\uparrow}^\dagger f_{j\uparrow} + f_{i\downarrow}^\dagger f_{j\downarrow}$ and pairing terms of the specific form $f_{i\uparrow} f_{j\downarrow} - f_{i\downarrow} f_{j\uparrow}$.

We now have to determine the coefficients $c_{E,P,D}^k$, such that the conditions of the recipe above are satisfied. We take the decoupling into exchange terms as an example. By commuting fermion fields one can write each $\hat{v}_{E,P,D}$ as a sum of squares of exchange terms:

$$\hat{v} = -\frac{1}{2}(c^0 + c^1 + c^2 + c^3) \left[(f_{i\uparrow}^\dagger f_{j\uparrow} + f_{i\downarrow}^\dagger f_{j\downarrow})(f_{j\uparrow}^\dagger f_{i\uparrow} + f_{j\downarrow}^\dagger f_{i\downarrow}) - n_i \right] \quad (\text{A.3})$$

$$-\frac{1}{2}(c^0 - c^1 - c^2 + c^3) \left[(f_{i\uparrow}^\dagger f_{j\uparrow} - f_{i\downarrow}^\dagger f_{j\downarrow})(f_{j\uparrow}^\dagger f_{i\uparrow} - f_{j\downarrow}^\dagger f_{i\downarrow}) - n_i \right] \quad (\text{A.4})$$

$$-\frac{1}{2}(c^0 + c^1 - c^2 - c^3) \left[(f_{i\uparrow}^\dagger f_{j\downarrow} + f_{i\downarrow}^\dagger f_{j\uparrow})(f_{j\downarrow}^\dagger f_{i\uparrow} + f_{j\uparrow}^\dagger f_{i\downarrow}) - n_i \right] \quad (\text{A.5})$$

$$-\frac{1}{2}(c^0 - c^1 + c^2 - c^3) \left[(f_{i\uparrow}^\dagger f_{j\downarrow} - f_{i\downarrow}^\dagger f_{j\uparrow})(f_{j\downarrow}^\dagger f_{i\uparrow} - f_{j\uparrow}^\dagger f_{i\downarrow}) - n_i \right]. \quad (\text{A.6})$$

In order that \hat{v}_E decouples into exchange terms of the form $f_{i\uparrow}^\dagger f_{j\uparrow} + f_{i\downarrow}^\dagger f_{j\downarrow}$, we need (A.4)-(A.6) to vanish. That implies $c_E^k = c_E^0$ ($k = 1, 2, 3$). In order that $\hat{v}_P + \hat{v}_D$ does not generate exchange terms already generated by \hat{v}_E , we need (A.3) to vanish for $\hat{v} = \hat{v}_P + \hat{v}_D$, i.e. $c_P^0 + c_D^0 = -\sum_{k=1}^3 (c_P^k + c_D^k)$.

Using the same arguments for the decoupling into pairing terms, we find $c_P^k = -c_P^0$ and $c_D^0 + c_E^0 = \sum_{k=1}^3 (c_D^k + c_E^k)$. Finally remark that Eq. (A.1) gives the relationships $c_E^0 + c_P^0 + c_D^0 = 0$ and $c_E^k + c_P^k + c_D^k = \frac{1}{4}$ (for $k = 1, 2, 3$). Putting everything together, the coefficients $c_{E,P,D}^k$ are determined uniquely:

$$\begin{aligned} c_E^0 &= \frac{3}{16}, & c_E^k &= \frac{3}{16}, \\ c_P^0 &= -\frac{3}{16}, & c_P^k &= \frac{3}{16}, \\ c_D^0 &= 0, & c_D^k &= -\frac{1}{8}. \end{aligned} \quad (\text{A.7})$$

Having found all coefficients $c_{E,P,D}^k$, we can now rewrite $\hat{v}_{E,P,D}$ as

$$\begin{aligned} \hat{v}_E &= -\frac{3}{8}(f_{i\uparrow}^\dagger f_{j\uparrow} + f_{i\downarrow}^\dagger f_{j\downarrow})(f_{j\uparrow}^\dagger f_{i\uparrow} + f_{j\downarrow}^\dagger f_{i\downarrow}) + \frac{3}{8}n_i, \\ \hat{v}_P &= -\frac{3}{8}(f_{i\downarrow}^\dagger f_{j\uparrow}^\dagger - f_{i\uparrow}^\dagger f_{j\downarrow}^\dagger)(f_{j\uparrow} f_{i\downarrow} - f_{j\downarrow} f_{i\uparrow}), \\ \hat{v}_D &= -\frac{1}{2}\mathbf{S}_i \cdot \mathbf{S}_j. \end{aligned} \quad (\text{A.8})$$

For self-consistency we need that $\hat{v}_E + \hat{v}_P$ does not generate any direct terms at the mean-field level. This is equivalent to $\langle \mathbf{S}_i \rangle = 0$.

The last step is to introduce three Hubbard-Stratonovich fields, to decouple $\hat{v}_{E,P,D}$ into quadratic terms. This finally leads to the following decomposition of $\mathbf{S}_i \cdot \mathbf{S}_j$:

$$e^{-J \sum_{\langle i,j \rangle} \mathbf{S}_i \cdot \mathbf{S}_j} \propto \int \prod_{\langle i,j \rangle} d\chi_{ji}^* d\chi_{ji} d\Delta_{ji}^* d\Delta_{ji} \prod_i \prod_{k=1}^3 d\rho_i^k e^{-\sum_{\langle i,j \rangle} \mathcal{A}_{ji}(\chi, \Delta, \rho)} \quad (\text{A.9})$$

$$\begin{aligned} \mathcal{A}_{ji} = & \frac{3J}{8} \left[|\chi_{ji}|^2 + |\Delta_{ji}|^2 - \chi_{ji}^* (f_{j\sigma}^\dagger f_{i\sigma}) - c.c. + n_i \right. \\ & \left. - \Delta_{ji}^* (f_{j\uparrow} f_{i\downarrow} - f_{j\downarrow} f_{i\uparrow}) - c.c. \right] \\ & + \frac{J}{2} \left[|\rho_i|^2 - \sum_{k=1}^3 \rho_i^k (f_j^\dagger \sigma^k f_j) \right]. \end{aligned} \quad (\text{A.10})$$

Appendix B

Diagonalization of H^{MF}

By going to Fourier space the mean-field version of the Hamiltonian (2.4) can be written in matrix form:

$$H^{\text{MF}} = J' \sum'_k \eta_k^\dagger \mathbf{M}_k \eta_k + J' \sum'_k \zeta_k^\dagger \mathbf{N}_k \zeta_k \quad (\text{B.1})$$

(\sum'_k denotes a sum over half of the Brioullin zone and $J' \equiv 3/4J$). In the above formula

$$\eta_k = \begin{pmatrix} f_{k\uparrow} \\ f_{k+Q,\uparrow} \\ f_{-k\downarrow}^\dagger \\ f_{-k-Q,\downarrow}^\dagger \end{pmatrix}, \quad \zeta_k = \begin{pmatrix} b_k \\ b_{k+Q} \end{pmatrix}, \quad (\text{B.2})$$

and \mathbf{M}_k and \mathbf{N}_k are the matrices [27]:

$$\mathbf{M}_k = \begin{pmatrix} -\mu_f - \chi\gamma_k \cos \theta & -i\chi\varphi_k \sin \theta & -\Delta a_k^* & 0 \\ i\chi\varphi_k \sin \theta & -\mu_f + \chi\gamma_k \cos \theta & 0 & \Delta a_k^* \\ -\Delta a_k & 0 & \mu_f + \chi\gamma_k \cos \theta & -i\chi\varphi_k \sin \theta \\ 0 & \Delta a_k & i\chi\varphi_k \sin \theta & \mu_f - \chi\gamma_k \cos \theta \end{pmatrix},$$

$$\mathbf{N}_k = \begin{pmatrix} -\mu_b - 2t\chi\gamma_k \cos \theta & -2it\chi\varphi_k \sin \theta \\ 2it\chi\varphi_k \sin \theta & -\mu_b + 2t\chi\gamma_k \cos \theta \end{pmatrix} \quad (\text{B.3})$$

($a_{\mathbf{k}} = \gamma_{\mathbf{k}} \cos \tau + i\varphi_{\mathbf{k}} \sin \tau$, $\gamma_{\mathbf{k}} = \cos k_x + \cos k_y$ and $\varphi_{\mathbf{k}} = \cos k_x - \cos k_y$). All energies are written in units of $J' \equiv 3/4J$.

The matrices $\mathbf{M}_{\mathbf{k}}$ and $\mathbf{N}_{\mathbf{k}}$ can be diagonalized by means of a Bogoliubov transformation. This leads to the diagonal Hamiltonian in Eq. (2.8).

Appendix C

Calculation of ρ_{ret}^x

In this Appendix we evaluate the expression for $\rho_{\text{ret}}^x(u/2, R)$ in Eq. (3.33). This expression is different from the non-interacting density matrix $\rho_{1D}^0(u/2, R)$ due to the constraint $0 < x_1 < \dots < x_{N/2-1} < R$, which lowers the entropy of the particle. [Note: we renamed the variables x_{N-n} to x_n .] We will approximate the integrals in Eq. (3.33) by calculating successive integrals of the form

$$\begin{aligned}
 \rho_{n+1}(x_{n+1}) &= \int_0^{x_n} dx_n \rho_{1D}^0(x_n, n\tau_\phi) \rho_{1D}^0(x_{n+1} - x_n, \tau_\phi) \\
 &= \frac{\exp\left(\frac{-Mx_{n+1}^2}{2(n+1)\tau_\phi}\right)}{\sqrt{2\pi(n+1)\tau_\phi/M}} \int_0^{x_{n+1}} \frac{dx_n}{\sqrt{2\pi}} \sqrt{\frac{n+1}{n\tau_\phi/M}} \\
 &\quad \times \exp\left[-\frac{n+1}{2n\tau_\phi/M} \left(x_n - \frac{nx_{n+1}}{n+1}\right)^2\right] \\
 &= \rho_{1D}^0(x_{n+1}, (n+1)\tau_\phi) \times F_n\left(\frac{x_{n+1}}{n+1} \sqrt{\tau_\phi/M}\right),
 \end{aligned} \tag{C.1}$$

where the correction factor F_n is defined by

$$F_n(\alpha) = \int_{-\alpha\sqrt{n(n+1)}}^{\alpha\sqrt{\frac{n+1}{n}}} \frac{dy}{\sqrt{2\pi}} e^{-\frac{1}{2}y^2}. \tag{C.2}$$

Notice that $F_n(\alpha)$ approaches 1 for $\alpha \gg 1$, so that the non-interacting result is recovered for $\alpha \gg 1$. The approximation that we make is that we replace the argument of the correction factor F_n by its average value, i.e. we replace $x_{n+1}/(n+1)$ by

$R/(N/2)$, so that the argument of $F_n(\alpha)$ becomes $\langle \alpha \rangle = 2R/N/\sqrt{\tau_\phi/M}$. After this replacement F_n is independent of the integration variable x_{n+1} , which allows us to take F_n outside the integrals, and to repeat the integral in Eq. (C.1) successively for $n = 1, 2, \dots, N/2 - 1$. This leads to the following approximation for ρ_{ret}^x in Eq. (3.33):

$$\rho_{\text{ret}}^x(u/2, R) \simeq \rho_{1D}^0(u/2, R) \prod_{n=1}^{N/2-1} F_n \left(\frac{2R}{N\sqrt{\tau_\phi}} \right). \quad (\text{C.3})$$

In the limit $N \rightarrow \infty$ we can obtain an asymptotic expression for ρ_{ret}^x by using the following approximation for $F_n(\alpha)$:

$$F_n(\alpha) \simeq \int_{-\infty}^{\alpha + \frac{\alpha}{2n}} \frac{dy}{\sqrt{2\pi}} e^{-\frac{1}{2}y^2} \simeq \left[1 + \frac{\gamma'(\alpha)}{n} \right] F(\alpha), \quad (\text{C.4})$$

where in the limit $N \rightarrow \infty$ the constants F and γ' are given by

$$\begin{aligned} F(\alpha) &= \int_{-\infty}^{\alpha} \frac{dy}{\sqrt{2\pi}} e^{-\frac{1}{2}y^2} \\ \gamma'(\alpha) &= \frac{\alpha}{2F(\alpha)\sqrt{2\pi}} e^{-\frac{1}{2}\alpha^2}. \end{aligned} \quad (\text{C.5})$$

Substituting Eq. (C.4) into Eq. (C.3), and using that $\prod_n (1 + \gamma'/n) \sim (N/2)^{\gamma'}$, one obtains

$$\begin{aligned} \rho_{\text{ret}}^x(u/2, R) &\sim \rho_{1D}^0(u/2, R) N^{\gamma'} e^{\frac{1}{2}N \log F} \\ &\sim \rho_{1D}^0(u/2, R) \left(\frac{u}{\tau_\phi} \right)^{\gamma'} e^{-c'u/\tau_\phi}, \end{aligned} \quad (\text{C.6})$$

where $c' \equiv -\frac{1}{2} \log F$. The last two factors in Eq. (C.6) have the following physical interpretation. The exponential $\exp(-c'u/\tau_\phi)$ gives rise to a shift in the band edge of the density of states, which is equivalent to a shift in the chemical potential. The factor $(u/\tau_\phi)^{\gamma'}$ is more important, because it modifies the nature of the singularity of the density of states near the band edge. This is discussed in more detail at the end of Sec. 3.4. In Fig. C-1 we show a plot of the exponent γ' as a function of α , using the estimate in Eq. (C.5). Notice that for large α the exponent γ' vanishes exponentially.

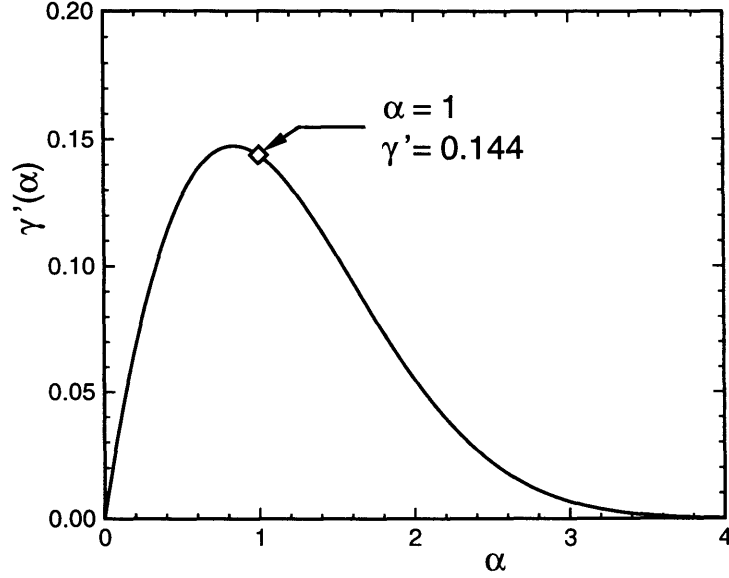


Figure C-1: The exponent γ' as a function of $\alpha = 2R/N/\sqrt{\tau_\phi/M}$. This exponent modifies the enhancement of the density of states near the band edge. For $\alpha \gg 1$ one approaches the non-interacting limit, and hence $\gamma' \simeq 0$. In this paper we use $\alpha = 1$, so that $\gamma' \simeq 0.144$. This is indicated by the diamond \diamond in the figure.

This is not surprising because this corresponds to the situation in which the boson has very little time to get from 0 to R in imaginary time u , so that the typical path will be almost straight. That means that the constraint $0 < x_1 < \dots < x_{N/2-1} < R$ is essentially irrelevant, and therefore one should recover the non-interacting result, i.e. $\gamma' = 0$. For our choice of R in Eq. (3.35), α is exactly equal to 1, and in that case γ' and c' are approximately

$$\begin{aligned} \gamma' &\simeq 0.144; \\ c' &\simeq 0.086. \end{aligned} \tag{C.7}$$

This particular value of γ' is indicated by the diamond in Fig. C-1.

Bibliography

- [1] J.G. Bednorz and K.A. Müller, *Z. Phys. B* **64**, 189 (1986).
- [2] K.A. Müller, *Physica C* **185-189**, 3 (1991).
- [3] S.S.P. Parkin *et al*, *Phys. Rev. B* **38**, 6531 (1988).
- [4] A. Schilling, M. Cantoni, J.D. Guo, H.R. Ott, *Nature* **363**, 56 (1993).
- [5] B. Keimer *et al.*, *Phys. Rev. B* **46**, 14034 (1992).
- [6] C.L. Kane, P.A. Lee, and N. Read, *Phys. Rev. B* **39**, 6880 (1989).
- [7] M.U. Ubbens and P.A. Lee, *Phys. Rev. B* **46**, 8434 (1992).
- [8] M.U. Ubbens, P.A. Lee, and N. Nagaosa, *Phys. Rev. B* **48**, 13762 (1993).
- [9] M.U. Ubbens and P.A. Lee, submitted to *Phys. Rev. B* (1993).
- [10] M.U. Ubbens and P.A. Lee, to appear in *Phys. Rev. B* (1994).
- [11] M.U. Ubbens and P.A. Lee, submitted to *Phys. Rev. Lett.* (1993).
- [12] M.U. Ubbens and P.A. Lee, M.I.T. preprint (1993).
- [13] P.W. Anderson, *Science* **235**, 1196 (1987).
- [14] G. Baskaran, Z. Zou, P.W. Anderson, *Solid State Commun.* **63**, 973 (1987).
- [15] A.E. Ruckenstein, P.J. Hirschfeld, J. Appel, *Phys. Rev. B* **36**, 857 (1987).
- [16] G. Kotliar, *Phys. Rev. B* **37**, 3664 (1988).

- [17] G. Kotliar, J. Liu, Phys. Rev. B **38**, 5142 (1988).
- [18] I. Affleck, J.B. Marston, Phys. Rev. B **37**, 3774 (1988).
- [19] J.B. Marston, I. Affleck, Phys. Rev. B **39**, 11538 (1989).
- [20] I. Affleck, Z. Zou, T. Hsu, P.W. Anderson, Phys. Rev. B **38**, 745 (1988).
- [21] J. Ye, S. Sachdev, Phys. Rev. B **44**, 10173 (1991).
- [22] T. Dombre, G. Kotliar, Phys. Rev. B **39**, 855 (1989).
- [23] L.B. Ioffe, A.I. Larkin, Phys. Rev. B **39**, 8988 (1989).
- [24] P. Lederer, D. Poiblan, T.M. Rice, Phys. Rev. Lett. **63**, 1519 (1989).
- [25] P.W. Anderson, Phys. Scr. **T27**, 60 (1989).
- [26] P.B. Wiegmann, Phys. Scr. **T27**, 160 (1989).
- [27] F.C. Zhang, Phys. Rev. Lett. **64**, 974 (1990).
- [28] G.J. Chen, R. Joynt, F.C. Zhang, C. Gros, Phys. Rev. B **42**, 2662 (1990).
- [29] G.J. Chen, R. Joynt, F.C. Zhang, J. Phys.: Cond. Mat. **3**, 5213 (1991).
- [30] J.W. Negele, H. Orland, *Quantum Many-Particle Systems*, p. 335 (Addison-Wesley, 1988).
- [31] P.A. Lee, Phys. Rev. Lett. **63**, 680 (1989).
- [32] M. Grilli and G. Kotliar, Phys. Rev. Lett. **63**, 1170 (1990).
- [33] N. Nagaosa, P.A. Lee, Phys. Rev. Lett. **64**, 2450 (1990).
- [34] N. Nagaosa and P.A. Lee, Phys. Rev. B **45**, 966 (1992).
- [35] P.A. Lee and N. Nagaosa, Phys. Rev. B **46**, 5621 (1992).
- [36] N. Nagaosa and P.A. Lee, Phys. Rev. B **43**, 1233 (1991).

- [37] L.B. Ioffe and G. Kotliar, Phys. Rev. B **42**, 10348 (1990).
- [38] M. Reizer, Phys. Rev. B **39**, 1602 (1989).
- [39] L.B. Ioffe and V. Kalmeyer, Phys. Rev. B **44**, 750 (1991).
- [40] K. Kuboki, J. Phys. Soc. Jpn. **62**, 420 (1993).
- [41] J.M. Wheatley and T.M. Hong, Phys. Rev. B **43**, 6288 (1991).
- [42] J.M. Wheatley, Phys. Rev. Lett. **67**, 1181 (1991).
- [43] J.M. Wheatley and A.J. Schofield, Int. J. of Mod. Phys. **6**, 665 (1992).
- [44] R.P. Feynman, *Statistical Mechanics* (Addison Wesley, Redwood City, CA, 1972), Chap. 3.
- [45] B.L. Altshuler and L.B. Ioffe, Phys. Rev. Lett. **69**, 2979 (1992).
- [46] D.S. Fisher and P.C. Hohenberg, Phys. Rev. B **37**, 4936 (1988).
- [47] V.N. Popov, Theor. Math. Phys. **11**, 565 (1972), *Functional Integrals in Quantum Field Theory and Statistical Physics* (Reidel, Dordrecht, 1983), Chap. 6.
- [48] D.A. Bonn *et al*, Phys. Rev. B **47**, 11314 (1993).
- [49] Z.-X. Shen *et al*, Phys. Rev. Lett. **70**, 1553 (1993).
- [50] T.R. Thurston *et al*, Phys. Rev. **46**, 9128 (1992).
- [51] S.E. Barrett *et al*, Phys. Rev. Lett. **66**, 108 (1991); N. Bulut and D.J. Scalapino, Phys. Rev. Lett. **68**, 706 (1992).
- [52] W. Hardy *et al*, PhysRev. Lett. **70**, 3999 (1993).
- [53] D.A. Wollman *et al*, Illinois preprint.
- [54] G. Baskaran and P.W. Anderson, Phys. Rev. B **37**, 580 (1988); G. Baskaran, Phys. Scr. T 27, 53 (1989).

- [55] R. Hlubina, W.O. Putikka, T.M. Rice, and D.V. Khveshchenko, Phys. Rev. B **46**, 11224 (1992).
- [56] S.E. Barnes, J. Phys. F **6**, 1375 (1976).
- [57] P. Coleman, Phys Rev. B **29**, 3035 (1984).
- [58] S. Sachdev, Phys. Rev. B **45**, 389 (1992).
- [59] A.J. Millis and H. Monien, Phys. Rev. Lett. **70**, 2810 (1993); **E 71**, 210 (1993).
- [60] T. Holstein, R. Norton, and P. Pincus, Phys. Rev. B **8**, 2649 (1973).
- [61] B.I. Halperin, T.C. Lubensky, and S.-k. Ma, Phys. Rev. Lett. **32**, 292 (1974).
- [62] D.C. Mattis and J. Bardeen, Phys. Rev. **111**, 412 (1958).
- [63] P.B. Miller, Phys. Rev. **118**, 928 (1960).
- [64] A.A. Abrikosov and L.P. Gorkov, Soviet Phys. JETP **35**, 1090 (1959).
- [65] For a derivation see for instance J.R. Schrieffer, *Theory of superconductivity*, (Addison-Wesley, Menlo Park, CA, 1964), section 8-4.
- [66] J.M. Tranquada *et al.*, Phys. Rev. B **46**, 5561 (1992).
- [67] B.J. Sternlieb *et al.*, Phys. Rev. B **47**, 5320 (1993).
- [68] S. Shamoto *et al.*, Phys. Rev. B (in press).
- [69] B.L. Altshuler and L.B. Ioffe, Solid State Commun. **82**, 253 (1992).
- [70] H. Fukuyama, Prog. Theor. Phys. Suppl. **108**, 287 (1992).
- [71] J.M. Tranquada *et al.*, Phys. Rev. B **40**, 4503 (1989).
- [72] T. Tanamoto, H. Kohno, and H. Fukuyama, J. Phys. Soc. Jpn. **61**, 1886 (1992);
J. Phys. Soc. Jpn. **62**, 717 (1993).
- [73] A.J. Millis, Phys. Rev. B **45**, 13047 (1992).

- [74] We are grateful to N. Bonesteel for a discussion on this point.
- [75] P.B. Wiegmann, Phys. Rev. Lett. **60**, 821 (1988); Physica (Amsterdam) **153-155C**, 103 (1988); X.G. Wen, Phys. Rev. B **39**, 7223 (1989).
- [76] A.J. Millis, H. Monien, and D. Pines, Phys. Rev. B **42**, 167 (1990).
- [77] H. Monien, D. Pines, and M. Takigawa, Phys. Rev. B **43**, 258 (1991).
- [78] J.P. Lu, Phys. Rev. Lett. **68**, 125 (1992).
- [79] W.L. McMillan, Phys. Rev. B **16**, 643 (1977).
- [80] M. Takigawa, to appear in Phys. Rev. B.
- [81] A. Sokol and D. Pines, Phys. Rev. Lett. **71**, 2813 (1993).